

Numerical Investigation of Transient Flow Responses in Fractured Tight Oil Wells

by

Min Yue

A thesis submitted in partial fulfillment of the requirements for the degree of

Master of Science

in

Petroleum Engineering

Department of Civil and Environmental Engineering
University of Alberta

© Min Yue, 2016

Abstract

Increasing demand of global energy and limited conventional resources force the petroleum industry to shift their focus towards the low permeability reservoirs such as shale or tight rock reservoir. Multi-fractured horizontal wells have economically unlocked the massive hydrocarbon resources from unconventional reservoirs. Horizontal drilling and hydraulic fracturing create a complex fracture network that could enhance reservoir contact area to achieve economic production rates.

In this study, we compute the transient response in a segment of a hydraulically fractured horizontal well using a triple-porosity model. Impacts of capillary discontinuity (fracture face-effect) and some limitations in analytical models such as sequential flow, single-phase flow and fully-connected symmetric fractures are investigated.

We find that the uncertainty in model history-matched parameters and assumptions associated with analytical models could potentially over- or under-estimate production by up to 30%. History-matching with analytical models alone and the assumption of uniformly-spaced fracture stages would tend to overestimate long-term production forecast. In contrast, the assumption of no solution gas in tight oil reservoir leads to underestimation of reservoir properties such as length of fracture and permeability. Moreover, the simulated production data indicates that fracture face-effect results in rapid production decline. Lower capillary contrast between fracture and matrix results in less water blockage and higher production.

*Dedicated to my parents, grandparents and fiancé,
who give me courage, support and endless love*

Acknowledgments

First, I would like to express my sincerest gratitude to my supervisors, Dr. Juliana Y. Leung and Dr. Hassan Dehghanpour, for supporting me, for their constant encouragement, guidance and help throughout my project with their patience.

I would like to thank Dr. Alireza Nouri and Dr. Yuntong She, my examining committee members.

I am thankful to support of Natural Sciences and Engineering Research Council of Canada (NSERC). Also I am thankful Computer Modelling Group Ltd. (CMG) for providing academic licenses of IMEX for my research.

I would like to thank Mingyuan who has given me his valuable suggestions in model building. I would like to extend my thanks to my dearest friends Yang, Xinming, Bo, Jingwen, Zhongguo, Cui, Song, Jindong and Yanming for their warm friendship.

Last but not the least, I would like to express my love to my family: my parents, my grandparents and Mingxiang, who have been with me through the best and worst times with their endless love and support.

Table of Content

1	General Introduction.....	1
1.1.	Overview and Background.....	1
1.2.	Problem Statement.....	3
1.3.	Research Objectives	4
1.4.	Thesis Layout.....	6
2	Literature Review.....	7
2.1	A Brief Background of Unconventional Reservoirs.....	7
2.2	Modeling and Analysis of Flow Response in Hydraulically-Stimulated Tight Reservoirs	8
2.3	Modeling and Analysis of Multiphase Flow Response in Tight Reservoirs.....	10
3	Geological and Production Characteristics of Tight Oil Reservoirs.....	12
3.1	Geological Characteristics.....	13
3.2	Hydraulic Fracturing.....	16
3.3	Natural Fracture (Secondary Fracture).....	20
4	Methodology.....	25
4.1	Rate Transient Analysis.....	26
4.2	Analytical Solution: Using Laplace Transform.....	27

4.3	History Matching and Sensitivity Analysis of Simulation Models	31
5	Numerical Investigation of Limitations and Assumptions of Analytical	
	Transient Flow Models	32
5.1	Configuration of Multistage Hydraulic Fracturing	34
5.2	Intensity/Spacing of Secondary Fractures	37
5.3	Non-Sequential Flow	42
5.4	Non-Symmetric Drainage	46
5.5	Heterogeneous Fracture Properties.....	54
6	Influence of Multi-phase Effects on oil Production.....	60
6.1	The Role of Gas Dissolution	60
6.2	The Role of Capillary Discontinuity	66
7	Conclusions and Future Work.....	90
7.1	Conclusions	90
7.2	Future Work	93
	References.....	94

List of Tables

Table 5.1 Known Field Data	32
Table 5.2 Unknown Data – Assumed based on typical values observed in Bakken reservoirs	33
Table 5.3 Unknown Data – Estimated based on rate transient analysis (RTA)	33
Table 5.4 Spacing between the four stages of hydraulic fractures for the Cardium well in Case A	34
Table 5.5 History-matched hydraulic fracture half-length and the corresponding number of natural fractures for the Bakken well.....	37
Table 5.6 Spacing between natural fractures for the Bakken well in Case A	46
Table 5.7 Natural fracture length for the Bakken well in Case B	50
Table 6.1 Water saturation at interface in dual-porosity and triple-porosity models with different capillary pressure (P_{c1} and P_{c3}).....	78
Table 6.2 Value of Δk_{row} in conditions of different relative permeability curvature	88

List of Figures

Figure 3.1 Schematic north-south cross section showing the Bakken and adjacent formations (USGS, 2013).....	13
Figure 3.2 Proppant distribution in hydraulic fracture (Cipolla et al. 2009).....	17
Figure 3.3 Horizontal well with transversely intersecting fracture (Phillips, et al., 2007)...	19
Figure 4.1 Top view of a horizontal well in triple-porosity model	25
Figure 4.2 Analysis of the Cardium well production data with analytical models	30
Figure 5.1 Pressure (in kPa) distribution at the end of production history (250 days) for the Cardium well with different distribution of L_F	35
Figure 5.2 Log-log plot of daily oil rate as a function of time for the Cardium well in Case A over 250 days	36
Figure 5.3 Relationship between $x_f - n_f$ for the Bakken well	38
Figure 5.4 Schematic of the base case with eight natural fractures for the Bakken well.....	40
Figure 5.5 Pressure (in kPa) distribution for the base case (Bakken well) at the end of production history (4.5 years).....	40
Figure 5.6 Log-log plot of daily oil rate as a function of time for the Bakken well	41
Figure 5.7 Pressure (in kPa) distribution for the sequential case (Bakken well) at the end of production history (4.5 years).....	42

Figure 5.8 Log-log plot of daily oil rate as a function of time for the base case and the sequential case (Bakken well) 43

Figure 5.9 Log-log plot of daily oil rate as a function of time for the base case and all sequential cases (Bakken well)..... 44

Figure 5.10 Log-log plot of daily oil rate as a function of time for non-sequential and sequential cases..... 45

Figure 5.11 Pressure (in kPa) distribution of the Bakken well at 4.5 years and the histogram of L_f for 47

Figure 5.12 Log-log plot of daily oil rate as a function of time of the Bakken well for Case A 48

Figure 5.13 Log-log plot of daily oil rate as a function of time of the Bakken well for Case A with higher matrix permeability (0.0026mD)..... 49

Figure 5.14 Schematic of non-symmetric drainage for the Bakken well..... 51

Figure 5.15 Pressure (in kPa) distribution of the Bakken well after 4.5 years for 52

Figure 5.16 Log-log plot of daily oil rate as a function of time of the Bakken well for Case B 54

Figure 5.17 Schematic of fully-connected and non-connected natural fractures for the Bakken well..... 55

Figure 5.18 Log-log plot of daily oil rate as a function of time of the Bakken well for cases

with varying natural fracture connectivity (4.5 years).....	56
Figure 5.19 Schematic of fully-connected and non-connected hydraulic fractures for the Bakken well.....	57
Figure 5.20 Log-log plot of daily oil rate as a function of time of the Bakken well for cases with varying hydraulic fracture connectivity (4.5years).....	58
Figure 5.21 Pressure (in kPa) distribution of the Bakken well after 4.5 years when $R_L=0.224$	59
Figure 6.1 Average gas saturation in hydraulic fracture during the first 30 days for the Bakken well.....	61
Figure 6.2 Input PVT data for the Bakken models with different bubble-point pressure ..	62
Figure 6.3 Log-log plots of production profiles for the Bakken models with different bubble-point pressure.....	63
Figure 6.4 Log-log plots of production profiles for the Bakken models with different relative permeability endpoints	64
Figure 6.5 Log-log plots of production profiles for the Bakken models with different relative permeability curvatures	65
Figure 6.6 Oil and water saturation profiles in matrix as a function of distance from the fracture-matrix interface for the dual-porosity model at:	68
Figure 6.7 Different capillary pressure curve for matrix.....	69

Figure 6.8 Oil and water saturation profiles in matrix as a function of time for the dual-porosity model with different capillary pressure:.....	70
Figure 6.9 Oil and water saturation profiles in saturation in matrix as a function of distance from the fracture-matrix interface for the dual-porosity models with different capillary pressure at 30 days:	71
Figure 6.10 Log-log plot of daily rate versus time for the dual-porosity models with different capillary pressure in matrix during 91 days:	72
Figure 6.11 Average oil saturation in fracture in models in as a function of time for the dual-porosity model different capillary pressure:	73
Figure 6.12 Log-log plot of cumulative oil versus time for the dual-porosity models with different capillary pressure in matrix during 91 days.....	74
Figure 6.13 Log-log plot of daily rate versus time for the dual-porosity models with different capillary pressure in matrix during 91 days:	75
Figure 6.14 Oil and water saturation profiles in matrix as a function of	77
Figure 6.15 Triple-porosity models with different capillary pressure:.....	78
Figure 6.16 Different relative permeability in matrix system by changing endpoint of k_{row}	80
Figure 6.17 Saturation profiles in saturation in matrix as a function of distance from the fracture-matrix interface with different endpoint of k_{row} at 30 days:.....	81
Figure 6.18 Log-log plot of daily rate versus time for the dual-porosity models with	

different kro endpoints in matrix during 91 days: 82

Figure 6.19 Different relative permeability in matrix system by changing curvature of k_{row}
..... 83

Figure 6.20 Saturation profiles in saturation in matrix as a function of distance from the
fracture-matrix interface with different curvature of k_{row} at 30 days:..... 84

Figure 6.21 Log-log plot of daily rate versus time for the dual-porosity models with
different k_{row} curvature in matrix during 91 days:..... 85

Figure 6.22 Schematic of calculation procedure for Δk_{row} :..... 86

Figure 6.23 Saturation profiles in saturation as a function of distance from the fracture-
matrix interface with different capillary pressure in matrix at 30 days: 87

Figure 6.24 Log-log plot of daily rate versus time for the dual-porosity models with
different capillary pressure in matrix during 91 days: 88

Figure 6.25 Δq as a function of time in models with different endpoint of k_{row} 89

Nomenclature and Greek Symbols

A_{cw} = cross-sectional area to flow defined as $2hX_e$, /m²

B_g = formation volume factor of gas, rm³/sm³

B_o = formation volume factor of oil, rm³/m³

c_t = total compressibility, kPa⁻¹

d_f = length of natural fracture, m

E_g = Gas expansion factor: $1/B_g$, sm³/rm³

$f(s)$ = transfer function

h = reservoir thickness, m

HF = hydraulic fracture

k_m = matrix permeability, mD

k_F = hydraulic fracture permeability, mD

k_f = natural fracture permeability, mD

k_{row}^o = endpoint of oil relative permeability

k_{rog} = oil relative permeability

k_{rw} = water relative permeability

L_F = hydraulic fracture spacing, m

L_f = natural fracture spacing, m

L_w = spacing between two horizontal wells, m

NF = natural (secondary) fracture

n_F = number of hydraulic fracture stages

n_f = number of natural fractures

P_b = bubble-point pressure, kPa

P_i = initial reservoir pressure, kPa

P_{wf} = minimum wellbore flowing pressure, kPa

Δq_{pc} = the difference in oil rate between models with different capillary pressure in matrix,
m³/day

$\overline{q_D}$ = dimensionless wellbore rate

R_s = solution gas-oil ratio, m³/m³

s = laplace variable, t⁻¹, s⁻¹

S_{orw} = residual oil saturation

S_w = water saturation

S_{wi} = initial water saturation

S_{wn} = normalized water saturation

SRV = stimulated reservoir volume

w_F = hydraulic fracture width, m

w_f = natural (secondary) fracture width, m

X_e = effective well length, m

y_{De} = dimensionless reservoir half-length

x_f = hydraulic fracture half-length, m

y_e = reservoir half-length, m

λ = interporosity transmissivity ratio

ω = storativity ratio, dimensionless

μ = viscosity, cp

ϕ_m = matrix porosity

ϕ_F = hydraulic fracture porosity

ϕ_f = natural (secondary) fracture porosity

1 General Introduction

1.1. Overview and Background

Unconventional resources have become an increasingly important energy supply in North America in the past two decades. Shale gas, tight oil, tight gas and coal-bed methane have been widely explored and exploited as commercial resources around the world. The proliferation of activity into shale plays has increased the production of shale gas. In North America, it makes the contribution of shale gas to total natural gas production from less than 1% in 2000, to 39% for the United States and 15% for Canada separately. (Stevens 2012; US Energy Information Administration, 2013a).

Unconventional resources are in the unconventional reservoirs that are with low matrix permeability in the order of nano darcies (10^{-6} mD) to micro darcies (10^{-3} mD) (Best and Katsube, 1995), small porosity (less than 10%) and small pore size in the order of nano meters (10^{-9} m) (Nelson, 2009). Large well-reservoir contact area is required to achieve commercial production from the unconventional reservoirs (Ning et al., 1993).

The use of multilateral horizontal drilling in conjunction with multi-stage hydraulic fracturing technologies has greatly expanded the ability to produce natural gas and oil profitably from unconventional plays (Wang et al., 2008; Medeiros et al., 2010). The first application of hydraulic fracturing can back to 19th century. In the 1970s, the developments of Devonian shale in the eastern US foster the crucial technologies for unconventional resources, which including horizontal drilling, multi-stage fracturing and slick water fracturing (US Energy Information Administration, 2013b). After the 1990s, the advances in horizontal drilling and hydraulic fracturing techniques, successful development of shale gas system such as Barnett Shale in

Texas, US have led to increased exploitation and development internationally and large-scale shale gas production in North America.

The decline in conventional resources and increasing demand for energy supply make oil companies more active to seek out new unconventional reservoirs for commercial development. However, development of unconventional formations still faces engineering challenges. Since the hydraulic fracturing system creates complex fracture network along horizontal wellbore, understanding the multiphase flow in the fracturing system is essential for reservoir estimation and production forecast, which can eventually lead to better optimization of drilling and production process. Moreover, because of the extremely small nano pore size in unconventional reservoirs, capillary end effect will play a more important role in hydrocarbon recovery, compared with inhigh permeability high porosity conventional reservoirs.

1.2. Problem Statement

Existing triple-porosity models typically assume sequential flow from matrix to micro fractures and from micro fractures to hydraulic fracture. Modeling simultaneous depletion of a matrix block into both micro and hydraulic fractures entails solution of a two-dimensional continuity equation that is challenging by analytical or even semi-analytical methods. In addition, production data analysis is an inverse problem with non-unique solutions. Analysis with analytical models and type-curves provides deterministic and homogeneous estimates, representing an average parameter value and rendering uncertainty analysis of fracture properties difficult. In other word, it is hard to capture the uncertainties associated with reservoir heterogeneity.

Field data usually show a rapid decline of oil production or low water flowback from fractured horizontal wells. It has been hypothesized that multiphase effects such as phase blockage are partly responsible for inefficient fracturing water and hydrocarbon recovery. Furthermore, recent imbibition experiments indicate the significance of capillary pressure during multiphase flow in unconventional rocks. In the late part of this thesis, we hypothesize that the discontinuity of capillary pressure at fracture-matrix interface leads to significant phase blockage and relative permeability effects, which in turn result in production decline. To test this hypothesis, we run a series of simulation case studies to investigate the role of capillary discontinuity on multi-phase production from fractured horizontal wells.

1.3. Research Objectives

In this thesis, we use a commercial reservoir simulator to compute the transient response in a segment of a hydraulically fractured horizontal well with a triple-porosity model, where matrix and fracture elements are explicitly discretized. Some limitations in analytical models such as sequential flow, single-phase flow and fully-connected symmetric fractures are investigated using the actual rate data from two tight oil wells completed in the Cardium and Bakken formations. An early drop in production, as commonly observed in many tight oil wells, could be attributed to gas dissolution with pressure decline and multiphase flow effects. Impacts of pressure interference between natural fractures and inter-well fracture communication are also investigated. Uncertainty in model parameter estimation is studied by assuming that results obtained from analytical solutions would characterize the mean estimate of the corresponding fracture parameters, additional heterogeneous models of natural/induced micro-fracture properties including its total number and intensity (spacing) are assigned stochastically. These models are subsequently subjected to flow simulations, and the variability in production performance captures the sensitivity due to model parameter uncertainties.

In addition to this, the simulated saturation profiles confirm the existence of fracture-face effect, which in principle is similar to the end-effect observed in laboratory coreflooding tests. Fracture-face effect is caused by seeking capillary equilibrium in two systems with different capillary pressures. The simulated production data indicate that fracture-face effect results in rapid production decline. Less water blockage and higher production are observed in cases with lower capillary contrast between fracture and matrix or higher relative permeability to the oil phase. It is also observed that initial oil production increases slightly due to the displacement of oil by water (wetting phase) near the fracture-matrix interface. This increase is more pronounced when

we increase the capillary pressure in matrix blocks. However, long-term production is hampered as a result of increased water blockage.

1.4. Thesis Layout

Most of the research is using numerical reservoir simulation. Methodology consists of rate transient analysis, history matching and sensitivity analysis.

The work in this thesis is divided into six chapters. Chapter 1 (the current chapter) provides the background and the scope of this research including problem statement and some hypotheses. Chapter 2 contains the introduction of modeling fractured well and transient flow. A detailed literature review on multi-phase effects on production is also included in this chapter. An overview of the geological features, reservoir heterogeneities and fracture characteristics for typical tight oil reservoirs is included in Chapter 3. A discussion of the hydraulic fracturing operation is also presented. This discussion serves as a basis for the numerical models employed in this thesis. Chapter 4 presents the details of the proposed modeling methodology. Rate transient analysis (RTA), Laplace transform and history matching are all explained in this chapter. Chapter 5 comprises numerical investigation of limitations and assumptions of analytical transient flow models. Several case studies are performed to highlight the non-uniqueness of fracture characterization in production data analysis. Chapter 6 investigates two multi-phase effects in tight oil production which are solution gas and capillary end effect. Some sensitivity including relative permeability, bottom-hole pressure and capillary pressure are tested in these two cases. Chapter 7 summarizes the major findings of the conducted research and presents suggestions for future research on this topic.

2 Literature Review

2.1 *A Brief Background of Unconventional Reservoirs*

Unconventional resources are hydrocarbon reservoirs which have low permeability and porosity, include shale gas, shale oil, tight gas, tight oil and coalbed methane. Tight gas and oil are the hydrocarbon gathered in small, poorly connected cavities between poorly porous sandstone. Shale gas and oil are the hydrocarbon which still remain in the bedrock where it formed instead of migrating to more permeable rock. Shale is characterized as a fine-grained, clastic sedimentary rock composed of clay minerals and quartz grains (Crain, 2012). It has lower permeability and porosity than tight sandstone reservoirs. The hydrocarbon in organic-rich shale reservoirs usually trapped in the surfaces of the shale rock particles (Curtis, 2002). Until 2013, there are 7,299 trillion cubic feet of shale gas and 345 billion barrels shale or tight oil which located in 95 basins around the world are identified as technically recoverable resources around the world (US Energy Information Administration, 2013b).

Stimulation techniques such as horizontal drilling, multi-stage fracturing and slick water fracturing are required for achieving economic hydrocarbon production from unconventional reservoirs. However, effective developments must consider the complex characteristics of hydraulic fracturing system, which make the reserve estimation and production forecast more difficult than conventional reservoirs. Accurate modeling and analysis on hydraulic stimulated reservoirs are essential for better optimization of drilling and production process.

2.2 Modeling and Analysis of Flow Response in Hydraulically-Stimulated Tight Reservoirs

Multi-fractured horizontal wells are required to enhance reservoir contact area in order to achieve economic production rates (Ning et al., 1993). Modeling and analysis of flow response in hydraulically-stimulated tight reservoirs are required for reserve estimation and production forecast. Works including Warren and Root (1963), Kazemi (1969) and Swaan (1976) have provided the basis for analyzing flow in a dual-porosity system. In these models, fluid flows from the low-permeability matrix into a high-permeability fracture network, which is connected to the production wellbore. El-Banbi (1998) extended the dual-media model for application in stimulated tight reservoirs. Five distinct alternating linear and bilinear flow regimes representing depletion in hydraulic fracture and surrounding matrix blocks can be identified (Bello, 2009). Abdassah and Ershaghi (1986) developed a triple-porosity model for analysis of pressure transient data, which could explain the anomalous slope changes observed during various transition periods. Since most tight reservoirs are also naturally fractured, more comprehensive triple-porosity models encompassing hydraulic fractures, natural fractures and matrix blocks were developed recently (Abdullah A G and Iraj E, 1996; Liu et al., 2003; Wu et al., 2004; Alahmadi, 2010, 2013; Dehghanpour and Shirdel, 2011; Abbasi et al., 2014; Ali A J et al., 2013). In these models, natural or secondary fracture is considered as the third porosity system (Gale et al., 2007), which can improve the stimulated reservoir volume as compared to a dual-porosity system involving only hydraulic fracture and matrix (Rogers et al., 2010; Castillo et al., 2011).

The aforementioned analytical models have been employed extensively in the areas of pressure transient (PTA) and rate transient (RTA) analysis. Many authors have also proposed simplified semi-analytical analysis equations that can be used to estimate various system parameters such as hydraulic fracture half-length and fracture-matrix contact area (Bello, 2009; Szymczak et al.,

2012; Ali et al., 2013). It should be emphasized that analytical or semi-analytical models are essentially simplified solutions to the detailed governing equations. Unfortunately, production data analysis is an inverse problem with non-unique solutions. Analysis with these analytical models would typically yield a homogeneous deterministic estimate, representing an average parameter value, but it fails to capture the uncertainties associated with reservoir heterogeneity (Al-Ahmadi and Wattenbarger, 2011). At last, assumptions associated with most (semi-) analytical models include single-phase flow (ignoring the effects of solution gas) and sequential depletion from matrix to natural fractures and from natural fractures to hydraulic fracture (Al-Ahmadi and Wattenbarger, 2011; Ali A J et al., 2013). These models also assume a fully-connected natural fracture system, rendering detailed transient flow analysis in a triple-porosity medium challenging.

In theory, numerical reservoir simulators can be used to estimate the transient flow response in a triple porosity medium in which matrix blocks deplete into the two fracture networks simultaneously within an arbitrary drainage volume; however, computational costs and complexities of simulation models often hinder their efficiency in practice (Alkough et al., 2012; Kalantari -Dahaghi et al., 2012; Lee and Sidel, 2010). We demonstrate with production data collected from two tight oil wells that the history matching process generates non-unique solutions. The effects of boundary conditions, pressure interference and gas dissolution would also introduce additional uncertainties in the parameters derived from analytical models. The analysis workflow adopted in this study presents a practical framework for integrating numerical simulations with analytical solutions to study the limitations of analytical transient flow models and to quantify the uncertainty in production performance predictions.

2.3 Modeling and Analysis of Multiphase Flow Response in Tight Reservoirs

Unconventional reservoirs have received a significant attention recent years due to recent advances in horizontal drilling hydraulic fracturing and the large amount of recoverable oil and gas (Isaacs 2008). Multi-hydraulically fractured horizontal wells could enhance production by connecting artificial fractures with micro fractures. Modeling and analysis of multiphase flow response in tight reservoirs with multiple fracture systems are required for reserve estimation and production forecast.

Works such as Clark (1962), Synder (1969) and Iwai (1976) have provided the basis for analyzing flow in a multi-phase fractured system. In these models, a set of differential equations which combine Darcy's law and the law of conservation of mass for each phase describe reservoir behavior. Based on this, Kazemi (1976) combined these flow equations to build a three dimensional, numerical simulator to simulate the water and oil flow in fractured reservoirs. Fetkovich (1980) developed type curve analysis method for oil wells based on the material balance equations and rate-time equations (Fetkovich, 1973). Fraim and Wattenbarger (1988) presented a method to analyze multiphase flow with Fetkovich (1980) type curves. Rossen and Kumar (1992) considered the effect of aperture distribution and gravity, developed a two-phase flow model using Effective Medium Approximation (EMA) (Kirkpatrick, 1973). Effect of fracture relative permeabilities on natural fractured reservoirs is investigated using Rossen and Kumar model. (Rossen and Kumar, 1994). Eker et al. (2014) modified a single-phase pressure drop equation, and introduced a multiphase flow model for analyzing well performance of fractured shale oil and gas reservoirs.

Brownscombe and Dyes (1952) performed water-oil imbibition experiments and observed oil can be displacement by water imbibition. The experiment results coupled with estimates of the

extent of fracturing, concluded the capillary pressure could be a main recovery mechanism in the highly fractured water-wet reservoir. Firoozabadi and Markeset (1992) performed drainage experiment on stacked block and stacked slab rock samples and observed the capillary cross flow enhanced the drainage rate. It is critical to know the capillary discontinuity in gravity drainage (Horie et al., 1988; Labastie, 1990). Ignorance of fracture-face effect result in erroneous results on relative permeability calculation in most of multiphase core flooding experiments (Qadeer et al., 1991; Huang and Honarpour, 1998). Rangel-German (2006) conducted water-air imbibition and oil-water drainage experiments, concluded that capillary continuity play more important role if the fractures are wider. Gupta et al. (2015) claimed that fracture-face effects have minimal impact on field-scale recovery according to their corefloods results. In this paper, we hypothesize that the discontinuity of capillary pressure at fracture-matrix may result in production decline.

Although experimental studies are useful in understanding the system physics, they are also costly and limited in study scale. Analytical models, though extensively employed in the areas of pressure transient (PTA) and rate transient (RTA) analysis, are essentially simplified solutions to the detailed governing equations; certain common assumptions include sequential depletion from matrix to a fully-connected secondary fracture system and from secondary fractures to hydraulic fracture (Al-Ahmadi and Wattenbarger, 2011; Ali et al., 2013) are often invoked. Numerical reservoir simulators offer a viable alternative to estimate the transient flow response in a complex medium in which fluids could flow into the two fracture networks simultaneously within an arbitrary drainage volume.

3 Geological and Production Characteristics of Tight Oil Reservoirs

In this chapter, geological characteristics, including those exhibited by complex multi-scale heterogeneous fractured systems, of typical tight oil reservoirs are summarized. In addition, completions/production technologies of horizontal wells and hydraulic fracturing are discussed, as these techniques are commonly adopted to unconventional reservoir development. The discussion would focus on two specific tight formations: Bakken and Cardium formations.

3.1 Geological Characteristics

Bakken Formation

Recently, the Bakken formation has been regarded as one of the largest contiguous deposits in North America due to its huge oil accumulation (US EIA, 2014). It is an interbedded sequence of rock unit from the Late Devonian to Early Mississippian age underlying large areas of northwestern North Dakota, Southern Saskatchewan, northeastern Montana and southwestern Manitoba (NoRDQuiST, 1953). The rock formation consists of three distinct members: lower and upper shale and middle member which is shown in Fig 3.1.

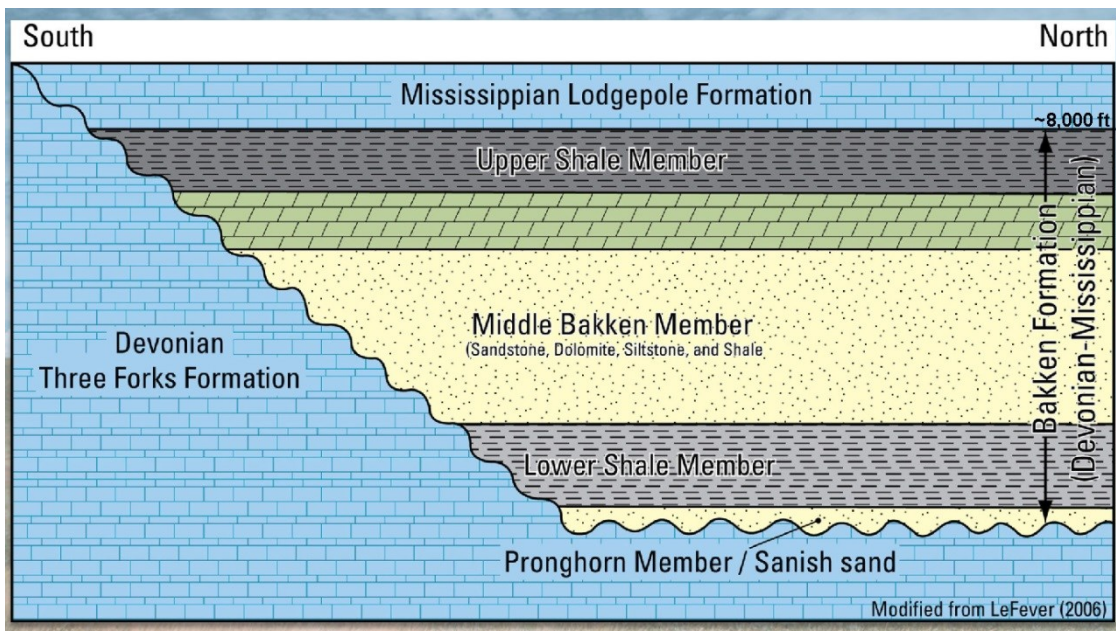


Figure 3.1 Schematic north-south cross section showing the Bakken and adjacent formations (USGS, 2013)

The upper and lower shale are organic-rich marine shale and share similar characteristics. Due to their low porosity and low permeability, upper and lower shale are acting as seals to the generated hydrocarbon (Wiley et al., 2004). The middle member is the main productive target of the current development. It is composed of marine sandstone or siltstone with large amount of

carbonate grains and cements (Cox et al., 2008).

Production in the Bakken can be divided into three development periods, that is, conventional vertical drilling (1953-1987), horizontal drilling in the upper shale (1987-2000) and horizontal drilling in the middle Bakken (2000-now) (LeFever, 2004). The application of horizontal well and hydraulic fracturing treatments have caused a considerable increasing in Bakken production since 2000 .

Although average porosity (5%) and permeability (0.04 md) are much lower than typical oil reservoirs, the existence of vertical secondary fractures have greatly enhanced the efficiency of horizontal drilling (Pitman et al., 2001). In this way, it is easy for a borehole to contact thousands of meters of oil reservoir rock with only about 40 m thickness (Baars, 1972). Also, production is increased by artificially fracturing the rock to have fracture with high conductivity for oil flowing into well (Yedlin, 2008). It has been proven that horizontal well with hydraulic fracturing is the most effective treatment to develop the middle Bakken formation (Tabatabaei et al., 2009).

Cardium Formation

The Cardium Formation is a stratigraphic unit of Late Cretaceous age and is a major source of oil and natural gas (Krause et al., 1994). It extends from northeastern British Columbia near Dawson Creek, to western Alberta. Oil is produced from Cardium formation in central Alberta, while natural gas is produced in western Alberta. The sandstones in formation have good storage ability and thick overlying becomes stratigraphic traps, while black shale, the underlying, is good source rock (Alberta Geological Survey, 2009).

Porosity of the Cardium formation is typically less than 9% with permeability being less than 1 md. Variation of porosity and permeability within the matrix can be ignored, considering their

intrinsically low values (Hoch et al., 2003). Horizontal well and hydraulic fracturing are also employed to connect to secondary fractures and enhance reservoir contact area or stimulated reservoir volume (Alberta Research Council et al., 1994).

3.2 Hydraulic Fracturing

Hydrocarbon in tight reservoir is difficult to be produced due to very low permeability in formation (Norbeck, 2011). Many unconventional reservoirs have recovery rate of less than 2% of OGIP which is much less compared with conventional reservoirs of 80% (King 2010; Moore 2010). Recently, hydraulic fracturing becomes a successful technology and widely used in tight reservoirs to improve hydrocarbon production performance (Hossain and Rahman, 2008).

Hydraulic fracturing is a formation stimulation technique used to create additional permeability by fracturing production formation with pressurized liquids (Veatch et al., 1989). Hydraulic fracturing operations are always performed by several portions of the lateral in horizontal well and fracturing of each portion is called a stage (DOE, 2009). Hydraulic fractures are induced in two phases (Weijers, 1995). At first, preparations such as perforation on casing and creating finger-like holes in formation are followed by pumping viscous fluids into well (Taleghani, 2009). A fracture is formed from perforation and develops into reservoir when bottom-hole pressure is above breakdown pressure and fracture width becomes relatively large during pumping (Cipolla et al. 2009). Next, fracturing slurry containing fluid and proppant is injected. This slurry increases width and length of fracture and transports the proppant into the end of fracture. Proppant is solid which can prevent the fractures from closing after finishing injection (Gandossi, 2013). Proppant distribution, controlled by proppant selection, fluids viscosity and fracture complexity, influences productivity of hydraulic fracture directly (Daneshy, 2004; Cipolla et al. 2009). Fig 3.2 shows a comparison that a fracture with or without proppant after pumping stops.

Cipolla et al. (2008) proposed that production enhancements in tight reservoir could be achieved by complex fracture and average proppant concentration would decrease with fracture

complexity increasing. Cipolla et al. (2009) claimed that proppant transport and proppant-filled height play important role in tight unconventional reservoirs. Using “waterfracs” which consists of treated water and very low proppant concentrations in recent hydraulic fracturing treatments has been successful in tight reservoirs (Fredd et al., 2000).

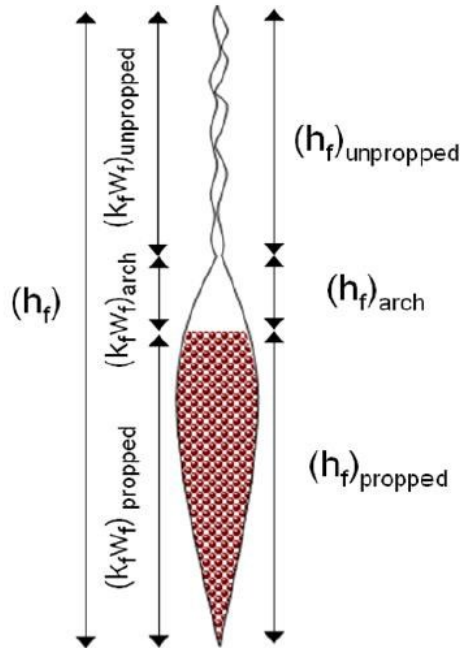


Figure 3.2 Proppant distribution in hydraulic fracture (Cipolla et al. 2009)

After slurry with proppant is pumped in, fluid with lower viscosity flows back out of the well, a fracture with high conductivity is formed (Veatch et al., 1989). Typical widths of hydraulic fractures are less than 0.6 cm, which is quite narrow. However, the effective length of hydraulic fracture can go as long as 900 m (Buchsteiner et al., 1993).

Hydraulic fractures are tensile fractures, and they always open in the direction of least resistance (Nolen-Hoeksema, 2013). Some geologic discontinuities (joints, bedding planes, faults and stress contrasts) have significant influences on hydraulic fracture, including reducing total

length of hydraulic fracture by fluid leak-off or difficulty of proppant transport and placement (Warpinski and Teufel, 1987). Microseismic imaging of fracture is relied on detection of micro-earthquakes or acoustic emissions associated with fracture (Urbancic et al., 1999). It can be used to characterize the fracture network (including fracture spacing, conductivity, degree of complexity, azimuth and fracture dimensions) and approximate fracture geometry (Fisher et al., 2002; Mayerhofer et al., 2006; Nejadi et al., 2015). Fractures are responsible for the main part of the permeability and mechanical closure of fracture is associated with pressure decline (Raaen et al., 2001). In other word, pressure declined can be a result of reduced fracture size, i.e. the pressure is less than or equal to the smallest principal stress in some part of the fracture (Fjar et al., 2008). Decreasing the fluid pressure causes the fracture to close, and the permeability decreases because of the smaller aperture (Walsh, 1981). Fracture closure can directly lead to production decline. Hence, modelling of fracture geometry is important in hydraulic fracturing for enhancing production in low-permeability reservoirs (Teufel and Clark, 1984).

For Bakken formation, horizontal well and hydraulic fracturing are used to achieve optimum recovery (Miller et al., 2008). Phillips, et al., (2007) highlighted the importance of fractures with high conductivity in Bakken horizontal wells and claimed that proppant characteristics are key parameter for transverse fractures (Fig 3.3). Due to low permeability in Bakken, horizontal well with multi-stage hydraulic fractures are required to increase oil production (Hassen et al., 2012). Others have suggested that the length of a hydraulic fracture is the most important factor influencing hydrocarbon productivity (Tabatabaei et al., 2009). It is also concluded that the optimum fracturing job would be the fracturing treatment that will cross and connect as much of the natural fracture system to the wellbore as possible. (Dahi, 2009).

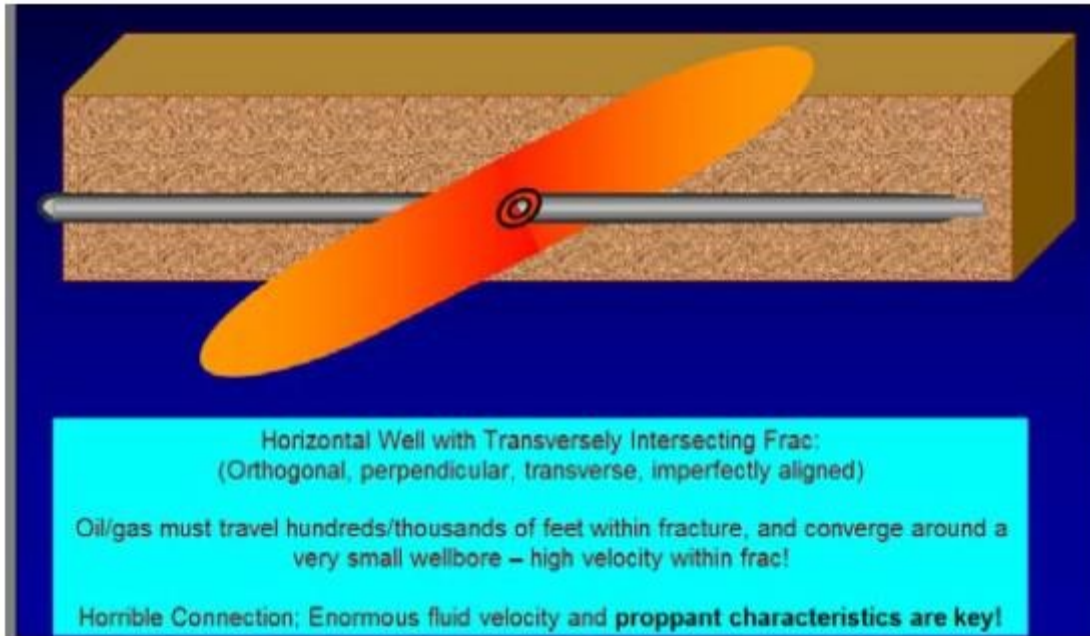


Figure 3.3 Horizontal well with transversely intersecting fracture (Phillips, et al., 2007)

3.3 Natural Fracture (Secondary Fracture)

Secondary or natural fractures have been recognized as an important factor for hydrocarbon recovery in unconventional reservoirs (Gale et al., 2014). Hydrocarbon recovery commonly exceeds the rate which is expected from hydraulic-fracture stimulation of intact host rock alone (Medeiros et al., 2010; Al-Ahmadi and Wattenbarger, 2011; Walton and McLennan, 2013; Yan et al., 2013). Natural fracture can be generated by many different process include 1) local stress perturbations; 2) regional burial; 3) stress change due to oil and gas generation or diagenetic reactions; 4) tectonic palaeostress; 5) accommodation effects around major faults and folds; 6) local structures and 6) stress release during uplift (Gale and Holder, 2010). The natural fractures in unconventional reservoirs are poorly connected to each other, rendering the formations economically unproductive. Without hydraulic fracturing stimulation, many tight gas reservoirs have been estimated to recover less than 2% of original gas in place (OGIP) (King, 2010; Moore, 2010). The connectivity of natural fractures can be effectively reactivated by hydraulic fracturing operations associated with complex microseismic event (Blanton, 1982; Warpinski and Teufel, 1987; Fisher et al., 2002, 2005; Dunphy and Campagna, 2011; Fisher and Warpinski, 2012), which will ultimate increase the estimated ultimate recovery (EUR) of tight gas reservoir to nearly 50% (King, 2010). Lack of site-specific natural fracture information is an impediment to understanding microseismic patterns and evaluating the hydraulic fracturing efficiency.

The overall productivity of a well and the role of natural fractures play as mechanical discontinuities and flow conduits depend on the number of fractures, fracture connectivity, and fracture characteristics (Wei and Economides, 2005). Understanding the characterization of the natural fracture has been considered as an important factor for determining the hydraulic fracturing, designing the well completion strategies and estimating the hydrocarbon production

performance (Aguilera, 2008). Fracturing properties such as fracture length, fracture width, fracture permeability, fracture conductivity, spatial arrangement, strength and cohesion and fracture mode (opening or shear) can be inferred from a variety of data including production data, core samples, resistivity image logs and cuttings and mud log data from drilling process (Norbeck, 2011).

Fracture abundance can be evaluated by fracture intensity or spacing, which is defined as number of fractures of a given size per unit of rock (scanline length, outcrop area or rock volume) (Ortega et al., 2006). It is more accurate when more fractures are sampled in a core or outcrop. However, sparse fractures are difficult to be captured in a limited area of outcrops, or the fracture clustering is easily misleading the fracture abundance observations. Another method to measure the fracture abundance is spacing, which is defined as separation between adjacent fractures, calculated as the inverse of intensity (Narr, 1996). Spacing is effectively analyzed in horizontal well data sets collected from a large outcrop. Fracture density or P_{32} is another measure of the fracture abundance, which is defined as the ratio of fracture surface area to rock volume (Dershowitz and Einstein, 1988). Fracture trace data in borehole images or whole core can be used to provide sufficient data sets for quantification of fracture density (Barthélémy et al., 2009). However, it is difficult to calculate or measure the fracture surface area and the micrometer wide fractures are difficult to be identified on chattered surfaces of the core. Vertical intensity of natural fractures are varies from 7 to 160 fractures per 100 ft for the unconventional reservoirs (Gale et al., 2014).

Geometry of an individual fracture is defined by its size (length and aperture) and orientation (i.e., dip and azimuth angle). Many unconventional formations exhibit a wide range of fracture size. Kinematic apertures range from micrometer to millimeter for both tight and shale reservoirs

(Laubach and Gale, 2006; Gale et al., 2014). The population of natural fracture usually follows a power-law size distribution (Marrett et al., 1999; Ortega and Marrett, 2000). Fracture length can be observed on some outcrop or quarry, but it is limited by the fracture exposure and the fracture may be not well preserved because of weathering (Olson, 2003). The maximum length observed by Gale et al.(2014) is around 40 m length with about 3 m height and 0.5 to 1 mm thick in Marcellus quarry outcrop. Natural fractures in shale are typically parallel arranged to the bedding plane, and propagate along the plane perpendicular to the least-compressive principal stress (Secor, 1966). Similar fracture orientations may indicate they formed under a similar stress regime (Hodgson, 1961; Hancock, 1985). Systematic regional patterns (consistent or gradually varying fracture patterns) of fracture strike has been observed in many basins include the Appalachian Plateau (Nickelsen and Hough, 1967; Engelder et al., 2009), the midcontinent New Albany (Ault, 1989) and the Michigan Basin Antrim Shales (Apotria et al., 1994). However, some formation also contain unsymmetrical fracture strike patterns. For example, fracture sets are not always follow the same sets in the outcrop in parts of the New Albany Shale (Gale and Laubach, 2009). This can be explained by weathering changes (Fidler, 2011), stress-field rotation (Rijken and Cooke, 2001).

Multiple orientation fracture patterns can be observed in shales with complex regional loading patterns and isotropic stress (Tuckwell et al., 2003; Fidler, 2011). Formation with such highly interconnected fracture pattern shows better production performance compare to the similar formation with a similar number of fractures but not well-connected (Philip et al., 2002).

Natural fracture permeability of a tight reservoir can be varied from 3 to 100 mD (Rubin, 2010; Cheng, 2012; Fakcharoenphol et al., 2013; Wattenbarger and Alkough, 2013). Natural fracture porosity can be typically varied from 0.1% to 8% in unconventional formations (Nelson, 1985;

Weber and Bakker, 1981). The natural fracture porosity can be underestimated because the size-dependent sealing patterns make the larger fractures tends to host great porosity (Laubach, 2003). Fracture porosity is far more compressible than normal matrix porosity (Ostensen, 1983). Fracture porosity usually decreases linearly with the log of confining stress (Walsh, 1981; Walsh and Grosenbaugh, 1979). Laboratory studies using tight sandstones shows the linear relation of fracture porosity and the log of confining stress (Jones and Owens, 1980; Sampath, 1982). The permeability of jointed natural fractures can be significantly reduced due to the stress decreasing. The fracture would not be fully closure and the permeability is still higher than matrix permeability (Gutierrez et al., 2000; Cho et al., 2013). For partly cemented natural fractures, the fracture is naturally propped with cement, which can prohibit closure from the stress decrease during production.

Not all natural fractures contribute to production. It depends on whether they are connected to the hydraulically fracture or activated according to the stress conditions (Cipolla et al., 2009). Natural fractures with high permeability and well-connected to the hydraulic fractures, usually have a positive effect on hydrocarbon recovery (Curtis, 2002; Engelder et al., 2009). High permeability natural fractures can also be a hindrance to hydrocarbon recovery (Dyke et al., 1995). For a conductive fracture system, water may only drain high permeability fractures but not low-permeability oil-saturated pores. Conductive fractures may also result in early breakthrough of water and hydrocarbon. For long-term production, natural fractures might close or be less contact with the hydraulic fracture system due to the fluid pressure depletion (Pagels et al., 2012; McClure, 2014). The horizontal natural fractures may act as barriers to hinder the hydraulic fracture propagate vertically when they intersect (Weng et al., 2011).

It is hard to measure natural fractures properties (such as permeability and length) by using log

imaging. In tight reservoir it is not practical to use well test analysis to estimate natural fracture properties because low reservoir permeability slows down the reservoir responses and testing time is long (Nejadi et al., 2014). Alternatively, analysis of dynamic production data has been adopted for estimations of fracture properties. However, production data analysis is an inverse problem with non-unique solutions (Nejadi et al., 2014). In this thesis, we have an integration of analytical solution and numerical solution to quantify uncertainties in reservoir and fracture properties.

4 Methodology

A commercial black-oil simulator (Computer Modeling Group, 2013) is used to construct a 2-D numerical model composed of three interacting media: natural fractures (*NF*), matrix blocks and hydraulic fractures (*HF*). There are no restrictions regarding the flow direction and the number of fluid phases. If we assume that hydraulic fracture stages are evenly spaced and symmetric, the simulation domain can be represented simply by a segment of a horizontal well with two bi-wing hydraulic fractures as shown in Fig 3.1. The top view of a horizontal well oriented along the x-direction with two additional fracture systems is illustrated. Perforation is placed in the center of the simulation model where the hydraulic fracture is intersecting with the horizontal well. Some natural fractures are positioned evenly at each side of horizontal well.

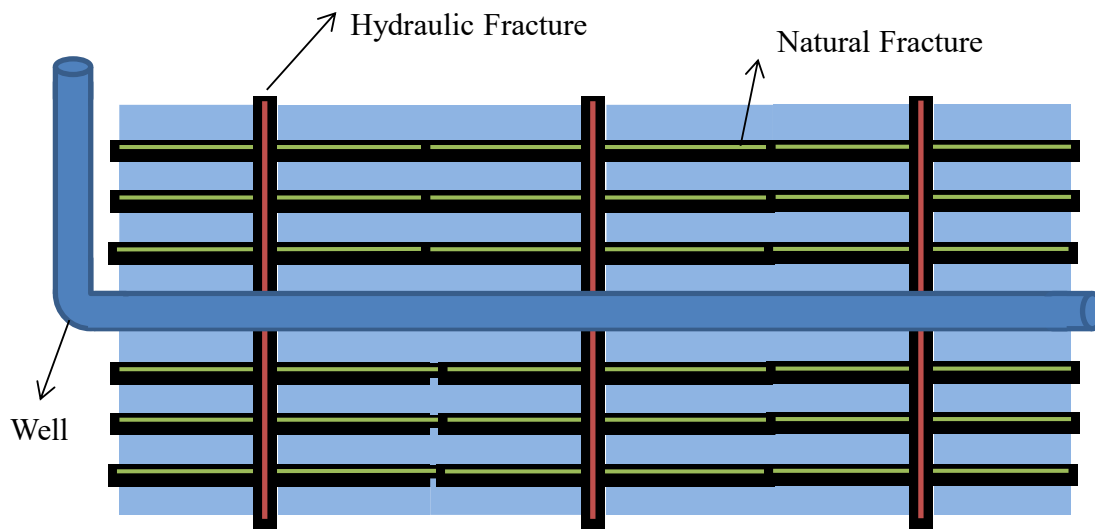


Figure 4.1 Top view of a horizontal well in triple-porosity model

The model depicts essentially a “single-porosity” medium, where matrix and fracture systems are explicitly discretized, and distinct properties are assigned to grid blocks that belong to each of the three systems. Due to the vast difference in the width dimensions of fractures and matrix, a logarithmic local grid refinement (LGR) scheme is employed to discretize regions around the

fractures, enhancing stability of the numerical solution while accurately capturing the transient responses within the fractures. The grid size varies from 0.05 m in the fracture cells to 10 m in the matrix cells that are located far away from the fracture.

4.1 Rate Transient Analysis

Parameters in the simulation model should be assigned according to known field observations/operating variables, as well as results obtained from RTA analysis. Analytical models such as Bello (2009) or Ezulike *et al.* (2015) can be used to estimate the system parameters pertinent to a dual-porosity or triple-porosity system, respectively. After identification of the observable flow regimes from the data, analysis equations can be applied to compute properties such as fracture permeability, fracture intensity, reservoir half-length (y_e) or stimulated reservoir volume (SRV). It is likely that a number of combinations of different parameter values could result in the same production data match.

4.2 Analytical Solution: Using Laplace Transform

The assumption of evenly-distributed hydraulic fracturing stages is explored in this section. Analytical models are applied to the Cardium well data to estimate a number of unknown parameters. First, the dual-porosity model of Bello (2009) is used to estimate the unknown hydraulic fracture properties such as half-length and permeability of hydraulic fracture. The rate-normalized pressure or RNP plots of three dominant flow regions are shown in Fig 3.2. For the bilinear region, a plot of RNP against $\sqrt[4]{t}$ (Fig 3.2a) yields a straight-line slope m_1 , which is substituted into Bello's region 2 analysis equation to obtain k_F :

$$\sqrt{k_F} = 966 \times \frac{\mu B_o}{A_{CW}} \sqrt{L_F}^4 \sqrt{\frac{1}{k_m(\phi c_t)_t \mu}} \times \frac{1}{m_1} \quad (1)$$

Where k_F = hydraulic fracture permeability; L_F = spacing between fracture stages; μ = fluid viscosity; c_t = total compressibility; ϕ = porosity; B_o = oil formation volume factor; k_m = matrix permeability; and A_{CW} = cross-sectional area to flow defined as $2hX_e$ (X_e = effective well length). The half-length of hydraulic fracture (x_F) is estimated by substituting the straight-line slope m_2 obtained from a plot of RNP against \sqrt{t} (Fig 3.2b) for the linear flow regime into Bello's region 4 analysis equation:

$$x_F = \frac{5.8B_oL_F}{A_{CW}} \sqrt{\frac{\mu}{k_m(\phi c_t)_t}} \times \frac{1}{m_2} \quad (2)$$

The values of k_F and x_F are estimated to be 1090 mD and 112 m, respectively.

Next, data from the boundary-dominated (linear pseudo steady state) flow regime is analyzed with the model described by Siddiqui *et al.* (2012). Assuming hydraulic fractures are fully

connected between wells (i.e., $y_e = x_F$), y_e and k_m can be estimated. A plot of RNP against material balance time (MBT) (Fig 3.2c) would yield a straight-line slope m_{ss} and intercept b_{ss} :

$$x_F = \frac{B_o}{2(\phi c_t)_m h n_F L_F} \times \frac{1}{m_{ss}} \quad (3)$$

$$k_m = \frac{\mu B_o L_F}{24 n_F x_F h} \times \frac{1}{b_{ss}} \quad (4)$$

Where h = formation thickness; x_F and k_m are evaluated to be 101 m and 0.034 mD, respectively. It is noticed that the correlation between RNP and MTB is not very strong in Fig 3.2c. This might introduce uncertainties in the estimation of x_F and k_m using this method. It is expected that some discrepancies would exist between x_F values estimated using the two different analytical models. Unlike Siddiqui's model, estimation of x_F from Bellos's model depends on the value of k_m . In this analysis, a permeability value of 1.34 mD was measured from core samples, and it was used as k_m in Bellos's analysis. This k_m value, however, is substantially larger than the estimate from Siddiqui's model, since micro fractures might exist in the core samples and true k_m is difficult to measure. Therefore, the value of k_m obtained from Siddiqui's model could serve as another estimate of the true matrix permeability.

Finally, a quadrilinear flow model (QFM) proposed by Ezulike and Dehghanpour (2013) is applied to estimate additional unknown parameters including number of natural fractures (n_f), natural fracture permeability (k_f), distance between two natural fractures (L_f). Laplace transform was used to solve a set of governing equations that describe simultaneous depletion of single-phase flow from matrix to natural fracture and hydraulic fracture under constant bottom-hole pressure or constant rate at the inner boundary. Type-curve solutions are subsequently constructed by inverting the solutions from the Laplace space (s) to real time numerically (Ezulike and Dehghanpour, 2013). Eqs.5-14 are the solutions in Laplace space for the

dimensionless rate at the wellbore with constant bottom-hole pressure.

$$\bar{q}_D = \frac{\sqrt{sf(s)}}{s \coth(\sqrt{sf(s)}y_{De})} \quad (5)$$

Where

$$f(s) = \omega_F + \frac{\lambda_{AC,Ff}}{3s} \sqrt{sf_f(s)} \tanh(\sqrt{sf_f(s)}) + \frac{\lambda_{AC,Fm}}{3s} \sqrt{f_m(s)} \tanh(\sqrt{f_m(s)}) \quad (6)$$

And

$$f_m(s) = \frac{3s\omega_2\omega_m}{\lambda_{AC,Fm}} \quad (7)$$

And

$$f_f(s) = \left\{ \frac{3\omega_f}{\lambda_{AC,Ff}} + \frac{\lambda_{AC,fm}}{s\lambda_{AC,Ff}} \sqrt{\frac{3s\omega_1\omega_m}{\lambda_{AC,fm}}} \tanh\left(\sqrt{\frac{3s\omega_1\omega_m}{\lambda_{AC,fm}}}\right) \right\} \quad (8)$$

Where

$$y_{De} = \frac{y_e}{\sqrt{A_{cw}}} \quad (9)$$

$$\omega_F = \frac{(\phi c_t)_F}{(\phi c_t)_t} \quad (10)$$

$$\omega_m = \frac{(\phi c_t)_m}{(\phi c_t)_t} \quad (11)$$

$$\lambda_{AC,fm} = \frac{12}{L_f^2} \frac{k_{m_1}}{k_F} A_{cw} \quad (12)$$

$$\lambda_{AC,Fm} = \frac{12}{L_F^2} \frac{k_{m_2}}{k_F} A_{cw} \quad (13)$$

$$\lambda_{AC,Ff} = \frac{12}{L_F^2} \frac{k_f}{k_F} A_{cw} \quad (14)$$

Here, ω_1 and ω_2 are weighting parameters, which control the fraction of fluid in the matrix that depletes into natural fracture and hydraulic fracture, respectively, during production; k_{m1} and k_{m2} denote matrix permeability in flow to natural fracture and hydraulic fracture, respectively. A match between QFM type-curves and production data is illustrated in Fig 3.2d.

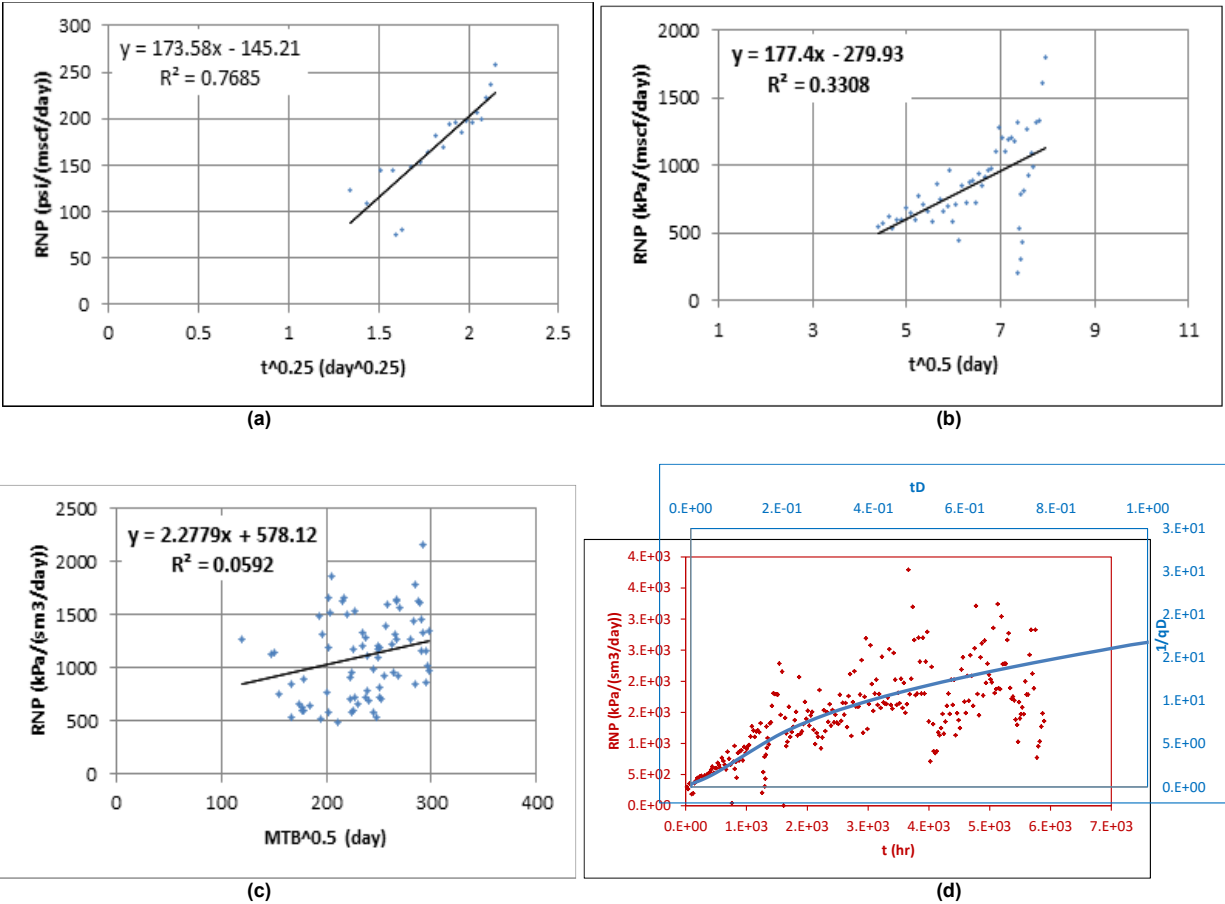


Figure 4.2 Analysis of the Cardium well production data with analytical models

- (a) – RNP against $\sqrt[4]{t}$ for bilinear flow; (b) – RNP against \sqrt{t} for linear flow;**
- (c) – RNP against MBT for boundary-dominated flow; (d) – QFM type-curve matching**

The same analysis is repeated for the second well completed in the Bakken formation. Results for x_F are in good agreement with those reported in the literature. Duhault (2012) and Quirk *et al.* (2012) have observed $60 \text{ m} < x_F < 300 \text{ m}$ in Cardium formation, while O’Brien *et al.* (2012) estimated $135 \text{ m} < x_F < 275 \text{ m}$ from micro-seismic studies in the Bakken formation.

4.3 History Matching and Sensitivity Analysis of Simulation Models

Additional adjustment or tuning of estimates derived from analytical models is required to achieve a final production history match with the simulation models. It is assumed that the results obtained from this history-matching process would characterize primarily the mean values of the corresponding fracture parameter distributions. A series of stochastic models are subsequently constructed and subjected to flow simulations in order to assess the uncertainties in fracture intensity (spacing) and the impacts of different assumptions associated with the analytical models. The variability (spread) in the simulation predictions would capture the sensitivity due to uncertainty in these model parameters.

5 Numerical Investigation of Limitations and Assumptions of Analytical Transient Flow Models

The RTA and history matching procedures described in the previous section have been applied in two case studies, where production data from two horizontal wells completed in the Cardium formation and Bakken formation are examined. Known model parameters summarized from field reports are shown in Table 5.1 (Ezulike and Dehghanpour, 2013). A few other unknown parameters are assigned based on typical values for these formations (Hlidek and Rieb, 2011; Alcoser *et al.*, 2012; Clarkson and Pederson, 2011) and RTA, as shown in Table 5.2. The value of fracture conductivity ($k_F \times w_F$) used in this study is comparable to typical field observation (Cinco, 1978). Although the assumed value for fracture porosity (ϕ_F) appears to be high in comparison to field observation, a sensitivity analysis reveals that the effects of ϕ_F on the numerical solution are minimal. This is because porosity influences primarily the accumulation term in the governing equations, and its impacts are subdued in a slightly-compressible system (e.g., oil). On the other hand, fracture permeability, k_F , has a strong influence on the simulated flow response, as it is used in the flux calculations. Table 5.3 is range of parameters estimated from RTA. Several cases for assessing the uncertainties and limitations of analytical models are presented next.

Table 5.1 Known Field Data

Parameter	Symbol	Cardium Well	Bakken Well	Unit
Formation volume factor of oil	B_o	1.221	1.329	m^3/m^3
Viscosity	μ	1.13	0.5643	cp
Initial reservoir pressure	P_i	15575	46884	kPa
Minimum wellbore flowing pressure	P_{wf}	1000	1000	kPa
Total compressibility	c_t	1.54×10^{-4}	2.51×10^{-6}	kPa^{-1}
Matrix permeability	k_m	-	0.0005	mD
Matrix porosity	ϕ_m	0.12	0.09	-

Effective well length	X_e	1370	1707	m
Reservoir thickness	h	7	5.8	m
Number of hydraulic fracture stages	n_F	-	16	-

Table 5.2 Unknown Data – Assumed based on typical values observed in Bakken reservoirs

Parameter	Symbol	Value	Unit
Natural fracture permeability	k_f	500	mD
Hydraulic fracture permeability	k_F	1000	mD
Natural fracture porosity	ϕ_f	0.6	-
Hydraulic fracture porosity	ϕ_F	0.8	-
Water saturation	S_w	0.2	-
Hydraulic fracture width	w_F	0.01	m
Natural fracture width	w_f	0.00005	m
Hydraulic fracture spacing	L_F	106	m
Hydraulic fracture half-length	y_e	200	m
Natural fracture length	d_f	106	m

Table 5.3 Unknown Data – Estimated based on rate transient analysis (RTA)

Parameter	Symbol	Value	Unit
Natural fracture permeability	k_f	104 – 520	mD
Hydraulic fracture permeability	k_F	245 – 1224	mD
Number of natural fracture	n_f	6-19	-
Hydraulic fracture half-length	y_e	141-235	m

5.1 Configuration of Multistage Hydraulic Fracturing

Next, a series of dual-porosity simulation models with four stages of hydraulic fracture are constructed to investigate the uncertainty in spacing between fracture stages on production performance of the Cardium well. Four different configurations or sets of L_F are tested (Table 5.4), and the corresponding pressure distributions at the end of production history (250 days) are illustrated in Fig 5.1. Fig 5.2 compares the production performances of all four cases, which deviate from each other with time. As expected, oil rate for the Base Case (where fracture stages are uniformly spaced) is the highest because pressure depletion and drainage is the most effective. In fact, a difference of 30% is observed between the Base Case and Case 0-3. This observation implies that if an analytical model assuming symmetry and uniform spacing between fracture stages is used to analyze production data from a well with asymmetric fracture stages and uneven spacing, a significant underestimation of the fracture half-length (and SRV) would be expected. The analytical solution, though not realistic, has provided an alternative (non-unique) estimation, which could be sufficiently useful for production forecast; however, underestimation of fracture half-length or SRV could potentially impact future field development decisions such as placement of nearby wells to maximize drainage.

Table 5.4 Spacing between the four stages of hydraulic fractures for the Cardium well in Case A

Case Number	Distribution of L_F	Unit
Case 0-1	146.4, 2.4, 147.6	m
Case 0-2	20.4, 146.4, 2.4	m
Case 0-3	87.6, 79.2, 69.6	m
Base Case	71.7, 71.7, 71.7	m

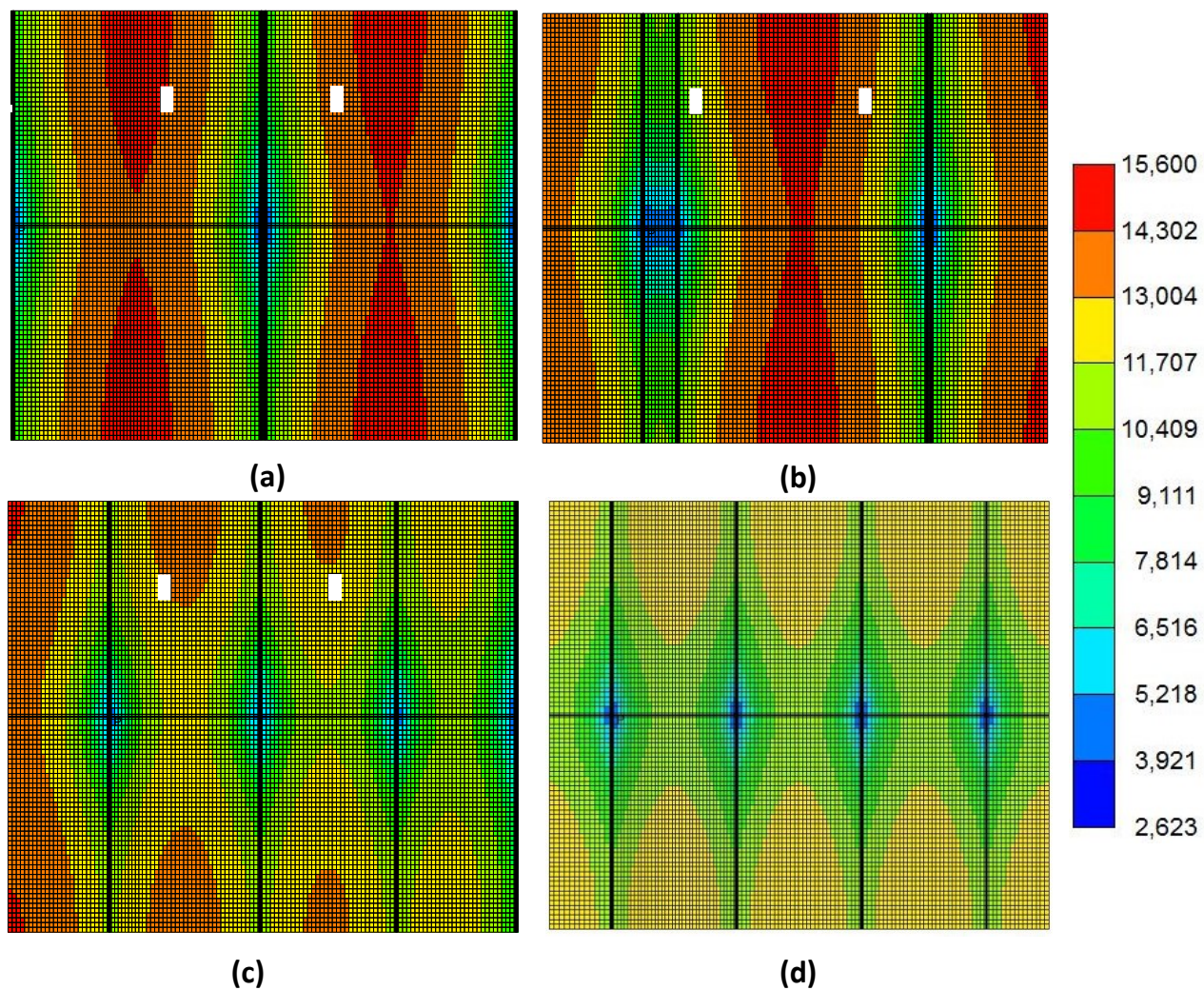


Figure 5.1 Pressure (in kPa) distribution at the end of production history (250 days) for the Cardium well with different distribution of L_F

(a) Case 0-1; (b) Case 0-2; (c) Case 0-3; (d) Base Case.

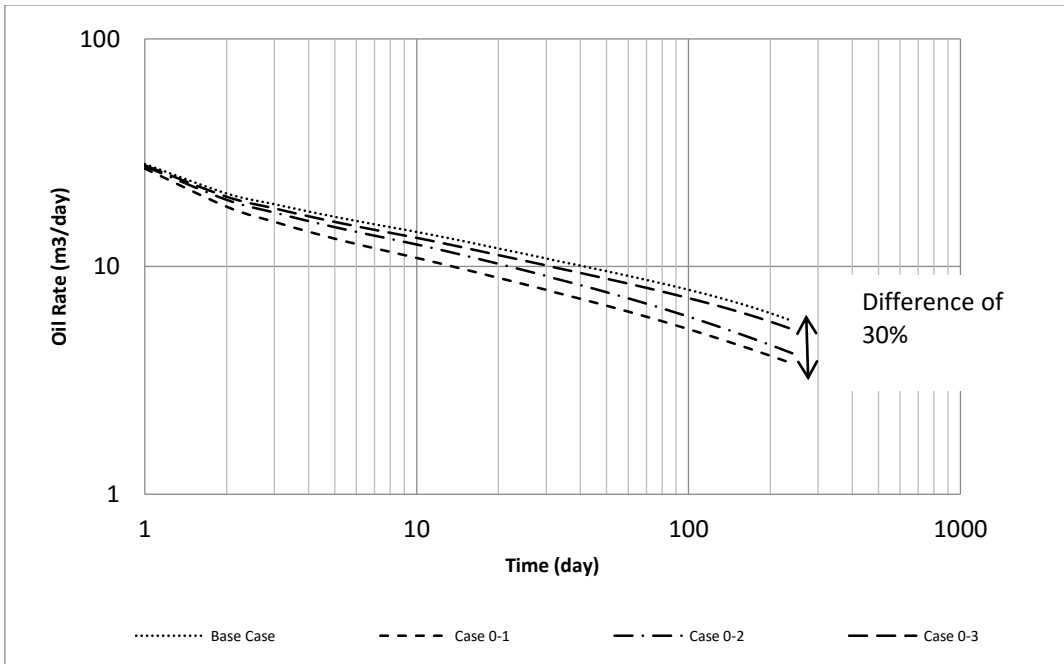


Figure 5.2 Log-log plot of daily oil rate as a function of time for the Cardium well in Case A over 250 days

5.2 Intensity/Spacing of Secondary Fractures

Approximate estimates of hydraulic fracture half-length (x_f) and spacing between natural fractures (or the number of natural fractures, n_f) are obtained from production data analysis with the triple-porosity analytical model described by Ezulike and Dehghanpour (2015). As discussed in the previous sections, solutions to production data analysis are non-unique, and many different combinations of these two parameters could yield the same data match. Therefore, based on the ranges of values derived from RTA, a set of simulation cases with different number of natural fractures (up to 20) are built and later matched with the production data. When the number of natural fractures becomes zero, the model converges to a dual-porosity model. To match the production data, different combinations of x_f and n_f are obtained. The final results for the Bakken well are tabulated in Table 5.5 and presented graphically in Fig 5.3.

Table 5.5 History-matched hydraulic fracture half-length and the corresponding number of natural fractures for the Bakken well

	Dual-Porosity Case	Case 1	Case 2	Case 3	Case 4	Case 5
n_f	0	2	4	8	12	20
x_f	315	280	250	200	150	114

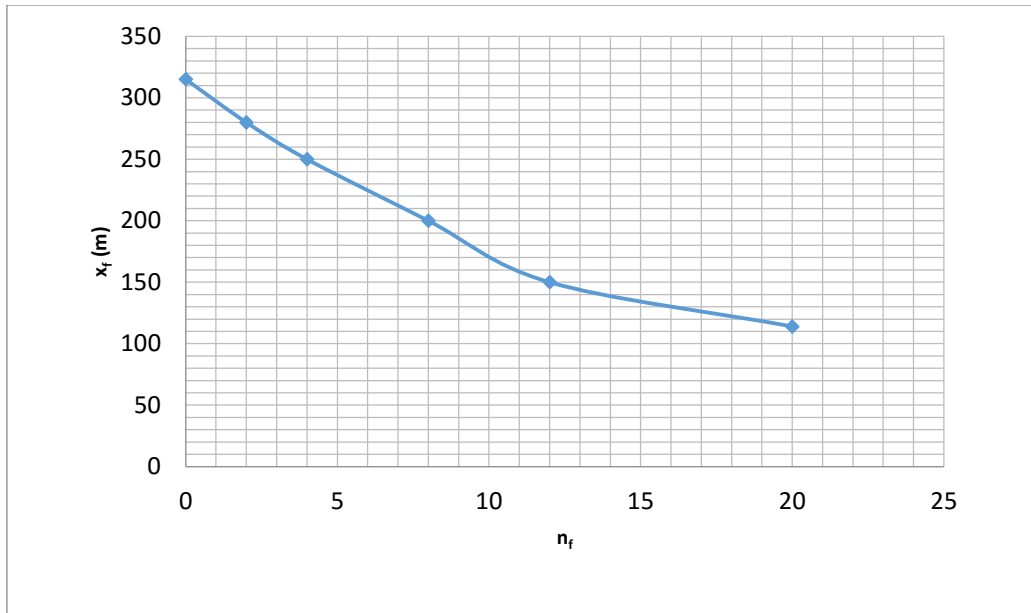


Figure 5.3 Relationship between x_f – n_f for the Bakken well

Interestingly, as the number of natural fractures increases, the history-matched hydraulic fracture half-length is reduced. This is because natural fractures provide additional interface for matrix depletion. In one extreme scenario where natural fractures are absent (representing a dual-porosity system), a maximum hydraulic fracture half-length of 315m is required to achieve a reasonable history match. This is almost three times the size in comparison to the other extreme scenario where there are 20 natural fractures and a hydraulic fracture half-length of 114m. This observation not only highlights the non-unique nature of production data analysis, but it also demonstrates the important role of n_f for production enhancement in a triple-porosity system.

In order to carry out further sensitivity analysis of other model parameters, a base case with $n_f = 8$ and $x_f = 200$ m is selected. A schematic of this base case is shown in Fig 5.4. Fig 5.5 shows the pressure distribution for the base case at the end of production history after 4.5 years. Fig 5.6 is a log-log plot of producing oil rate versus time for this base case along with the actual field data. The overall trend of the production decline of the base case is in good agreement with the actual

field observations, but it fails to accurately predict two spikes in the oil production. The first peak at 17 days corresponds to a drop in the bottom-hole pressure, while the second peak at 172 days is the result of reopening the well after a temporary shut-in. In this model, the bottom-hole pressure is assumed to be constant.

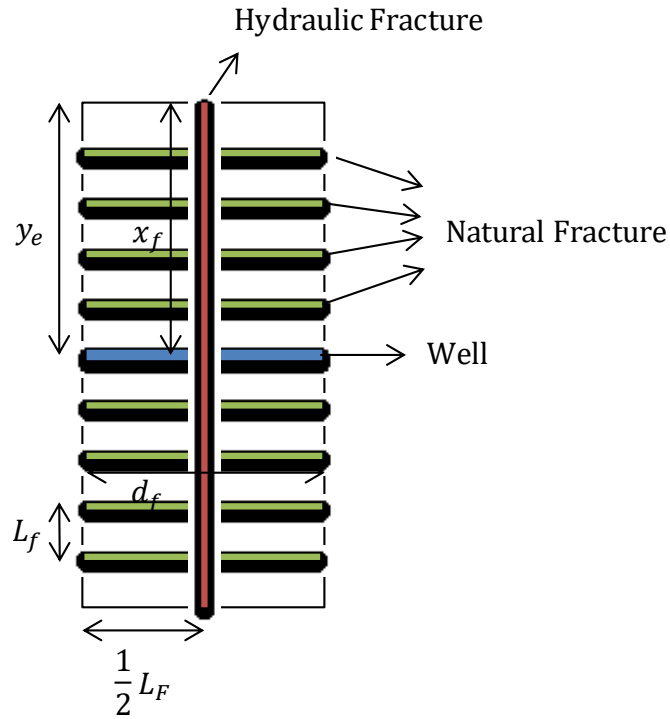


Figure 5.4 Schematic of the base case with eight natural fractures for the Bakken well

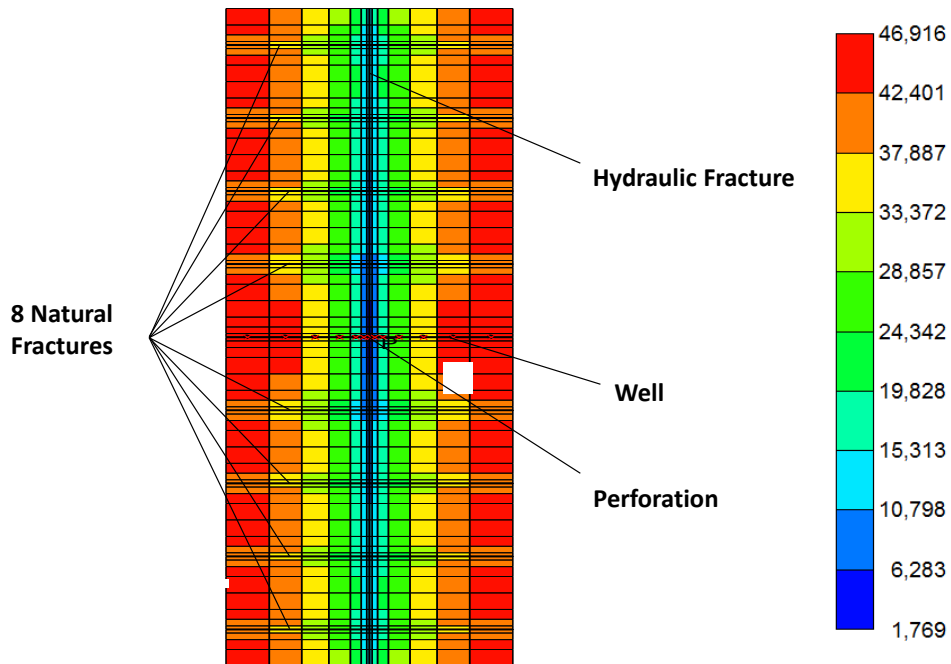


Figure 5.5 Pressure (in kPa) distribution for the base case (Bakken well) at the end of production history (4.5 years)

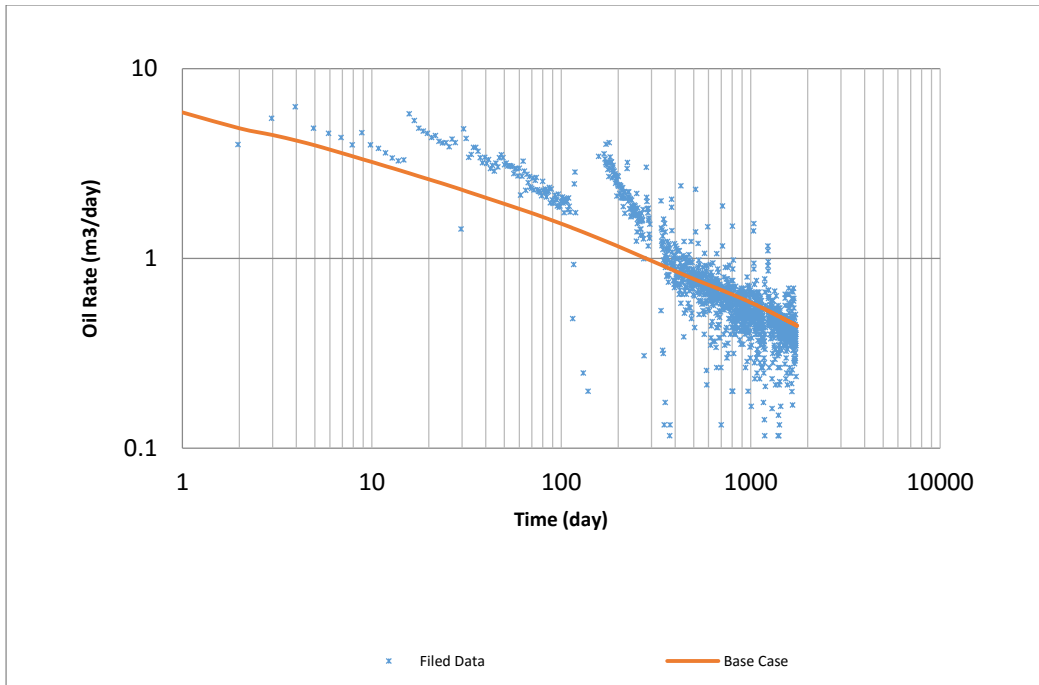


Figure 5.6 Log-log plot of daily oil rate as a function of time for the Bakken well

5.3 Non-Sequential Flow

In all analytical models, a series of 1-D sequential flows are assumed: fluid flows from matrix to natural fractures then from natural fractures to hydraulic fracture. Several simulation models are built to test this assumption for the Bakken well. All parameters are the same as described at beginning of this chapter; however, the i -direction permeability in matrix is reduced to nearly zero to simulate the sequential flow conditions. Therefore, pressure drop between natural fracture and matrix is uniform along the entire natural fracture. Fig 5.7 shows the pressure distribution for the sequential case at the end of production history after 4.5 years. The drainage area in matrix is reduced substantially, as compared with the base case shown in Fig 5.5, due to zero flux between matrix and hydraulic fracture.

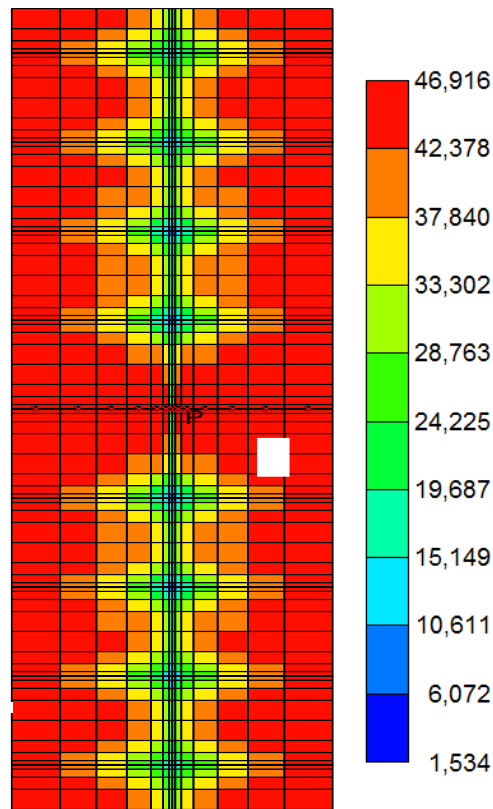


Figure 5.7 Pressure (in kPa) distribution for the sequential case (Bakken well) at the end of production history (4.5 years)

Fig 5.8 compares the oil rate versus time for the sequential case and the base case. It can be observed that the sequential model underestimates the oil rate as compared with the non-sequential model, especially at early time. This observation implies that history matching with sequential model, especially at early time. This observation implies that history matching with analytical models would overestimate n_f and x_f to compensate the ignorance of matrix-hydraulic fracture communication.

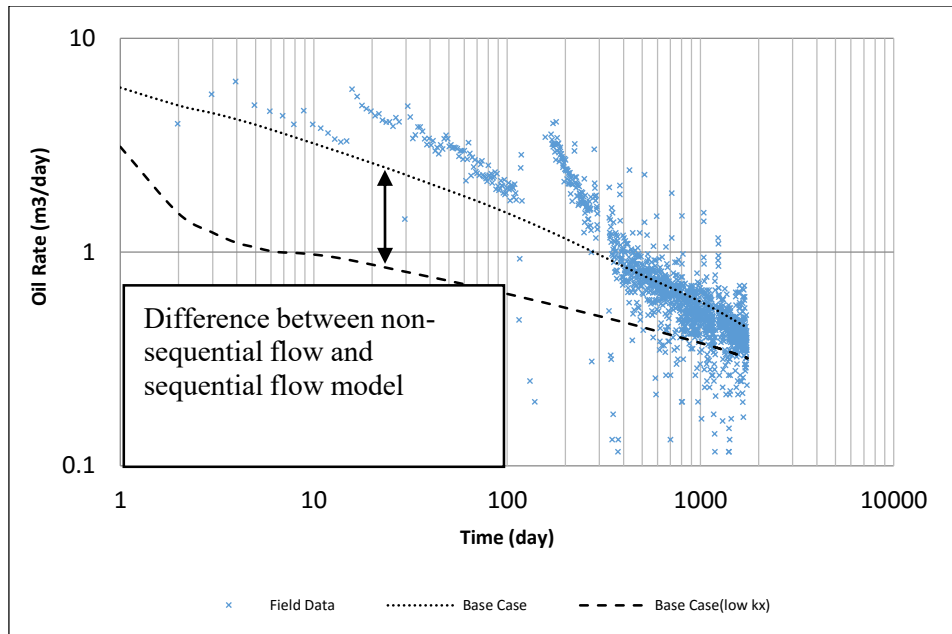


Figure 5.8 Log-log plot of daily oil rate as a function of time for the base case and the sequential case (Bakken well)

To verify this hypothesis, more natural fractures are added to this sequential-flow case; two additional models with 12 and 20 natural fractures are built. Fig 5.9 compares the daily oil rate versus time for the base case and all three sequential cases ($n_f = 8, 12$ and 20). As the number of natural fractures increases the response of sequential flow case converges to that of the simultaneous flow case (base case) with only 8 natural fractures. However, the difference between the three sequential flow models with different values of n_f is not obvious at early time scales. This is because during early time, flow from hydraulic fracture to well contributes

primarily to the production. Therefore, increasing the number of natural fractures does not have a significant influence on early time production. However, as production continues, drainage from natural fractures and matrix becomes important; increasing the number of natural fractures in the sequential model would enhance the contact area with the matrix and allow increased drainage from matrix to natural fractures. This would essentially compensate for the reduction in fluid transfer from the matrix to hydraulic fracture due to the near-zero permeability in i -direction.

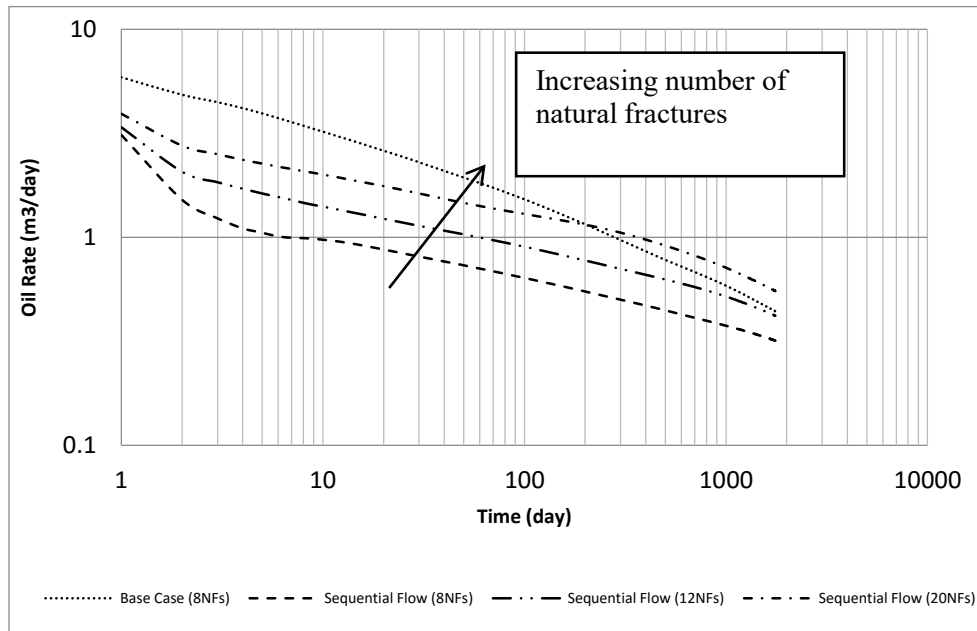


Figure 5.9 Log-log plot of daily oil rate as a function of time for the base case and all sequential cases (Bakken well)

Fig 5.10 shows the daily oil rate versus time for the non-sequential and sequential cases with certain number of natural fractures (e.g., $n_f = 8$ and 20). A transient flow in the hydraulic fracture system is observed at early time. This is followed immediately by a bilinear flow (1/4 slope) period in hydraulic fracture and natural fracture. Another short transient linear flow emerges, which is followed by a period of bilinear flow (1/4 slope) in matrix and natural fracture. This sequence of observable flow regimes is similar to the model #3 described by Al-Ahmadi (2011).

It is obvious that the difference between non-sequential and sequential with twenty natural fractures is much less than the difference between two cases with eight natural fractures. In other word, the difference between the two models diminishes as n_f increases. That means the impact of sequential flow assumption is less important when n_f increases. This result suggests that for forecasting gas or oil production production, especially at late time scales, sequential triple porosity models may work for situations when n_f is high enough. This observation also suggests that analytical solutions may lead to an overestimation of n_f or conductivity of the secondary fracture network.

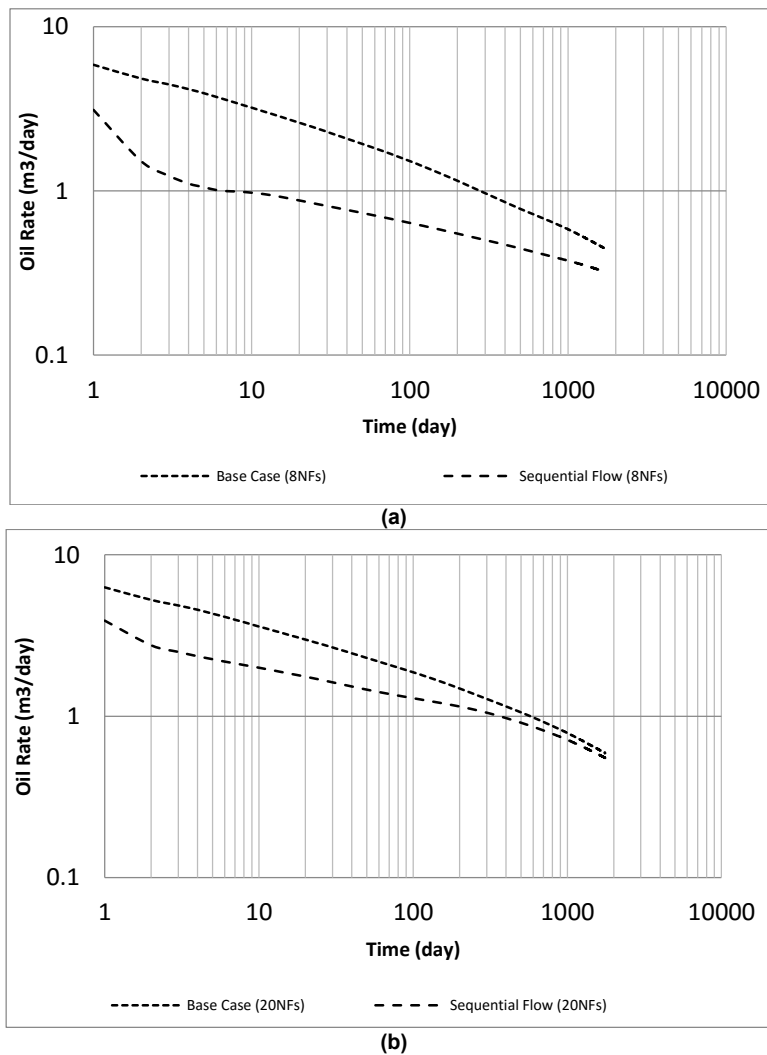


Figure 5.10 Log-log plot of daily oil rate as a function of time for non-sequential and sequential cases

(Bakken well): (a) – $n_f = 8$; (b) – $n_f = 20$.

5.4 Non-Symmetric Drainage

In most analytical models, the spacing between natural fractures and length of natural fractures are assumed to be uniform. Hence, for $n_f = 8$ in the history-matched base case, a value of natural fracture spacing (L_f) of 44.4 m should be considered as an average or mean estimate, while the length of each natural fracture is approximately 106 m (spacing between individual hydraulic fracturing stages).

Firstly, a series of models (Case A) for the Bakken well with varying spacing between the eight individual natural fractures are employed to investigate the impact of local heterogeneity of L_f on production prediction. Four different distributions of L_f are tested, and their values are summarized in Table 5.6. The degree of variability (heterogeneity) increases from Case A-1 through Case A-4.

Table 5.6 Spacing between natural fractures for the Bakken well in Case A

Case Number	Distribution of L_f	Unit
Case A-1	22.2 13.6 13.6 133 35.2 133 13.6 13.6 22.2	m
Case A-2	28.4 28.4 28.4 28.4 28.4 28.4 97.6 66 68	m
Case A-3	22.2 22.2 22.2 22.2 22.2 22.2 22.2 22.2 222.4	m
Case A-4	4 4 4 4 4 4 4 4 340	m

In Case A-1 (Fig 5.11a), four natural fractures are placed on each side of the horizontal well, with one being very close to the perforation point while the other three fractures are located much further away. The pressure map at the end of 4.5 years and the corresponding histogram of L_f for Case A-1 are shown in Fig 5.11a. Results for Case A-2, which consists of six evenly-

distributed natural fractures on one side and two more on the other side, are shown in Fig 5.11b. Fig 5.11c shows a case where all eight natural fractures are located on the same side of the horizontal well. Fig 5.11d illustrates an extreme scenario where all natural fractures are located on the same side of and far away from the well. It is clear that larger pressure drop, and thus more drainage, can be experienced in the areas close to the natural fractures.

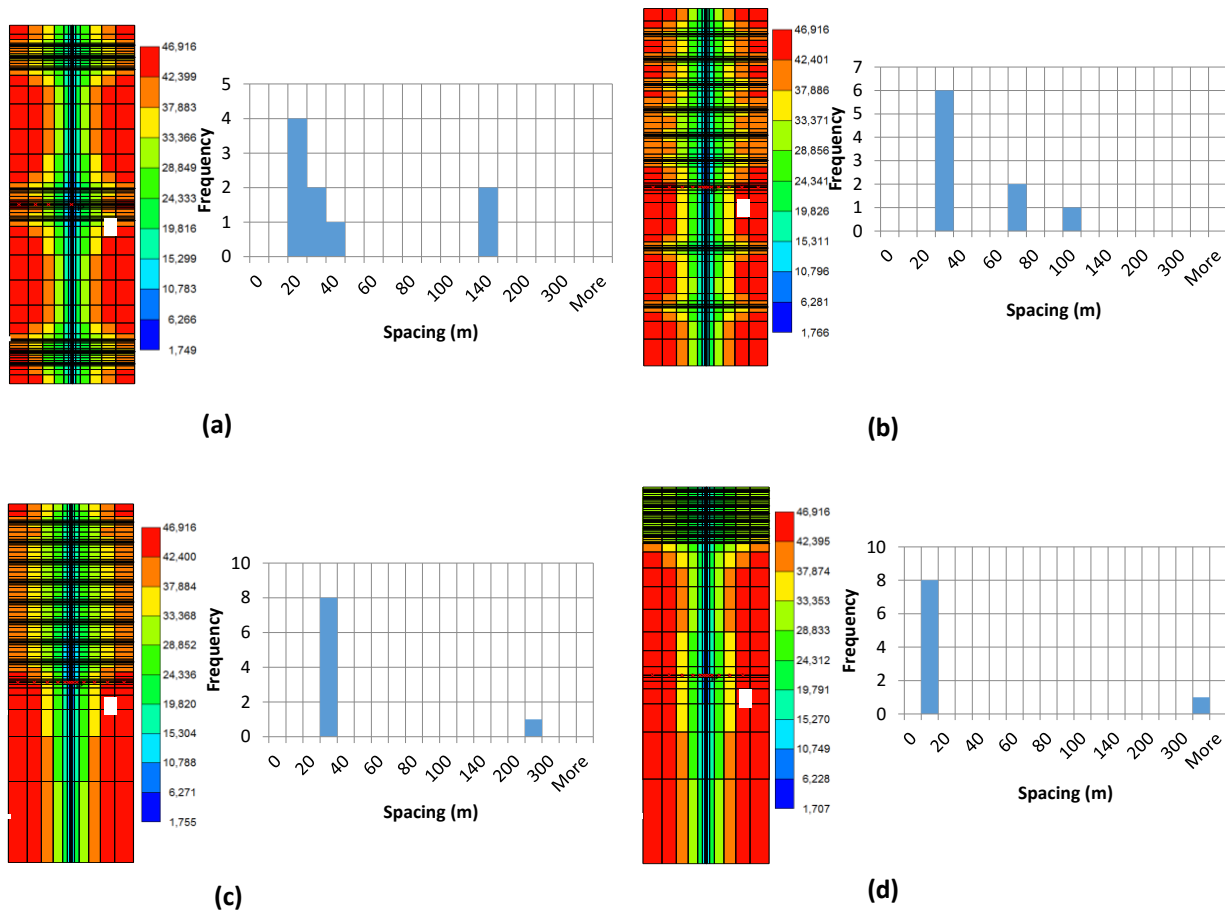


Figure 5.11 Pressure (in kPa) distribution of the Bakken well at 4.5 years and the histogram of L_f for
 (a) – Case A-1; (b) – Case A-2; (c) – Case A-3; (d) – Case A-4.

Fig 5.12 compares the match with production history for the four cases, and the differences between each case at early times shown in Fig 5.12a are not noticeable. However, when

comparing the production performance from 1000 days to 20 years illustrated in Fig 5.12b, the effect of natural fractures becomes dominating. It is obvious that the differences between these five profiles become more pronounced with time. It can be noted that oil rate for Case A-4 is much lower than that for other cases because pressure depletion and drainage is much less effective on the side of the horizontal well where the natural fractures are absent. The base case, on the other hand, gives the highest production rate at all times because natural fractures are evenly distributed, allowing more effective drainage across the entire domain.

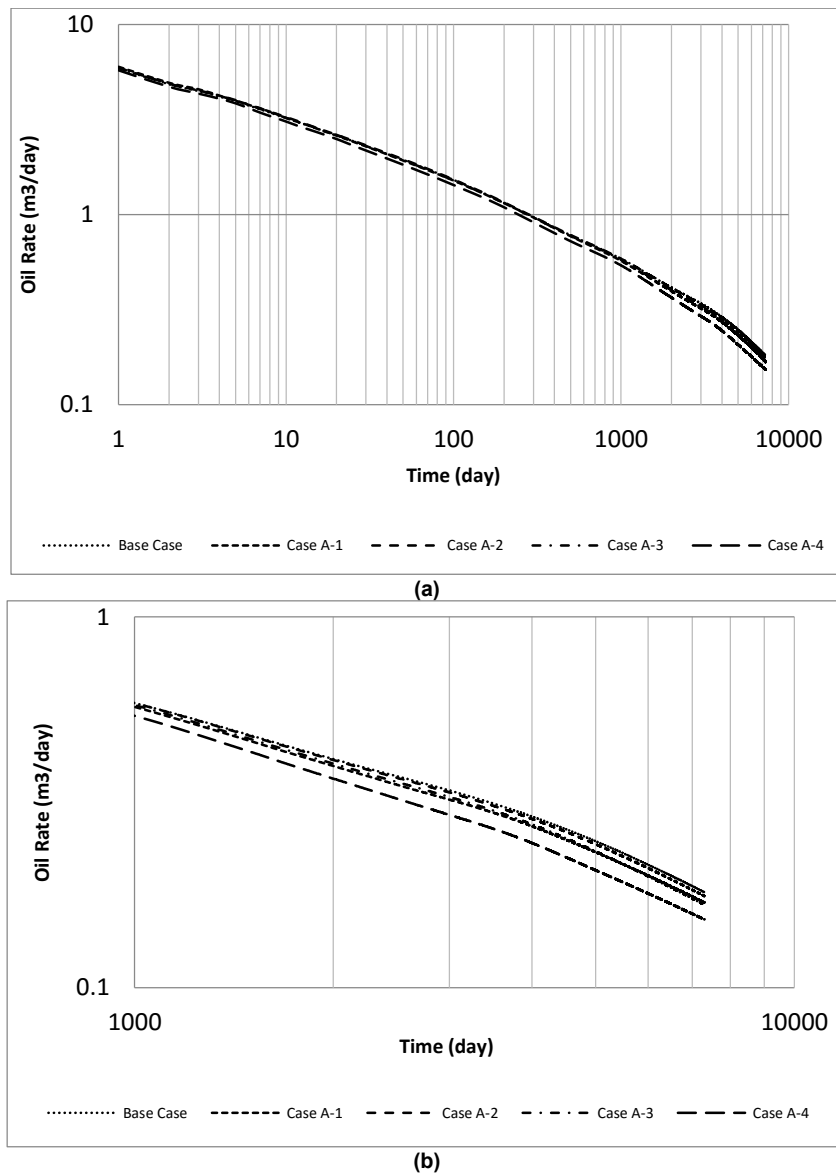


Figure 5.12 Log-log plot of daily oil rate as a function of time of the Bakken well for Case A

(a) – entire history for 20 years; (b) – late-time history after 1000 days.

Next, the four cases are repeated with matrix permeability increased by approximately 5 times (i.e., $k_m = 0.0026$ mD) to investigate the interplay between matrix permeability and heterogeneity in natural fracture spacing. Fig 5.13 shows the production history for these four new cases, and the differences among them are negligible.

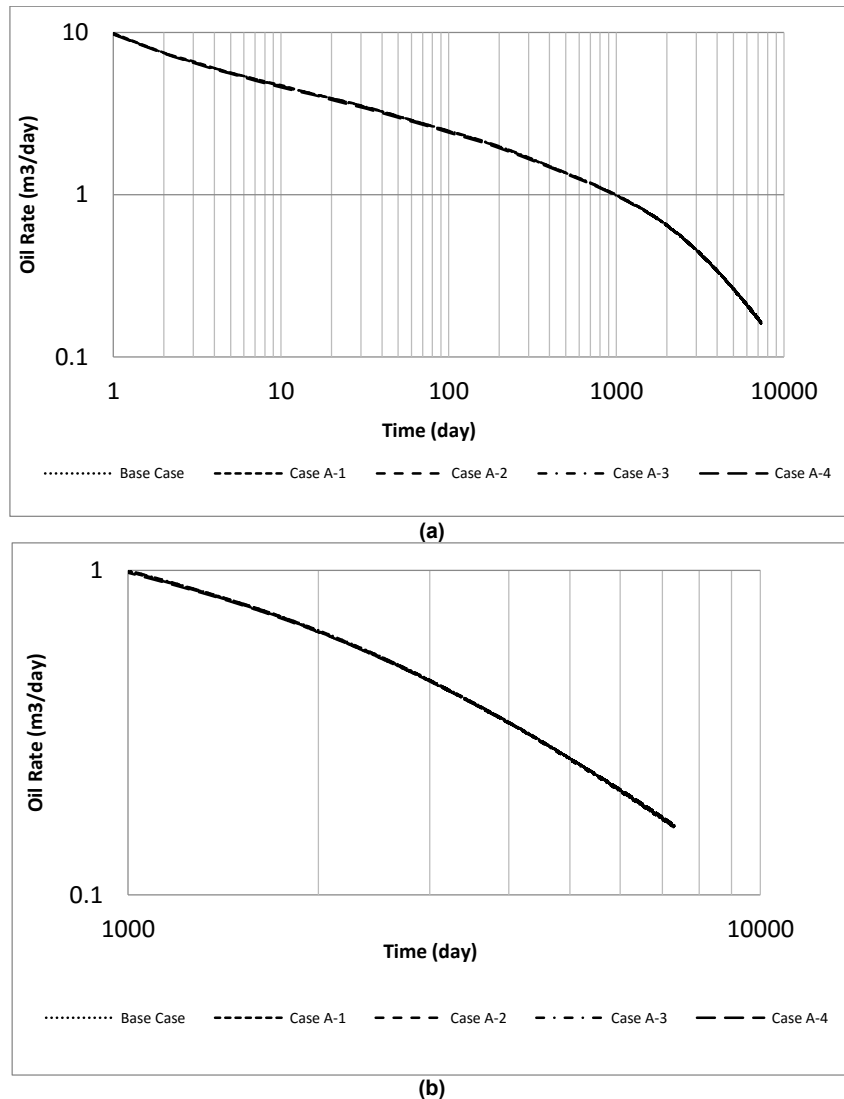


Figure 5.13 Log-log plot of daily oil rate as a function of time of the Bakken well for Case A with higher matrix permeability (0.0026mD)

(a) – entire history for 20 years; (b) – late-time history after 1000 days.

One possible explanation is that for this particularly high matrix permeability, specific locations of a fixed number of natural fractures do not have significant impacts. With high k_m , relatively uniform pressure depletion and oil drainage can be achieved readily, irrespective of the NF locations. In other words, the contribution of natural fractures is not essential. On the other hand, when k_m is low, drainage in regions with low *NF* density remains limited, significantly hampering the ensuing production. Overall, the comparative analysis suggests that the impact of natural fracture spatial distribution is more pronounced for low-permeability reservoirs.

As discussed before, most analytical models assume that all natural fractures are uniform in length. In the next set of models (case B), length of individual natural fractures is varied, allowing only a portion of the natural fractures to be fully connected. The case with natural fractures length being half the distance between two hydraulic fractures ($R_l=0.5$) is chosen as the base scenario here. R_l is defined as the ratio of natural fracture length d_f to hydraulic fracture spacing L_F . A series of models (Cases B-1 to B-3) are constructed where the length of individual natural fractures is sampled from different distributions with the same average (mean) value of 50 m. The idea is to ensure that average length of the eight natural fractures remains identical.

Three different distributions, as summarized in Table 5.7, are tested to investigate the effects of local heterogeneity in natural fracture length on production performance. All cases have the same average natural fracture length as in the new base case.

Table 5.7 Natural fracture length for the Bakken well in Case B

Case Number	New Base Case	Case B-1	Case B-2	Case B-3
Natural Fracture Length (m)	50	26 or 74	26 or 74	38, 74, 4, 62, 54, 18, 90, 60

Fig 5.14 shows a schematic of each model set-up including the new base case. In Case B-1, two sets of natural fractures with different lengths are placed alternatively. Case B-2 consists of four evenly-distributed short natural fractures on one side and four long ones on the other side. Case B-3 shows a case where eight natural fractures with different lengths are randomly placed along the bi-wings of the hydraulic fracture. The pressure distributions at the end of 4.5 years for all four cases are shown in Fig 5.15.

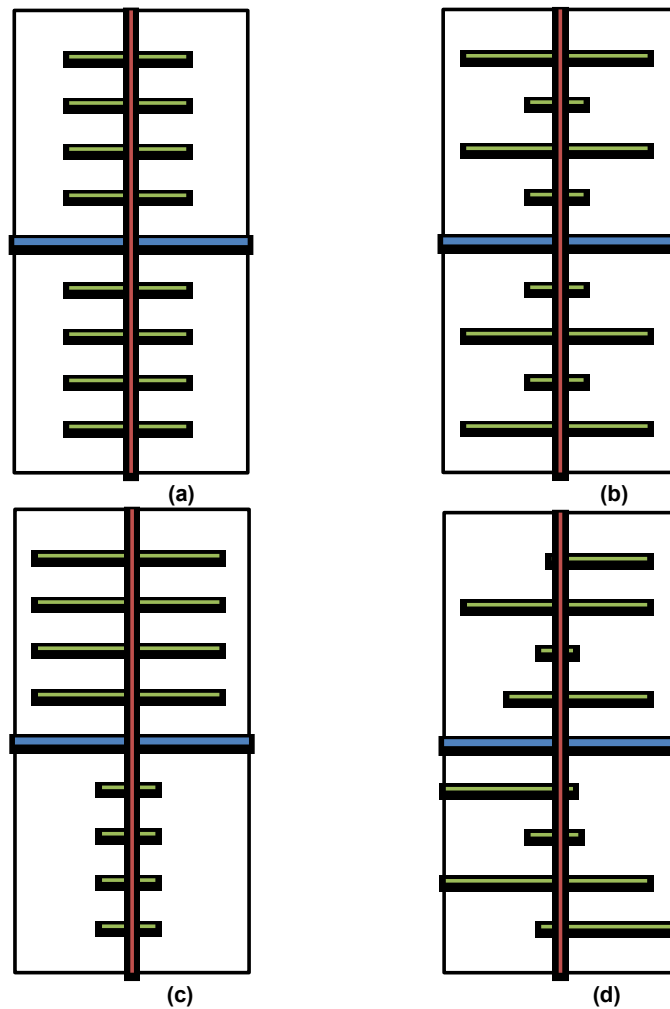
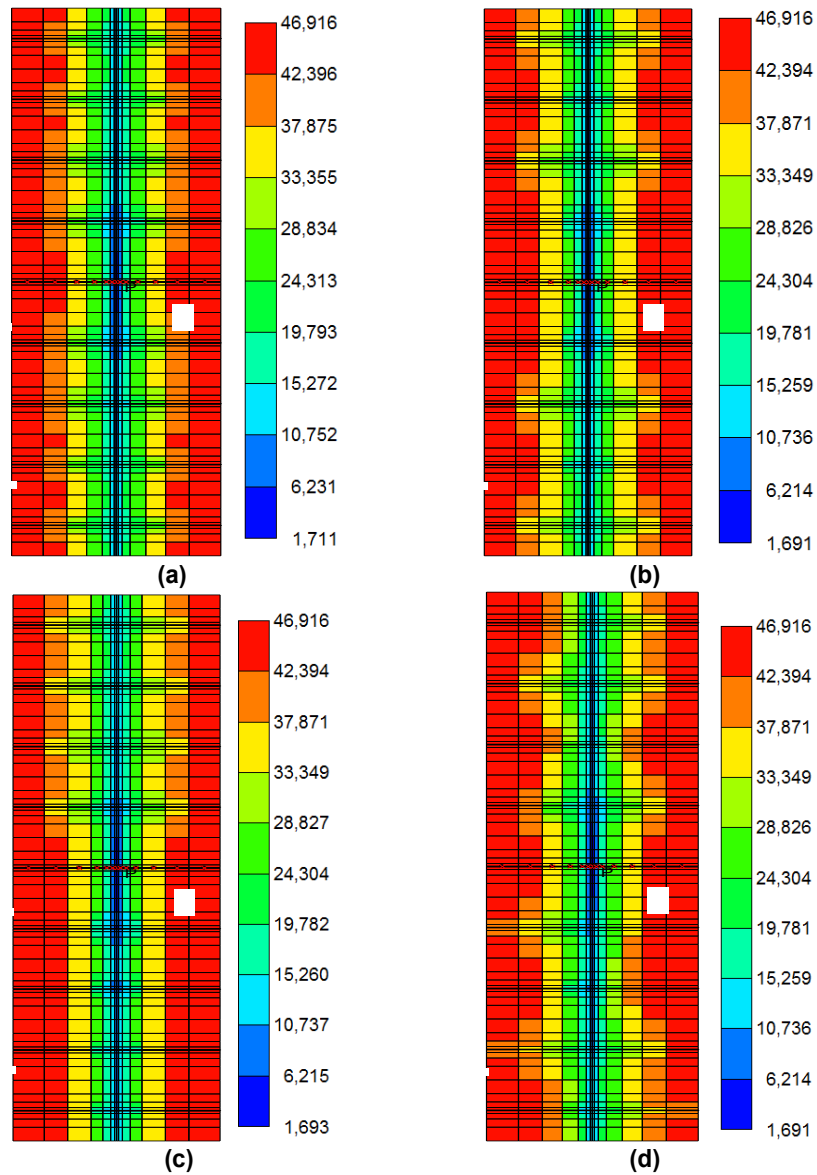


Figure 5.14 Schematic of non-symmetric drainage for the Bakken well

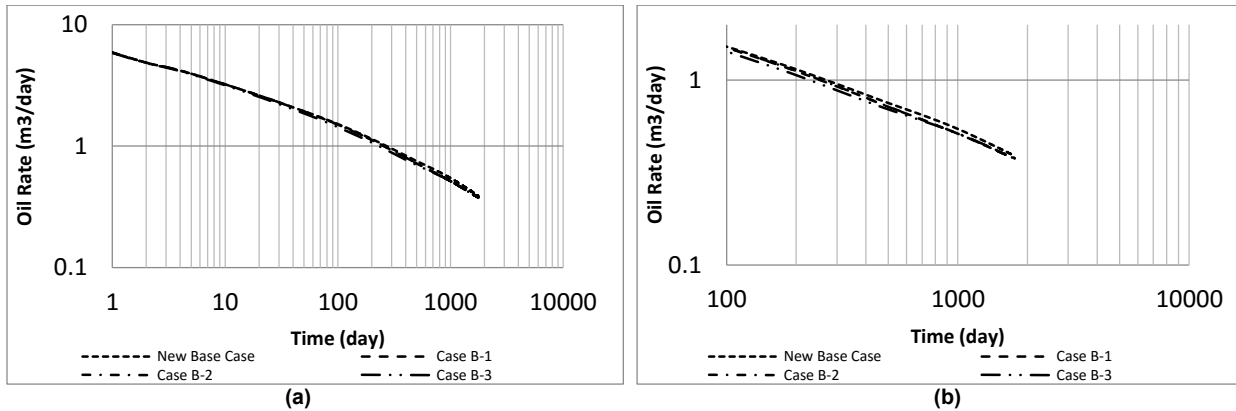
(a) – New Base Case; (b) Case B-1; (c) – Case B-2; (d) – Case B-3

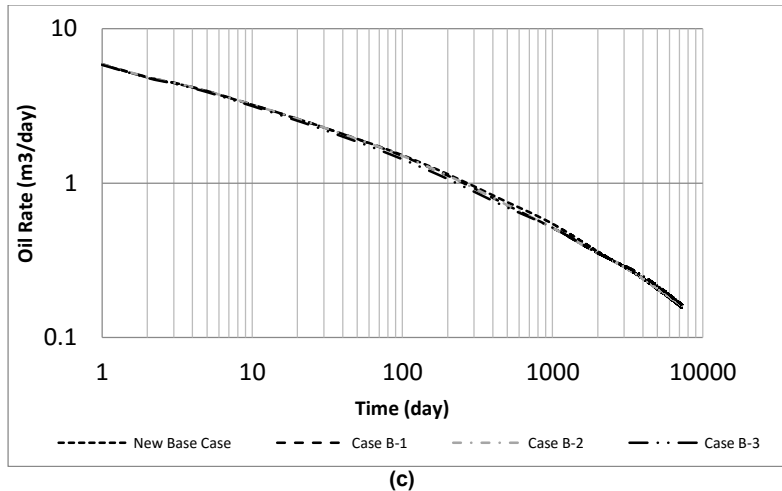


**Figure 5.15 Pressure (in kPa) distribution of the Bakken well after 4.5 years for
 (a) – New Base Case; (b) Case B-1; (c) – Case B-2; (d) – Case B-3**

Fig 5.16 compares the production performances of the three cases with that of new base case, and the differences at early times are not noticeable. Once again, at early times, flow contribution from natural fractures and matrix are not important. When comparing the production performance from 100 days to 4.5 years, the effects of natural fractures become more apparent. All three cases of B-1 to B-3 have the same average natural fracture length, and the resultant

total area available for flow between natural fracture and matrix would also be nearly identical. The minor observable difference would most likely due to the heterogeneous distribution of natural fracture lengths. It can be noted that oil rate for Case B-3 is slightly lower than those for other cases. That is because arrangement of natural fractures in Case B-3 does not allow even symmetric drainage from both sides of the hydraulic fracture. Pressure depletion and ensuing drainage are less effective on the side of the horizontal well with less contact area between natural fractures and matrix. The new base scenario gives the highest production rate because natural fractures are evenly distributed, allowing more effective drainage across the entire domain. All cases would converge again in long-term production (shown in Fig 5.16c) when transient flow in matrix begins. Similar to the observations in section 3.1, the results presented in this section would imply that the assumption of symmetric drainage in analytical solutions may lead to underestimation of fracture half-length and the associated *SRV*.





(c)
Figure 5.16 Log-log plot of daily oil rate as a function of time of the Bakken well for Case B

(a) – early-time history for 4.5 years; (b) – mid-time history between 100 to 10000 days; (c) – entire history for 20 years.

5.5 Heterogeneous Fracture Properties

The effect of fracture connectivity on rate transient response is studied next. Another assumption which plays an important role in analytical models is that natural fractures are fully connected between hydraulic fracture stages. That means for a fixed number of hydraulic fracturing stages with uniform spacing, the natural fractures are connected across all stages (i.e., $d_f = L_F$ in Fig.3). The ratio of natural fracture length d_f to hydraulic fracture spacing L_F is defined as R_l , which reflects the degree of natural fracture connectivity. As shown in Fig 5.17, if R_l equals to zero, the model is equivalent to a dual-porosity model. On the other hand, if R_l equals to one, the model has fully-connected natural fractures. Models with different values of R_l (0, 0.1, 0.3, 0.5, 0.7 and 1.0) are constructed by reducing the value of d_f , in order to study the relationship between natural fractures connectivity and rate transient response for the Bakken well.

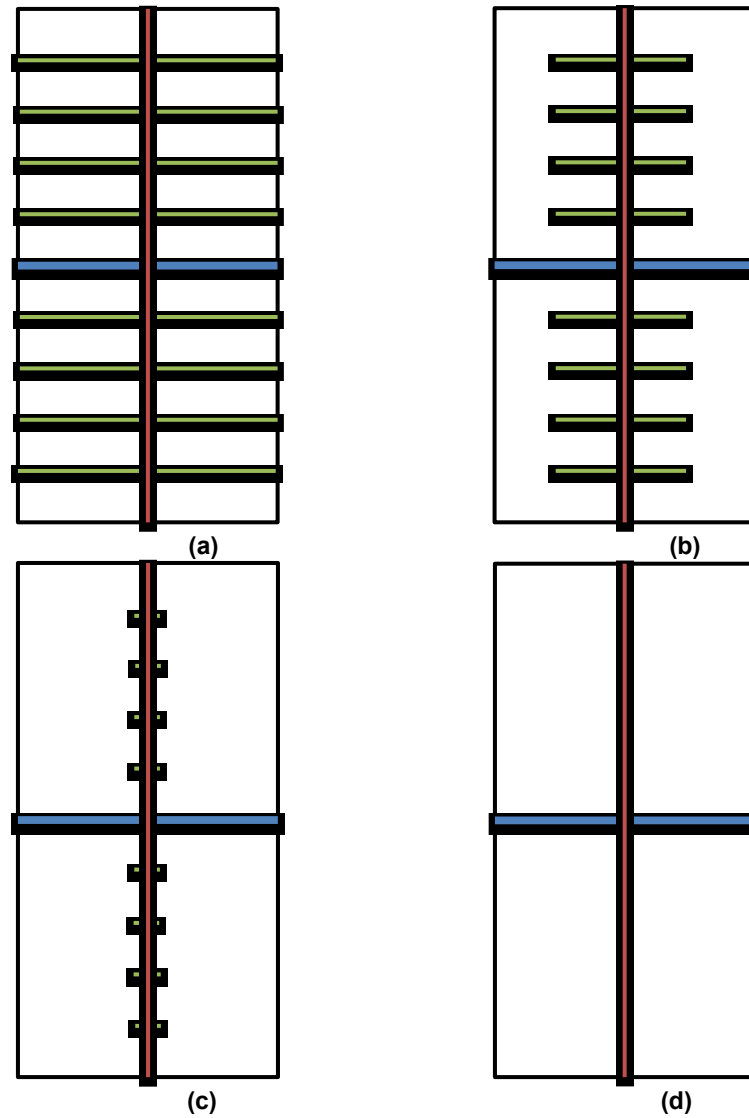


Figure 5.17 Schematic of fully-connected and non-connected natural fractures for the Bakken well

(a) – $R_l=1.0$; (b) – $R_l=0.5$; (c) – $R_l=0.25$; (d) – $R_l=0$

It is evident in Fig 5.18 that as the value of R_l increases, oil production would also increase, especially during later time when the drainage is dominated by linear flow in natural fractures and bilinear flow in matrix and natural fractures. This observation implies that the assumption of fully-connected natural fractures in the analytical model may underestimate n_f .

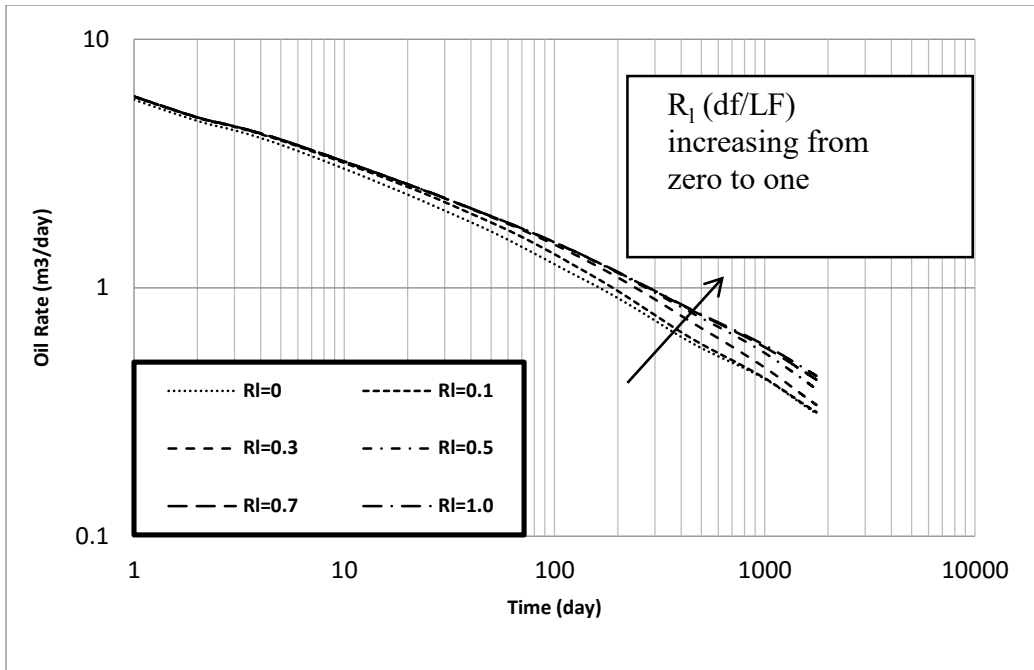


Figure 5.18 Log-log plot of daily oil rate as a function of time of the Bakken well for cases with varying natural fracture connectivity (4.5 years)

Another assumption of analytical models is that hydraulic fractures between two parallel horizontal wells are fully-connected. That means the distance between two parallel horizontal wells is the same as length of one hydraulic fracture (i.e., $2x_f = L_w$). The ratio of hydraulic fracture length $2x_f$ to distance between two parallel horizontal wells L_w is defined here as R_L . Several schematics with different values of R_L are shown in Fig 5.19. $R_L = 1$ represents a dual-porosity system, while $R_L = 0$ represents a single porosity system.

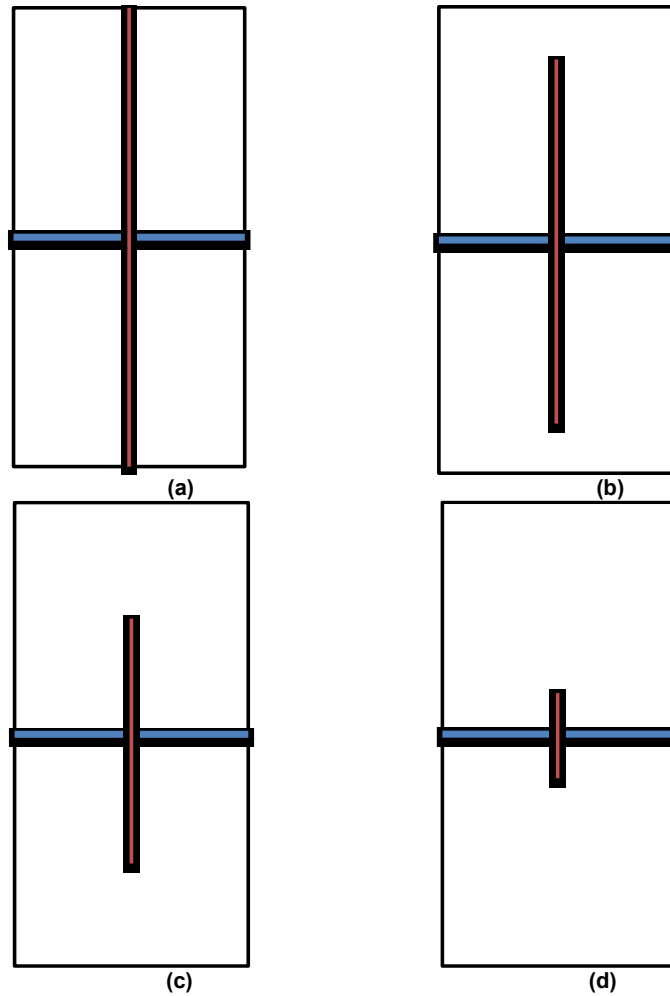


Figure 5.19 Schematic of fully-connected and non-connected hydraulic fractures for the Bakken well

(a) – $R_L=1.0$; (b) – $R_L=0.75$; (c) – $R_L=0.5$; (d) – $R_L=0.25$

Fig 5.20 shows that as the value of R_L increases, oil production would also increase. Interestingly, when hydraulic fracture length is very short ($R_L = 0.224$), the signatures and slopes of production plot are very different from dual-porosity ($R_L = 1.0$) plot. The slope is expected to change from a half slope to a quarter slope and finally to a half slope in a normal dual-porosity system (Fig 5.20). This sequence of slope change represents linear, bilinear and linear flow in fracture, matrix-fracture and matrix, respectively. However, when R_L equals to 0.224, we observe a change from unit slope to half slope. The occurrence of early unit-slope and the absence of

early half- and quarter-slope indicate that the transient flow in relatively small hydraulic fractures is masked by pseudo steady-state pressure depletion. In other words, the transient behavior has quickly reached the tip of short hydraulic fractures.

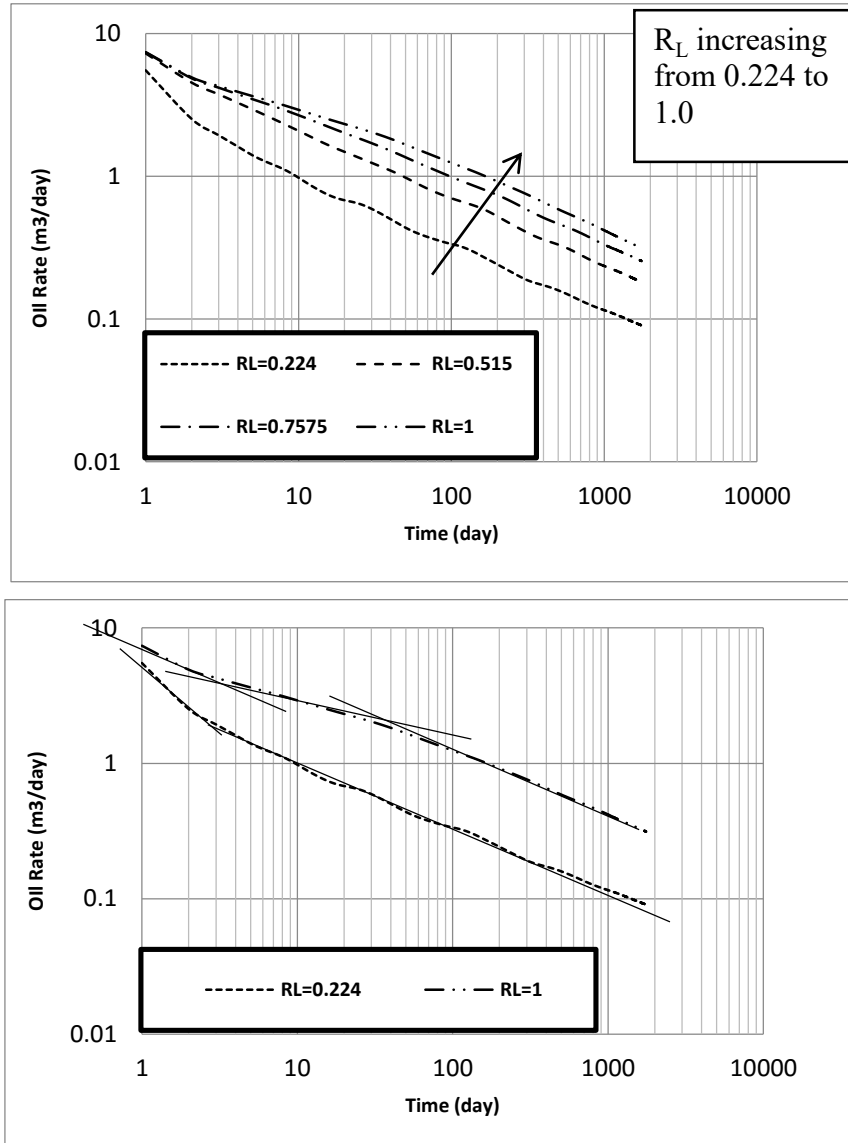


Figure 5.20 Log-log plot of daily oil rate as a function of time of the Bakken well for cases with varying hydraulic fracture connectivity (4.5years)

Furthermore, pressure map shown in Fig 5.21 indicates that there is pressure drop at the tips of hydraulic fractures. This observation could explain why signatures of rate-time plot for relatively

small R_L would be different from those with high R_L value. It also implies that the occurrence of early unit slope could be an indication of limited hydraulic fracture penetration. Similar to the effects of fully-connected natural fractures, the assumption of fully-connected hydraulic fracture may underestimate the distance between two horizontal wells, which could potentially impact future development design such as optimal well spacing.

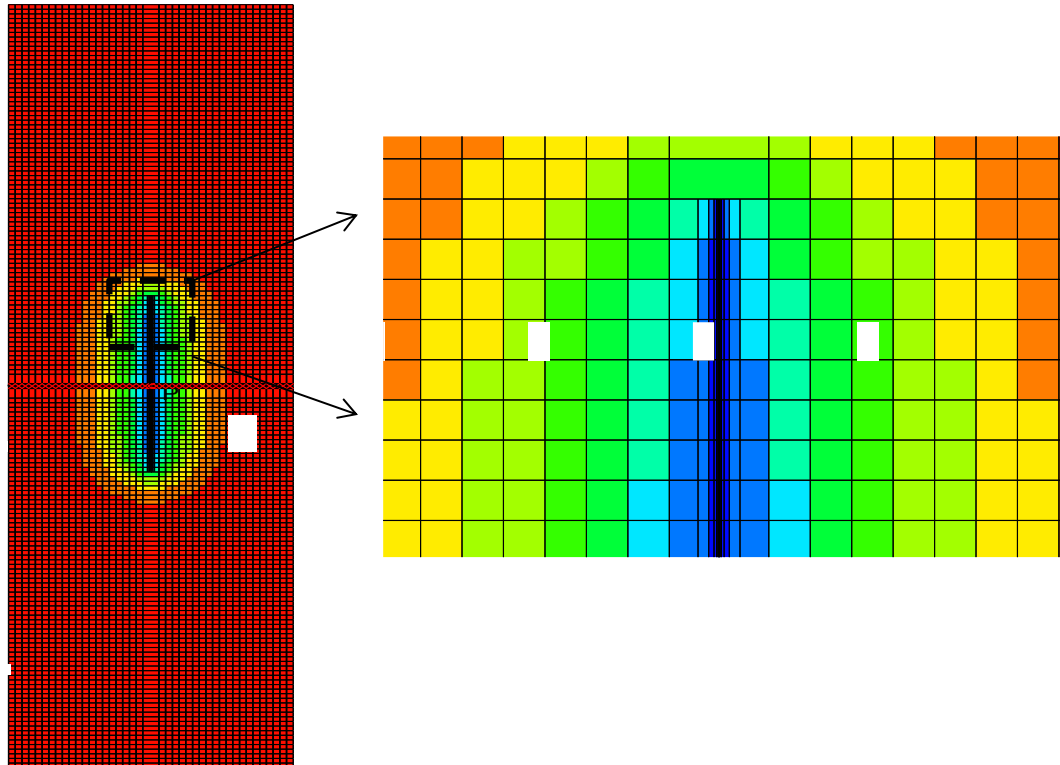


Figure 5.21 Pressure (in kPa) distribution of the Bakken well after 4.5 years when $R_L=0.224$

6 Influence of Multi-phase Effects on oil Production

6.1 *The Role of Gas Dissolution*

Gas dissolution and multiphase flow effects could potentially contribute to early decline in production, as often observed in many tight oil wells. However, these effects are typically ignored in most analytical models. To understand how solution gas may influence two-phase oil-gas flow, a model based on the Bakken well base case is considered. In order to provide a more detailed description of the matrix-fracture interface, of the model size has been reduced to $10.6\text{m} \times 20.5\text{m}$. The model is initialized with no free gas and zero water saturation. The relative permeability and capillary pressure relationships for matrix and fracture system are assigned according to the multiphase flow functions presented in Gdanski and Fulton (2009). Zero capillary pressure and linear relative permeability functions (stick curves with exponent = 1.0) are assigned in the fractures (Papatzacos and Skjæveland, 2002). The effects of gas adsorption are ignored in this work, since Wu *et al.* (2014) estimated the contribution of gas adsorption/desorption to the total gas production to be approximately 13%. Gas saturation profile in the hydraulic fracture is shown in Fig 6.1. The initial increase and decrease in gas saturation during the first few days may be attributed to the large disparity between initial reservoir pressure and bottom-hole pressure; pressure in the hydraulic fracture drops suddenly, and a significant amount of solution gas has evolved and is produced immediately.

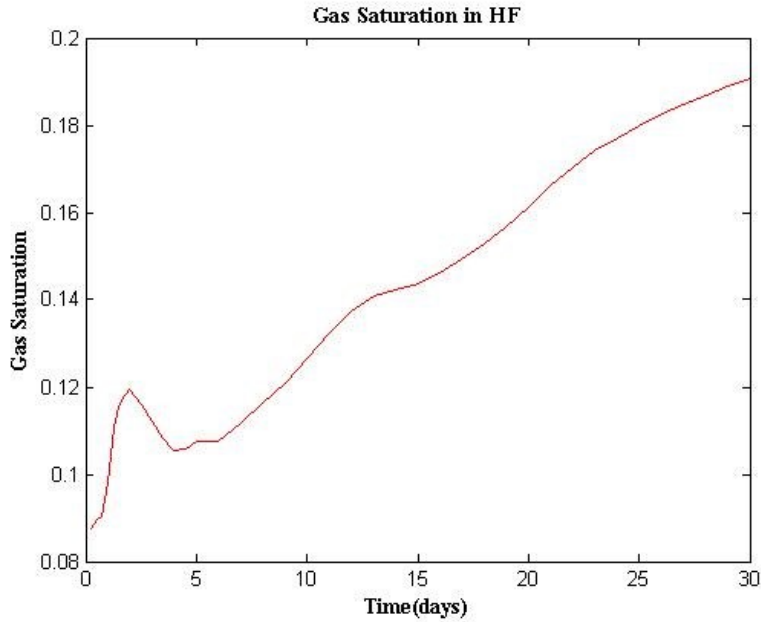


Figure 6.1 Average gas saturation in hydraulic fracture during the first 30 days for the Bakken well

Next, a set of triple-porosity model with two natural fractures placed evenly on each side of the horizontal well is constructed to assess the impacts of the amount of gas dissolution and multiphase flow functions on production performance. The relative permeability and capillary pressure functions in the natural fracture is assigned according to Iwai (1976) and Killough (1976). The amount of solution gas is varied with different bubble-point pressure (P_b). The bottom-hole flowing pressure, P_{wf} , is kept constant to ensure that variation in production is attributed to solution gas alone. The production profiles and input PVT data for $P_b = 10$ and 35 MPa are compared in Fig 6.2 and Fig 6.3. In order to compare the combined energy content obtained from the produced oil and gas, the total hydrocarbon rate based on the approximate energy released by burning one barrel of oil is computed (British Petroleum, 2011).

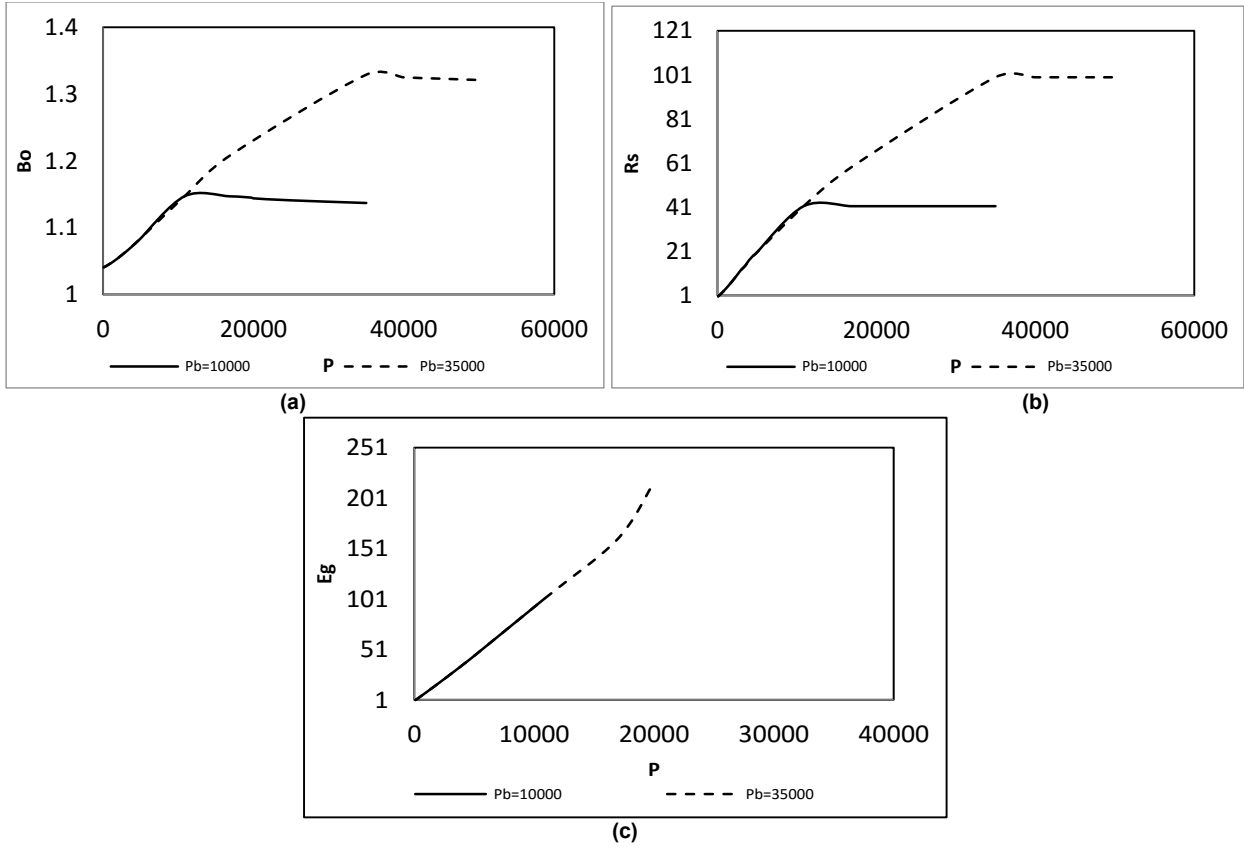
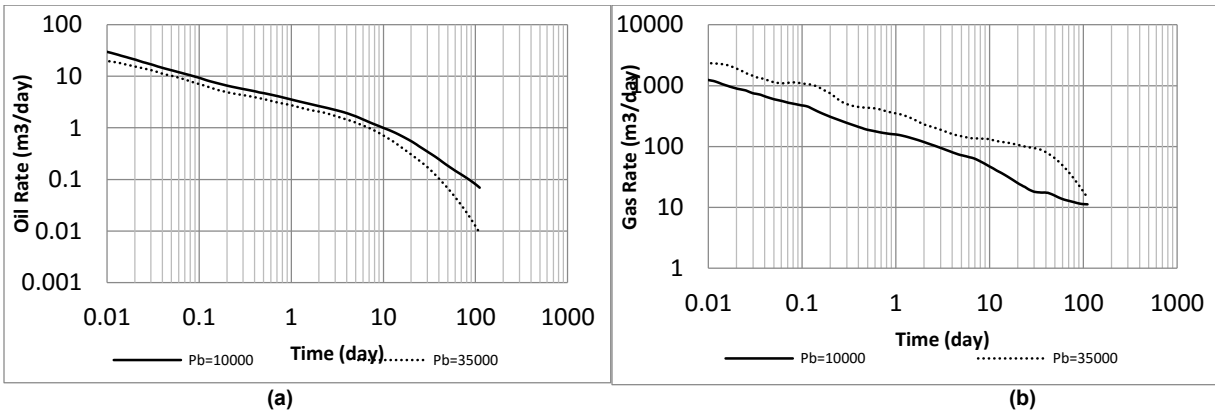


Figure 6.2 Input PVT data for the Bakken models with different bubble-point pressure
 (a) – oil formation volume factor; (b) – solution gas-oil ratio; (c) – gas expansion factor.



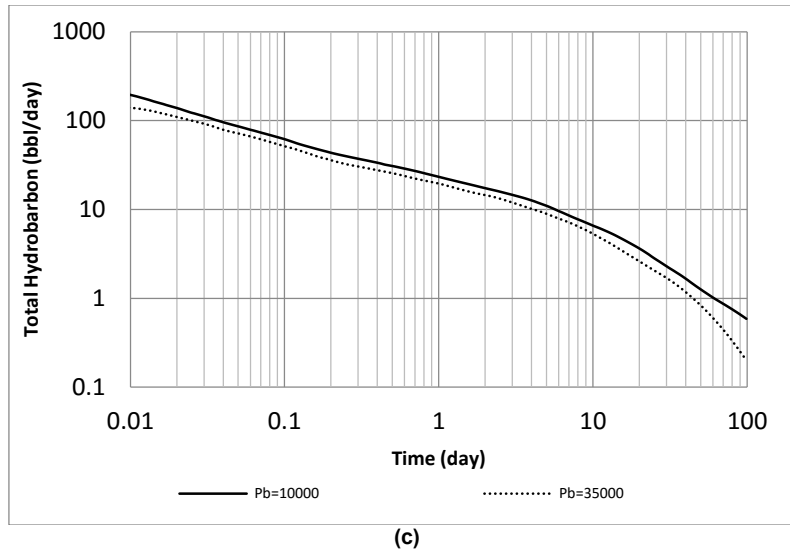


Figure 6.3 Log-log plots of production profiles for the Bakken models with different bubble-point pressure

As P_b increases, both the oil rate and total hydrocarbon rate are reduced, while gas rate is increased. This is because with the same initial pressure, higher P_b implies a larger pressure range over which free gas would exist. Given that the mobility for the gas phase is higher than that of the oil phase, oil production is reduced. Therefore, ignoring the presence of two phase oil-gas flow in analytical models could lead to an overestimation of fracture parameters such as effective fracture volume and fracture length.

The influences of relative permeability functions in the natural fracture are studied next. Fig 6.4 compares the production profiles for cases with different k_{rog} endpoint ranging from 0.1 to 1.0. As the value of k_{rog} endpoint decreases, lower oil production can be achieved. The reasoning for this decrease in production is two folds: decrease in hydraulic connection for the oil phase and shifting the intersection of oil and gas relative permeability curves towards the higher liquid saturation scale (i.e., there is a smaller saturation range over which the mobility of the oil phase is higher than the gas phase).

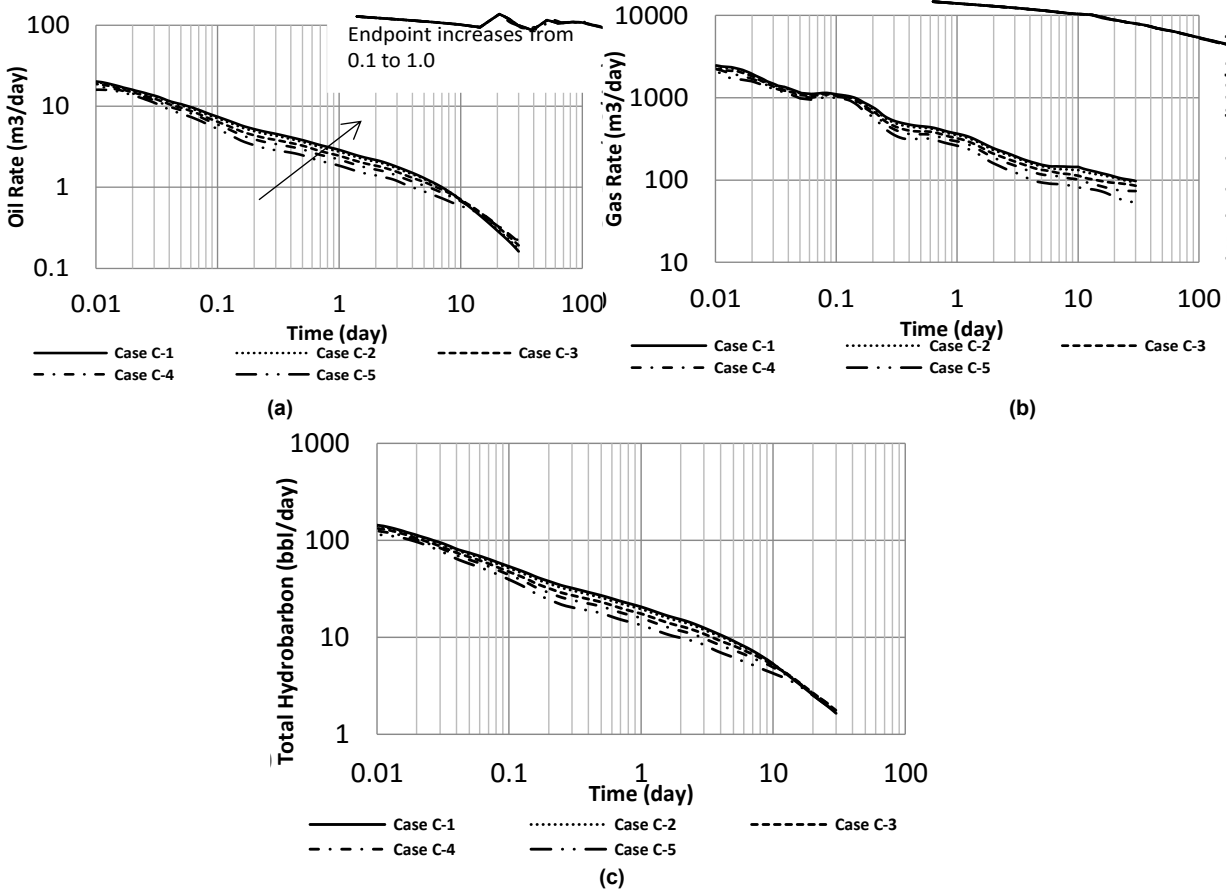


Figure 6.4 Log-log plots of production profiles for the Bakken models with different relative permeability endpoints

Fig 6.5 compares the production profiles for cases with different gas relative permeability exponent, a_1 , ranging from 1.0 to 3.0. Slightly lower oil and hydrocarbon production rates are observed for the case with higher values of a_1 , especially at late time. It has already been highlighted that ignoring the presence of two phase oil-gas flow could lead to an underestimation of fracture parameters such as effective fracture volume and fracture length; the conclusions derived from Figs 6.4-6.5 would imply that this underestimation would be more severe, if k_{rog} is low and/or gas relative permeability exponent (a_1) is high.

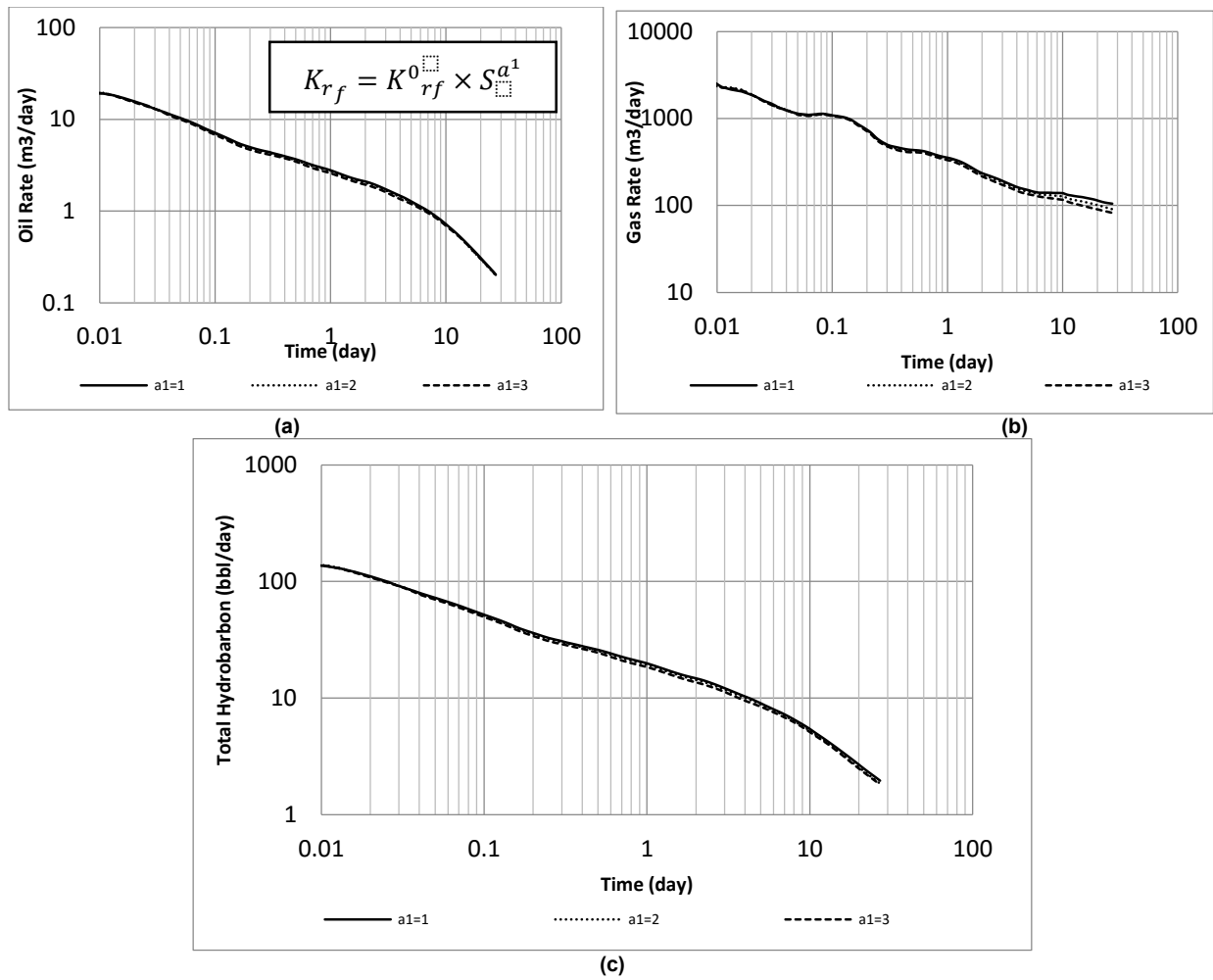


Figure 6.5 Log-log plots of production profiles for the Bakken models with different relative permeability curvatures

6.2 The Role of Capillary Discontinuity

Unlike most experiments and analytical models that use coreflood to present capillary discontinuity, we have models under reservoir conditions with a high capillary pressure difference between fractures and matrix. Since hydraulic fracture has high conductivity, its corresponding capillary pressure is significantly lower than that in the rock matrix (Aguilera, 1980). Therefore, zero capillary pressure and linear relative permeability functions are assigned in the fractures (Papatzacos and Skjæveland, 2002). This zero capillary pressure in the hydraulic fracture is to imitate the zero capillary pressure boundary condition in core-flooding experiments. A section of the reservoir between two hydraulic fractures showing in Fig 4.1 is modeled.

We use a typical correlation, Corey correlation, to represent relative permeability in the matrix (Brooks and Corey, 1964).

Correlations of oil relative permeability can be defined as below:

$$k_{row}(S_w) = k_{row}^o (1 - S_{wn})^{C_o} \quad (5)$$

Where S_{wn} is defined as a normalized water saturation value:

$$S_{wn} = S_{wn}(S_w) = \frac{S_w - S_{wi}}{1 - S_{wi} - S_{orw}} \quad (6)$$

Where S_{wi} is irreducible water saturation; S_{orw} is residual oil saturation.

C_o is empirical parameters obtained from measured data or history matching; k_{row}^o is called the end point of oil relative permeability.

Capillary pressure in matrix is assigned according to the correlation in Eq. (7) (Gdanski et al., 2009).

$$P_c = \frac{\sigma'}{a_2 (S_w)^{a_1}} \left(\frac{\phi}{k} \right)^{a_3} \times 6.89476 \quad (7)$$

σ' is the interfacial tension of water and oil (30 dynes/cm). For the matrix, a measure of pore structure a_3 equals to 0.5 (Bradley, 1992). To represent low-permeability reservoirs, a_1 and a_2 equal to 1.86 and 6.42 respectively (Holditch, 1979).

Dual-porosity and triple-porosity models with one hydraulic fracture in the middle and perpendicular to the horizontal wellbore were built. By using these models, influences of fracture face-effect on production profile in fractured reservoir can be investigated. We use logarithmic grid size distribution near fracture to capture flow behavior by using saturation profile. In this part, a dual-porosity model called base case B is built. Since the irreducible water saturation is 0.2, the initial water saturation is to 0.5 to model mobile water and no free gas at initial conditions. To ensure that only two flowing phases exist and that there is zero gas production, the bubble-point pressure is set at 15000 kPa, in comparison with initial reservoir pressure of 48630 kPa. Fig 6.6 shows the simulated saturation versus distance to the fracture-matrix interface for a dual-porosity model at different times.

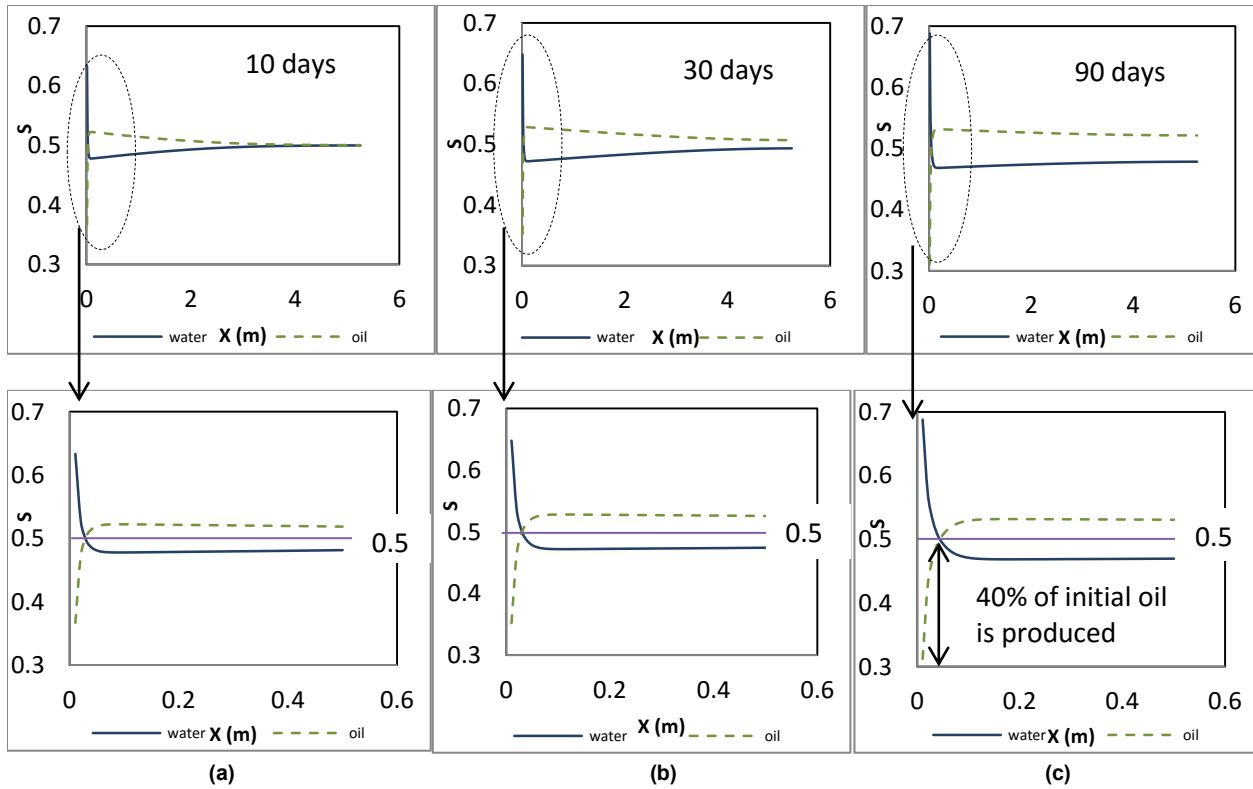


Figure 6.6 Oil and water saturation profiles in matrix as a function of distance from the fracture-matrix interface for the dual-porosity model at:

(a)- 10 days; (b)- 30 days; (c)- 90 days

The interface between fracture and matrix is located at $x = 0$. Oil saturation in matrix increases from its initial value due to oil expansion with pressure decline. Highest water saturation is observed at the interface, and as production continues, this highest value increases from its initial value (0.5) as a result of enlarged water blockage at the interface. This water blockage is a distinctive characteristic of fracture-face effect and may have influences on production.

Water imbibition due to capillary pressure during extended shut-in can lead to the transfer of oil from matrix into fracture (Cheng, 2012). In this part, we try to investigate the relationship between capillary pressure functions and fracture-face effect under reservoir conditions. We are

investigating the effect of matrix capillary pressure by running three dual-porosity models with different capillary pressure functions as shown in Fig 6.7.

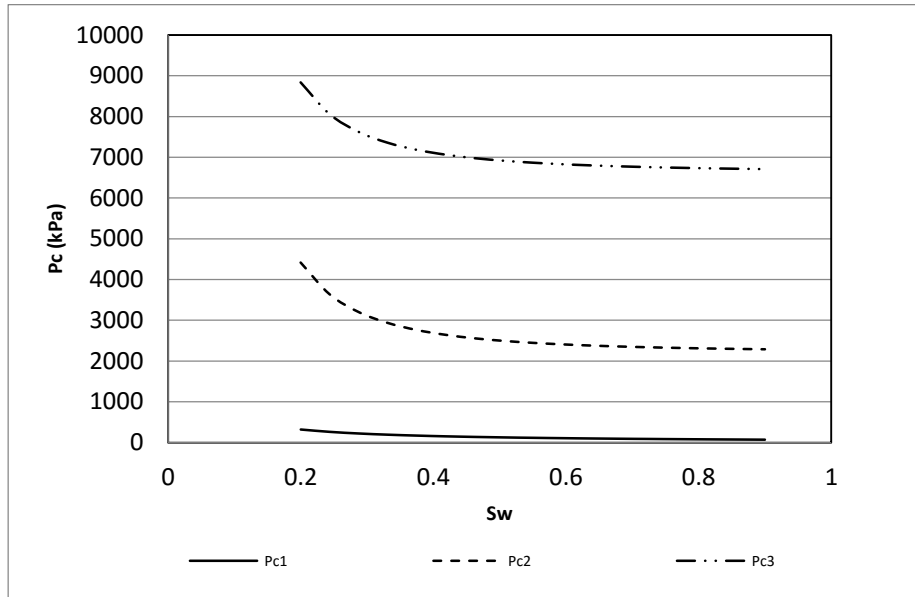


Figure 6.7 Different capillary pressure curve for matrix

We use three different capillary pressures curves to investigate the effects of fracture-face effect at fracture-matrix interface. Here, we hypothesize that with higher P_c of matrix, capillary end-effect becomes more pronounced and oil production rate drop. Higher P_c of matrix may cause larger water blockage near the interface of matrix and fracture, and therefore, oil flow from matrix to fracture can be hindered.

Fig 6.8 shows oil saturation in matrix close to frac-matrix interface (0.01025 m) in models with different capillary pressure in the first day. It is shown in Fig 6.8 that after 1 hour of production, oil saturation in matrix close to frac-matrix interface decreases. It is observed in Fig 6.8 that oil saturation drop is sharper for the case with higher capillary pressure. And low oil saturation at the interface (which means high water saturation) leads to water blockage around fracture-matrix interface.

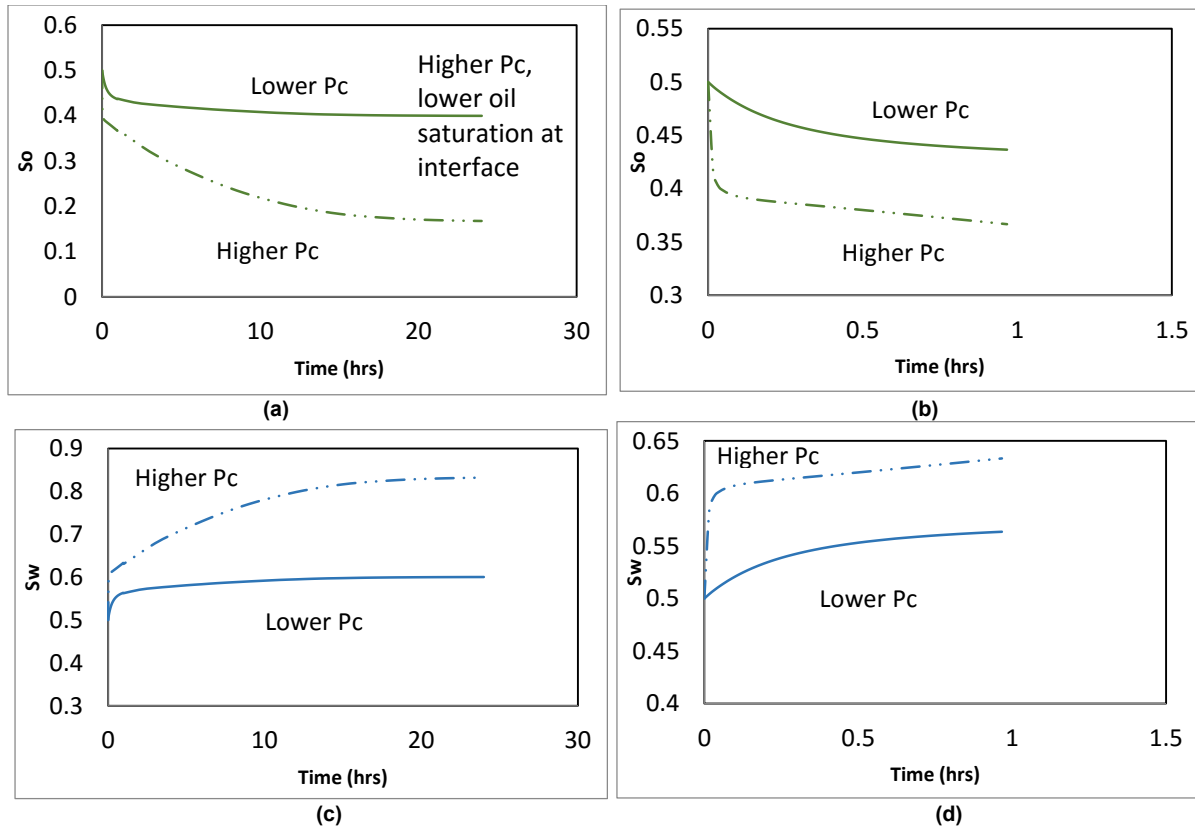


Figure 6.8 Oil and water saturation profiles in matrix as a function of time for the dual-porosity model with different capillary pressure:

- (a)- oil saturation in 1 day; (b)- oil saturation in 0.04 day**
(c)- water saturation in 1 day; (b)-water saturation in 0.04 day

Saturation comparisons of models with different capillary pressure in matrix at 30 days are plotted in Fig 6.9. Both oil saturation and water saturation versus distance to frac-matrix interface are shown. It can be seen that higher capillary pressure in matrix causes higher water saturation at interface. This higher water saturation leads to water blockage around the interface.

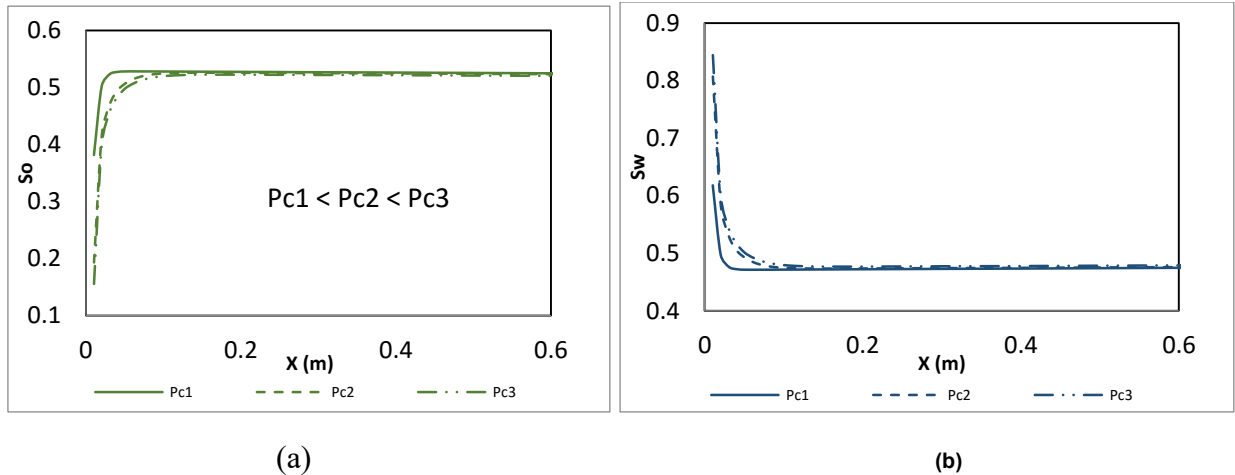
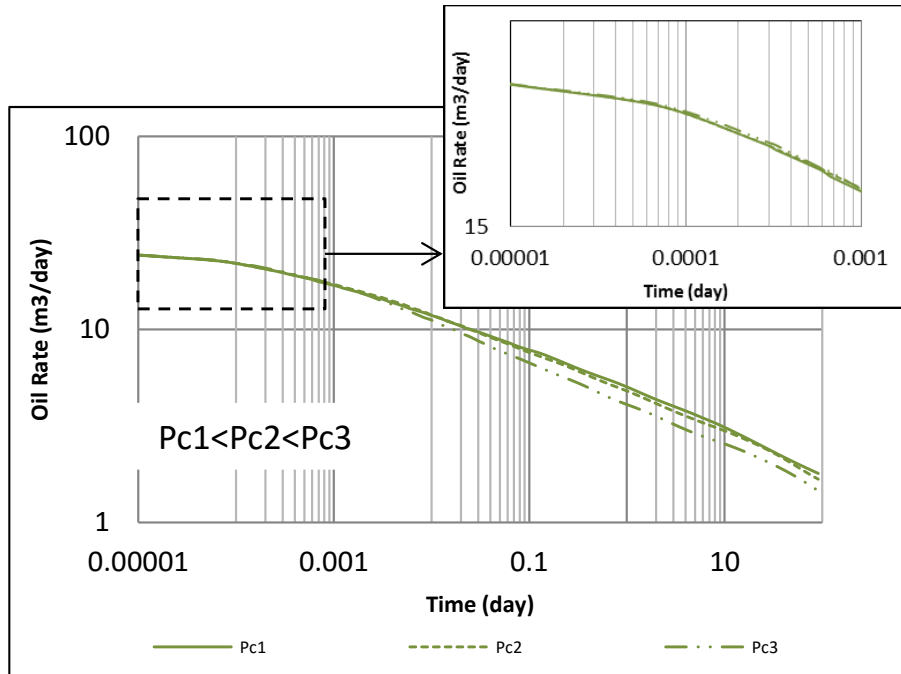


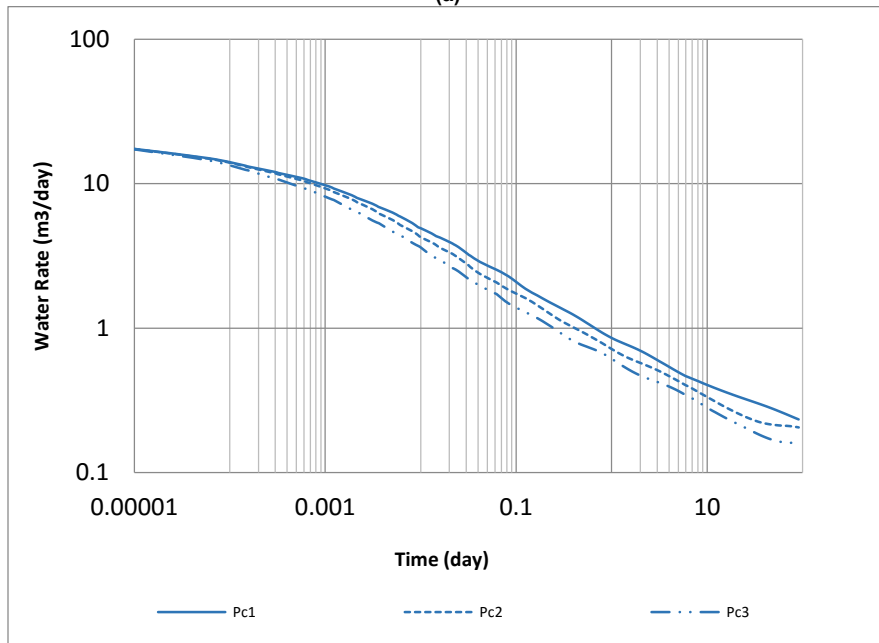
Figure 6.9 Oil and water saturation profiles in saturation in matrix as a function of distance from the fracture-matrix interface for the dual-porosity models with different capillary pressure at 30 days:

(a)-oil saturation in 0.6 m; (b)-water saturation in 0.6 m

Fig 6.10 shows production comparison of models with various capillary pressure in matrix. Fig 6.10 (a) and Fig 6.10 (b) are oil rate and water rate during the whole production process. Both oil rate and water rate decrease with increasing of capillary pressure in matrix after one day. As we mentioned above, higher capillary pressure brings more water blockage around frac-matrix interface and this water blockage prevents both oil and water in matrix from going into fracture. An interesting thing to note is that in production profile shown Fig 6.10, oil rate increases as capillary pressure increases while water rate has a sharp drop in the first day.



(a)



(b)

Figure 6.10 Log-log plot of daily rate versus time for the dual-porosity models with different capillary pressure in matrix during 91 days:

(a)-oil rate from very beginning; (b)- water rate from very beginning

Both oil rate and water rate decrease with increasing of capillary pressure in matrix after one day.

As we mentioned above, higher capillary pressure brings more water blockage around frac-

matrix interface and this water blockage prevents both oil and water in matrix from going into fracture. An interesting thing to note is that in production profile shown in Fig 6.10 (a) and Fig 6.10 (b), oil rate increases as capillary pressure increases in the first day. This increasing of oil rate can be explained by Fig 6.11. Fig 6.11 shows average oil saturation in fracture by using time scale.

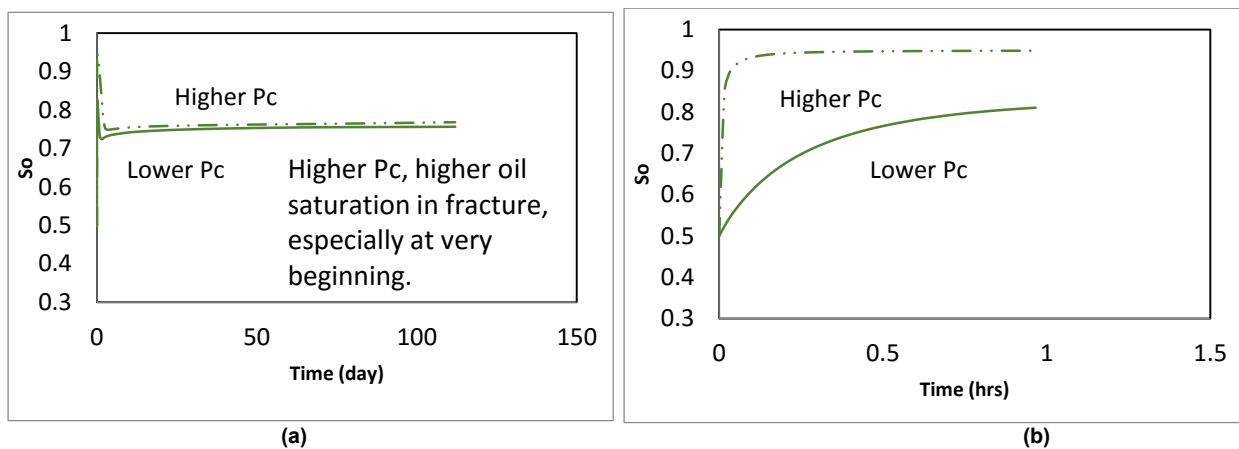


Figure 6.11 Average oil saturation in fracture in models in as a function of time for the dual-porosity model different capillary pressure:

(a)- in 112 days; (b)- at 1 hour

We observe in Fig 6.11 that oil saturation in fracture is higher for the model with higher capillary pressure in matrix, after 1 hour of production. With higher capillary pressure in matrix, it is harder for both oil and water in matrix to flow into fracture. In the beginning, with higher Pc, the difference of oil phase pressure between in the nearby matrix and the fracture is higher, leading to higher oil drainage in the matrix. Therefore, higher oil rate and lower water rate can be achieved. As production continues, fracture-face effect becomes more important, and water blockage is slowing down both oil and water flows.

Fig 6.12 compares cumulative oil of models with various capillary pressure models in matrix. It is easy to see that although capillary pressure changed, cumulative oil production does not change much. In Wang and Leung's (2015) paper, quite similar results are observed in soaking models.

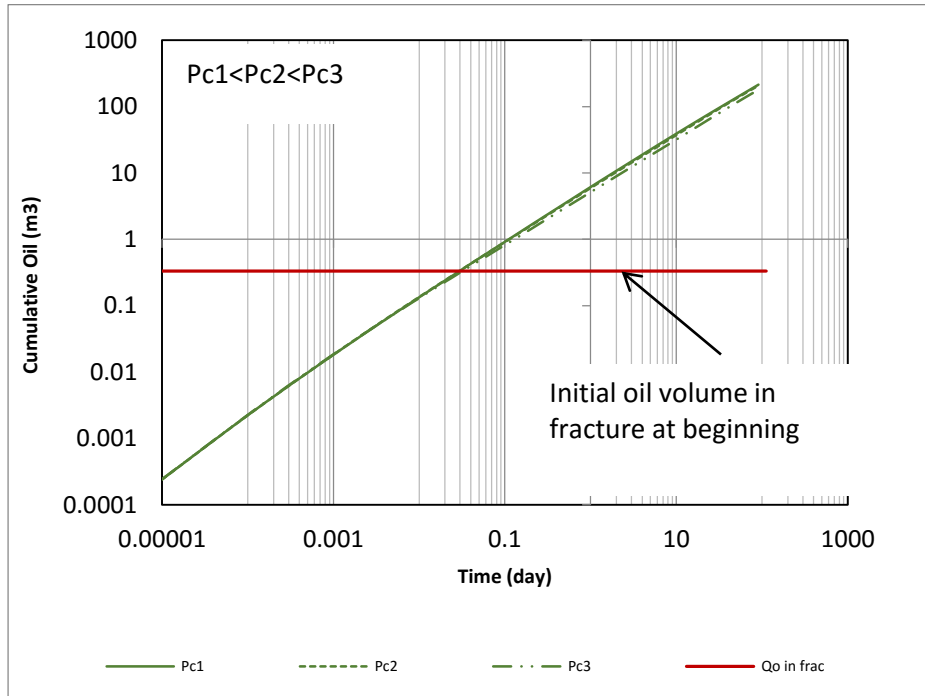


Figure 6.12 Log-log plot of cumulative oil versus time for the dual-porosity models with different capillary pressure in matrix during 91 days

The bold horizontal line represents initial oil volume in fracture at initial conditions. Based on Fig 6.12 and Fig 6.10 (a), we hypothesize that most of produced oil comes from fracture at beginning (less than 3 hrs). However, cumulative oil in 3 hours is beyond initial oil volume in fracture. This is because some oil in matrix goes into fracture due to the draw down at early times.

Another set of models with different initial water saturation in matrix are constructed to investigate influences of initial water saturation on production under different capillary pressure. Results of oil rate with different capillary pressure in models with three different initial water saturation levels are shown in Fig 6.13.

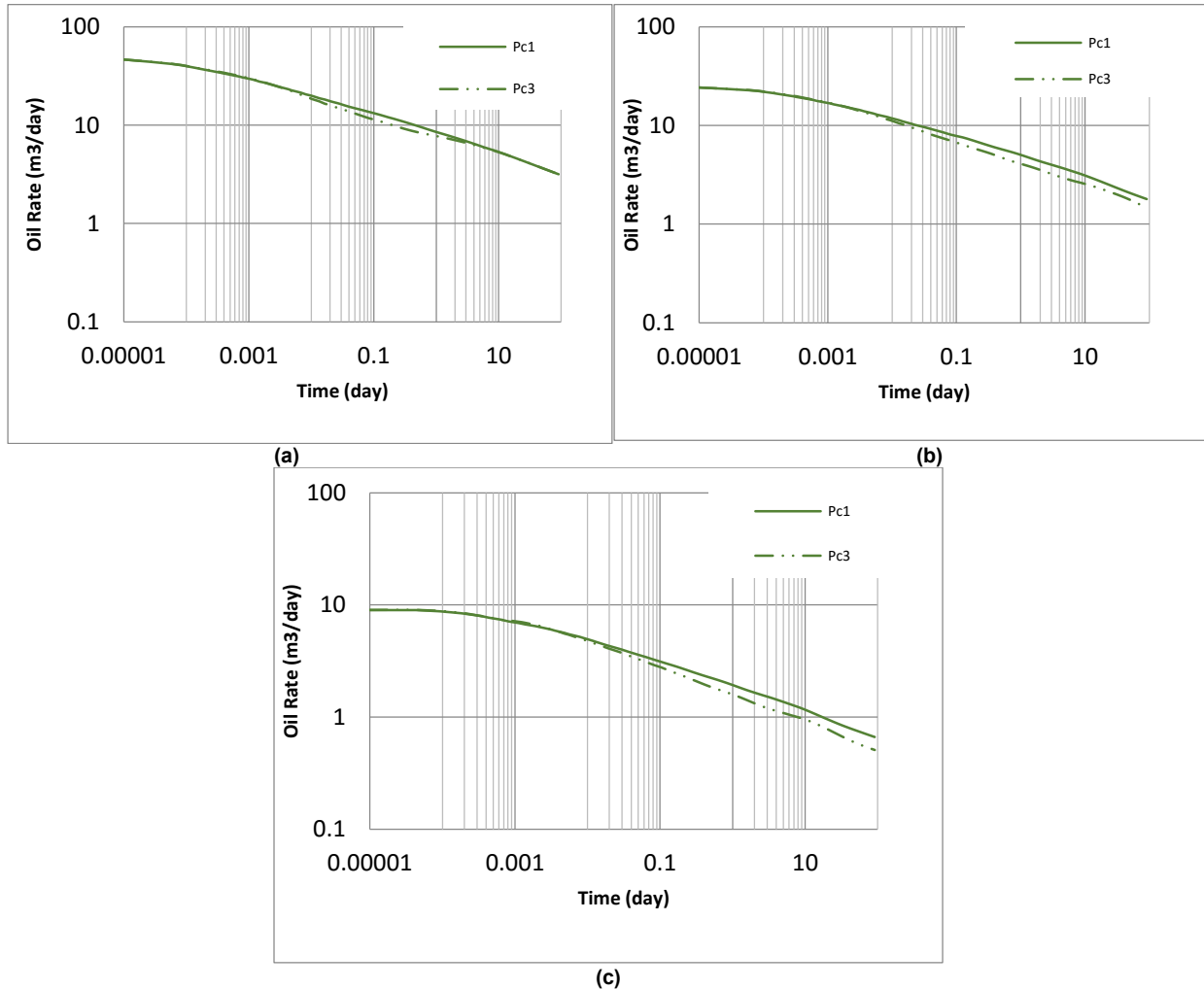


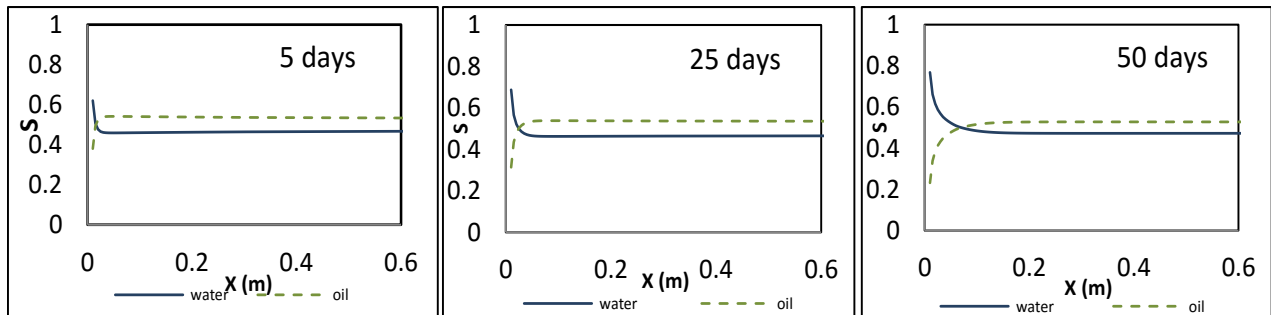
Figure 6.13 Log-log plot of daily rate versus time for the dual-porosity models with different capillary pressure in matrix during 91 days:

Initial water saturation in matrix equals to (a)-0.3; (b)- 0.5; (c)-0.7

We observe that oil rate decreases with increasing initial water saturation in matrix. Here, we define Δq_{Pc} to be the difference in oil rate between models with lower and higher capillary

pressure in matrix. In Fig 6.13, Δq_{pc} increases with increasing initial water saturation. We compute Δq_{pc} as a function of time. When initial water saturation reaches to 0.7, its average differential ($\Delta q_{pc} / q_{pe1} \times 100\%$) value over the entire production period is around 30%. This is because with higher initial water saturation in matrix, there is more mobile water in matrix. More mobile water in matrix provides more favorable conditions for the occurrence of fracture-face effect. This leads to more water blockage around interface which decreases oil production.

After discussing impacts of capillary pressure with dual-porosity models, triple-porosity models with one hydraulic fracture and eight secondary fractures are constructed. Relative permeability functions in secondary fracture are adopted from Aguilera et al. (1980). And a capillary function for secondary system is assigned from Eq. (7) before. We expected with more frac-matrix interfaces in triple-porosity model, fracture-face effect became more obviously. Fig 6.14 is water and oil saturation profiles in matrix as a function of distance from the hydraulic fracture interface (X) and secondary (micro) fracture interface (Y) at different times.



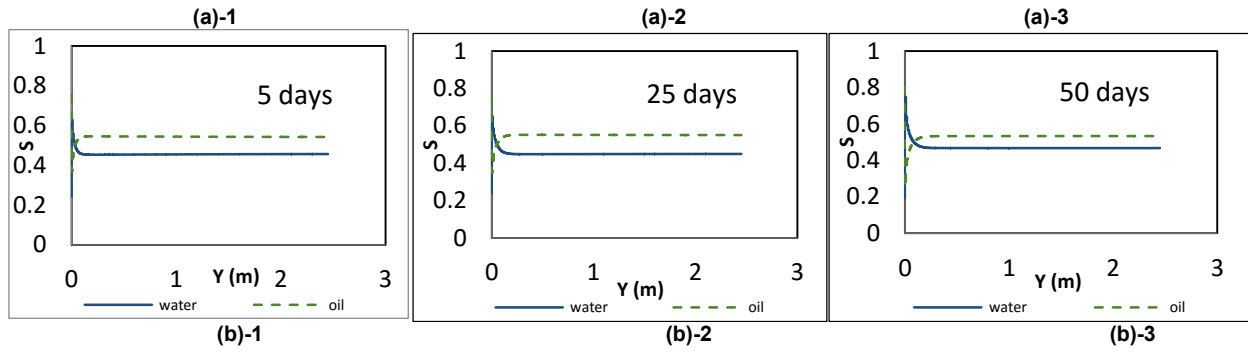


Figure 6.14 Oil and water saturation profiles in matrix as a function of

(a) distance from the hydraulic fracture-matrix interface X and (b) distance from the secondary fracture-matrix interface Y for the triple-porosity model at

(1): 5 days; (2); 25 days; and (3) 50 days.

Fig 6.14 (a) shows the evolution of saturation profiles in matrix as a function of distance from the hydraulic fracture-matrix interface with time. The region near the interface is enlarged to illustrate the fracture-face effect more clearly. Similarly, Fig 6.14 (b) presents the saturation profiles matrix as a function of distance from the hydraulic fracture-matrix interface at different time. It is shown in both Fig 6.14 (a) and Fig 6.14 (b) that as time goes by, water saturation close to frac-matrix interface increases. It is discovered that fracture-face effect appears in two different systems (hydraulic fracture-matrix, secondary fracture-matrix) in triple-porosity models (Fig 6.14) due to high P_c difference between matrix and fracture.

The effects of capillary pressure functions in matrix on water saturation and on oil production are shown in Fig 6.15. Three triple-porosity models with varying capillary pressure in matrix are constructed.

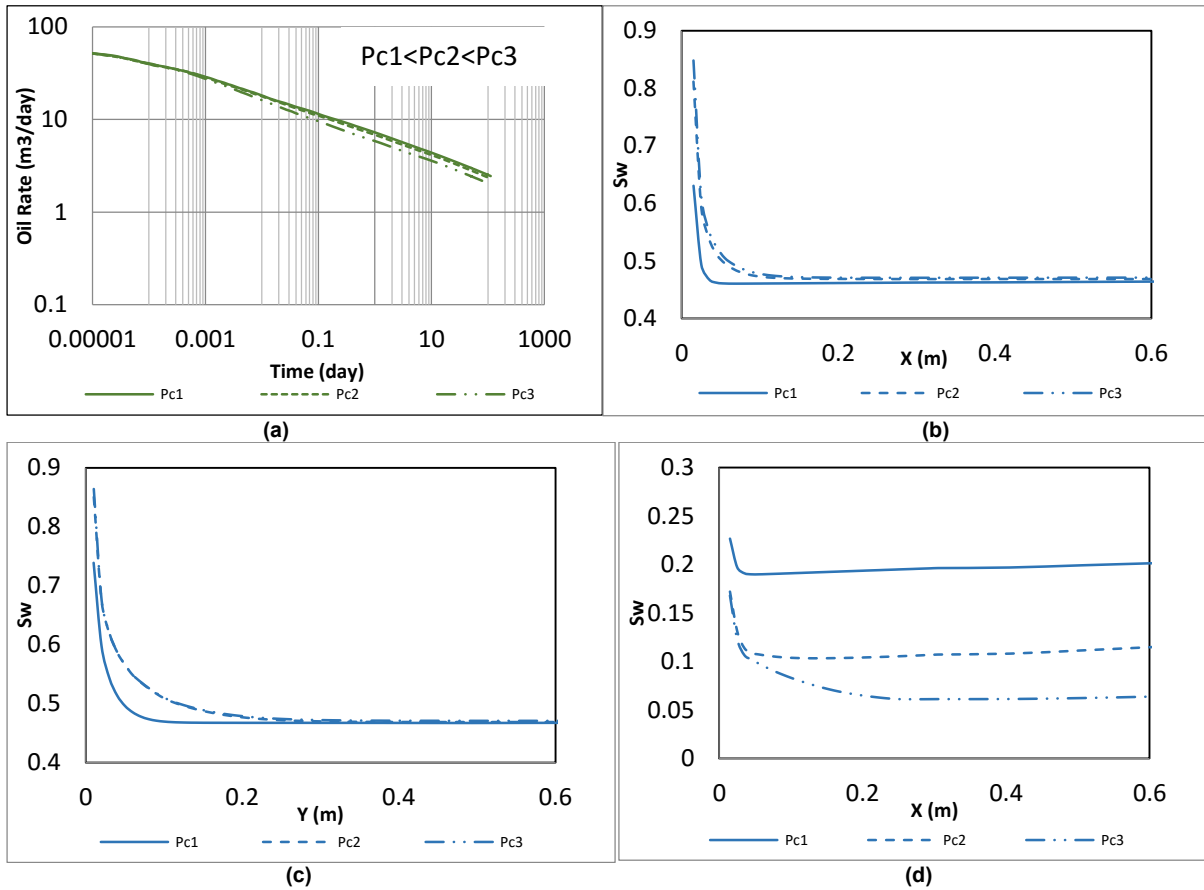


Figure 6.15 Triple-porosity models with different capillary pressure:

(a)- Log-log plot of daily oil rate versus time during 91 days; (b)- Water saturation of HF-M system at 30 days; (c)- Water saturation of SF-M system at 30 days; (d)- Water saturation of SF-HF system at 30 days.

(Values of Pc_1 , Pc_2 and Pc_3 are shown in Fig 6.7)

With increasing capillary pressure in matrix, water saturation in matrix close to frac-matrix interface increases, while oil rate decreases. These observations are quite similar to the results in dual-porosity model. However, the difference in oil rate shown in Fig 6.15 (a) is not pronounced. Table 6.1 shows a comparison between dual-porosity and triple-porosity models on water saturation at the interface in *HF-M* system and *SF-M* system.

Table 6.1 Water saturation at interface in dual-porosity and triple-porosity models with different capillary pressure (Pc_1 and Pc_3)

$S_{W_{inter}}$	$S_{W_{inter}} (P_c=P_{c1})$	$S_{W_{inter}} (P_c=P_{c3})$	$\Delta S_{W_{inter}}$
Dual-porosity (HF-M)	0.6181	0.8445	0.2264
Triple-porosity (HF-M)	0.6305	0.8479	0.2174
Triple-porosity (SF-M)	0.7388	0.8641	0.1253

Compared with dual-porosity model in Table 6.1, triple-porosity model has higher water saturation in both *HF-M* and *SF-M* systems. This means fracture-face effect becomes more pronounced in models with more interfaces. However, the difference in oil production (Δq_{Pc}) that we compute as a function of time in triple-porosity model does not increase compared with Δq_{Pc} in dual-porosity models. The contrast between different porosity systems in a medium consisting of matrix, secondary fractures and hydraulic fracture is less in comparison to a medium consisting of matrix and hydraulic fracture only. Fracture-face effect has fewer influences on oil rate in triple-porosity models compared with impacts on oil rate in dual-porosity models shown in Fig 6.10 (a). Since the fracture-face effect is more pronounced between *HF* and *M*, the dual-porosity model is employed in the next section to study the impacts on matrix relative permeability functions.

Next, we investigate possible relationships between relative permeability and production performance. Two models with different values of relative permeability endpoint and curvature in matrix are tested

According to Eq. (5) and Eq. (6) shown before, two parameters determine value of relative permeability, k_{row}^o and C_o . By changing these two parameters, sensitivity of relative permeability value on production are assessing. The first parameter tested here is value of k_{row}^o .

This value we call it endpoint of k_{row} in matrix and it changes from 0.4 to 0.9, as shown in Fig 6.16.

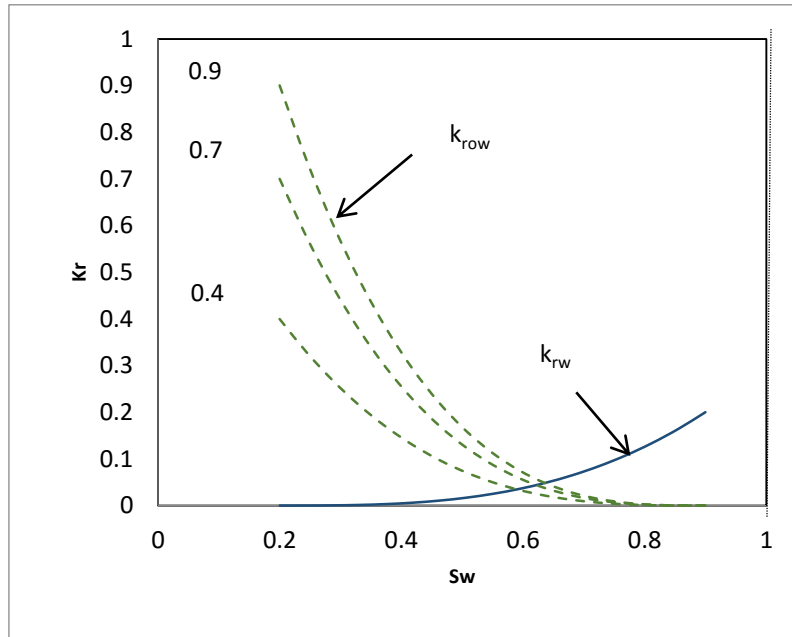


Figure 6.16 Different relative permeability in matrix system by changing endpoint of k_{row}

Fig 6.16 shows that as the endpoint of k_{row} increases, the value of oil relative permeability in matrix increases. Fig 6.17 presents the oil and water saturation profiles in matrix as a function of distance from the HF-M interface by using models with different endpoint of k_{row} . It is observed that as the endpoint of k_{row} increases, oil saturation decreases while water saturation increases. According to Fig 6.16, the intersection point of oil and water relative permeability curves goes to right, as the endpoint of k_{row} increases. This observation means that matrix becomes more water-wet and capillary end effect becomes more pronounced.

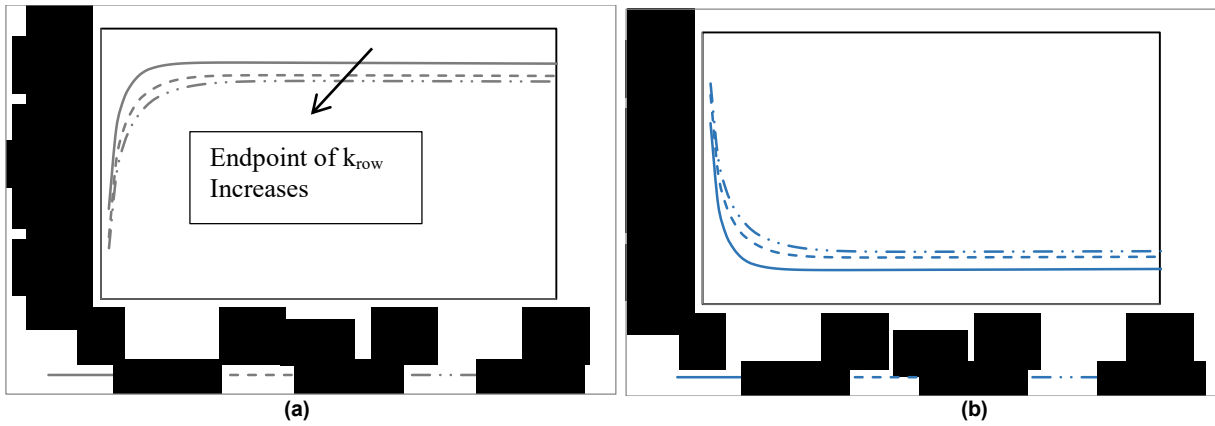
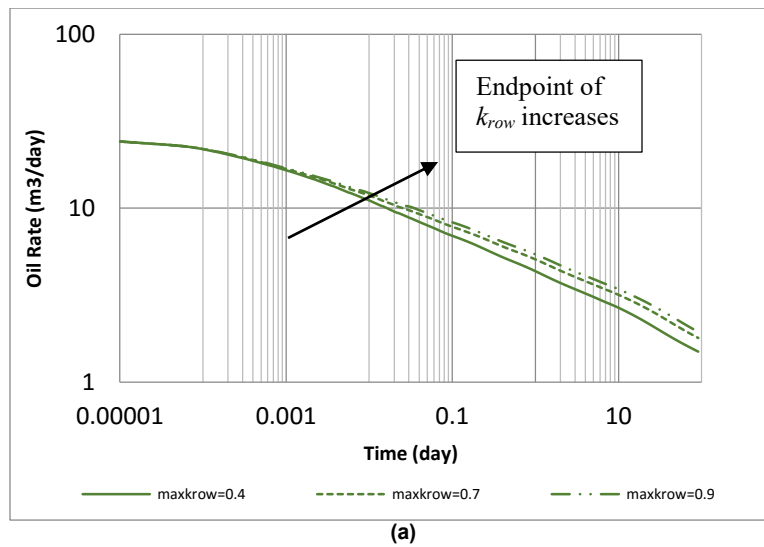
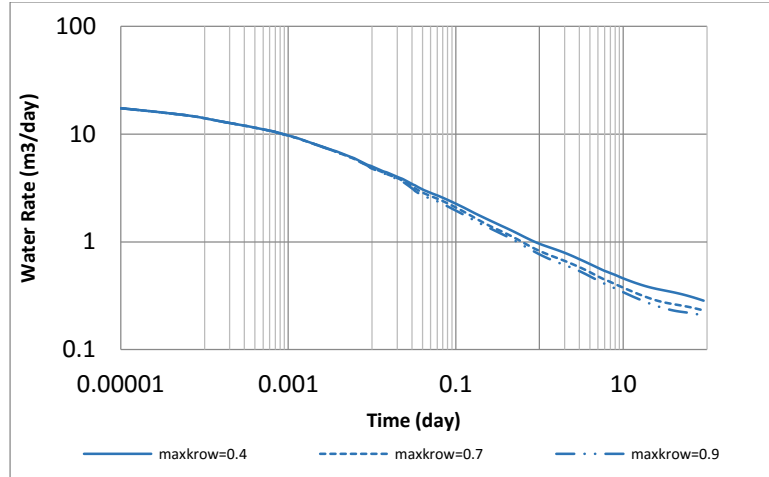


Figure 6.17 Saturation profiles in saturation in matrix as a function of distance from the fracture-matrix interface with different endpoint of k_{row} at 30 days:

(a)-oil saturation; (b)- water saturation

Fig 6.18 shows the results of log-log plot of daily production versus time during 112 days using models with different k_{row} endpoints in matrix.





(b)

Figure 6.18 Log-log plot of daily rate versus time for the dual-porosity models with different kro endpoints in matrix during 91 days:

(a)-oil rate; (b)- water rate

Oil rate increases as oil relative permeability increases. On the other hand, water rate decreases by increasing endpoint of k_{row} . Although water saturation at interface is larger which means more water blockage around interface as endpoint of k_{row} increases, higher k_{row} endpoint gives higher value of k_{row} at interface water saturation. This leads to higher oil transmissibility and lower water transmissibility.

The second sensitivity testing is curvature of oil relative permeability in matrix. This curvature is C_o in equation (1) which influences relative permeability directly. When this exponent equals to 1.0, relative permeability curves become straight line. Exponent of oil relative permeability curvature in matrix defined as C_o changes from 2.0 to 5.0 which is shown in Fig 6.19.

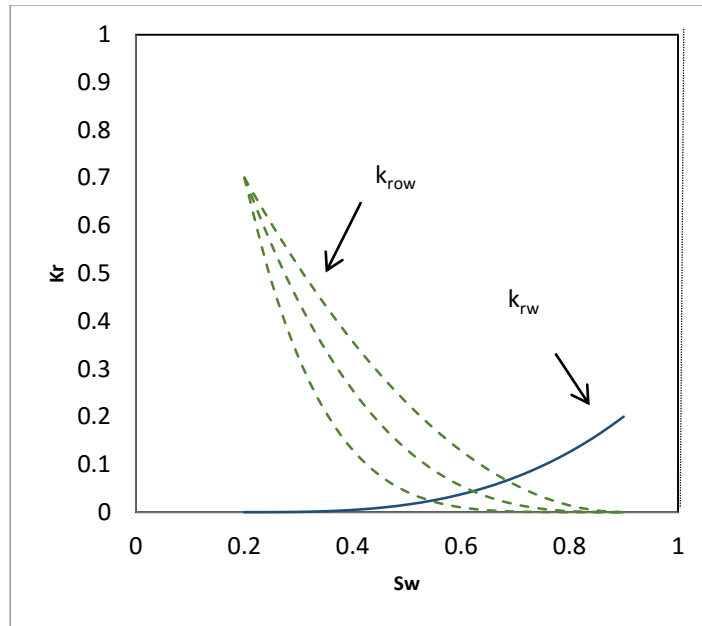


Figure 6.19 Different relative permeability in matrix system by changing curvature of k_{row}

We hypothesize that due to increasing C_o , changing of water saturation have stronger impacts on oil relative permeability. It will result in fracture-face effect increasing and leads to oil rate reduction. Fig 6.20 is oil and water saturation in matrix close to fracture. It shows that when C_o in matrix is higher, more water blockage appears near fracture which means fracture-face effect becomes more pronounced, and it hinders oil transport from matrix to fracture.

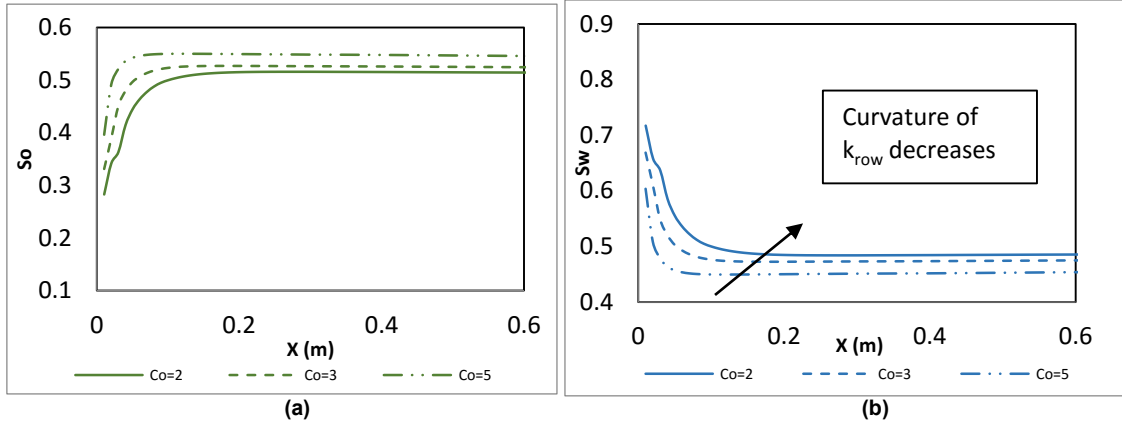
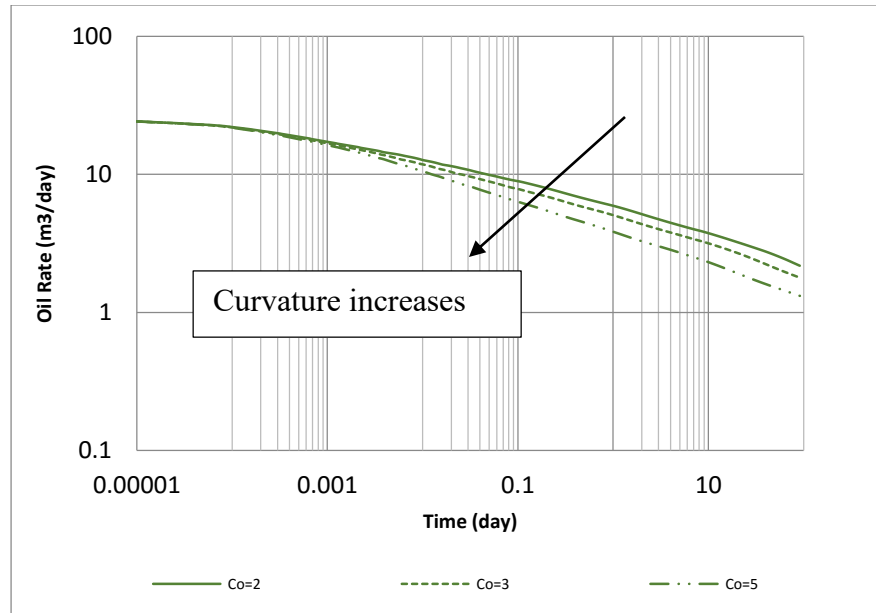


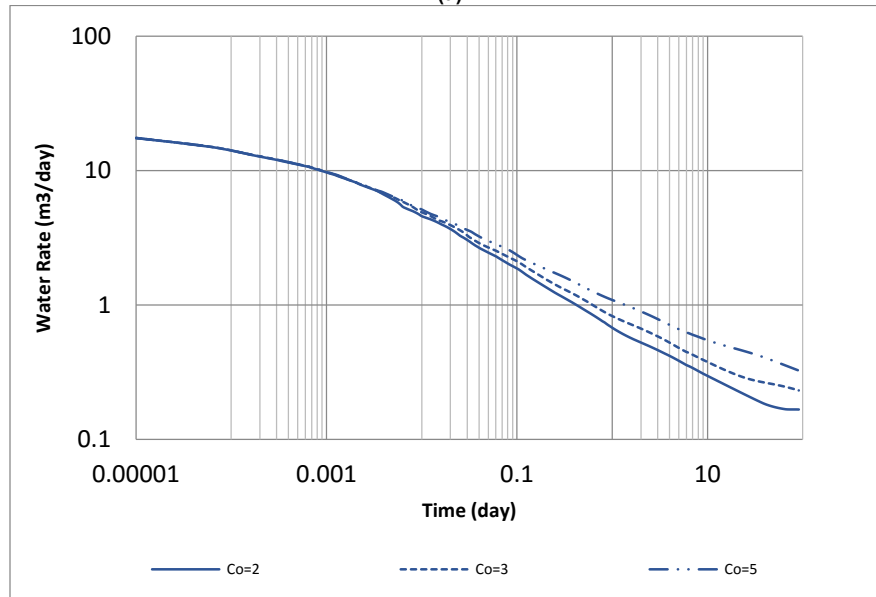
Figure 6.20 Saturation profiles in saturation in matrix as a function of distance from the fracture-matrix interface with different curvature of k_{row} at 30 days:

(a)-oil saturation; (b)- water saturation

Similar to the observation in Fig 6.6 for the base case, oil saturation in matrix increases due to oil expansion with reservoir pressure decline during production. Fig 6.21 is log-log plot of daily production versus time during 112 days. Oil rate shown in Fig 6.21 decreases while water rate increases with C_o increasing. This observation is consistent with the characteristics of oil saturation profiles shown in Fig 6.20. With C_o increasing, more oil remains in the matrix due to lower k_{row} at a given saturation; therefore, oil rate decreases.



(a)



(b)

Figure 6.21 Log-log plot of daily rate versus time for the dual-porosity models with different k_{row} curvature in matrix during 91 days:

(a)-oil rate; (b)- water rate

To investigate how much capillary pressure and relative permeability influence production. We do an additional sensitivity. Here, we do a combination sensitivity with capillary pressure and relative permeability curvature. Fig 6.22 is a schematic of the whole procedure. Firstly, P_{c1} and

P_{c3} shown in Fig 6.7 are used in Matrix. Water saturation profile at particular day can be obtained by using models with different capillary pressure in matrix. Different value of S_w close to frac-matrix interface (0.01025 m) in models with P_{c1} and P_{c3} can be read in water saturation profiles (S_{w1} and S_{w3} in Fig 6.22 (b)). According to Fig 6.16, when endpoint of k_{row} equals to 0.9, Δk_{row} can be obtained. Then this whole procedure is repeated by using endpoint of k_{row} equals to 0.4. Fig 6.23 is saturation profile at 30 days by using P_{c1} and P_{c3} on matrix with different relative permeability curvature. We use these plots to obtain water saturation at interface.

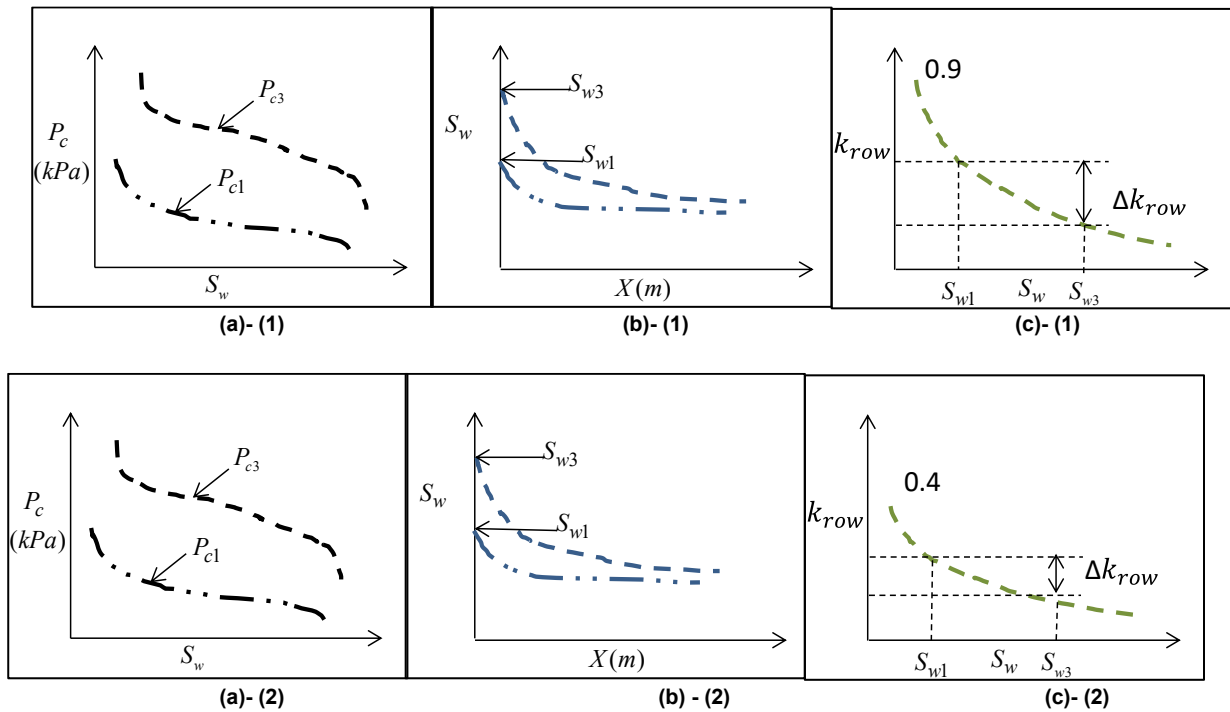
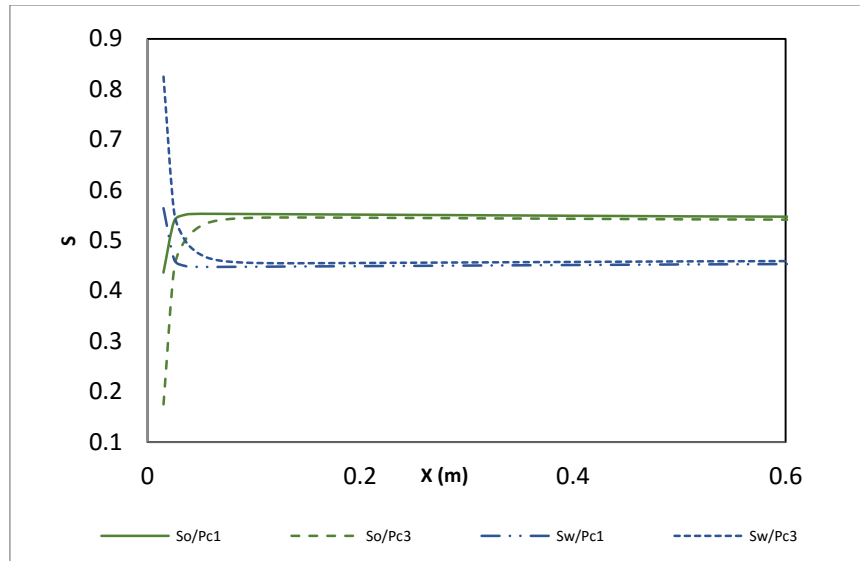


Figure 6.22 Schematic of calculation procedure for Δk_{row} :

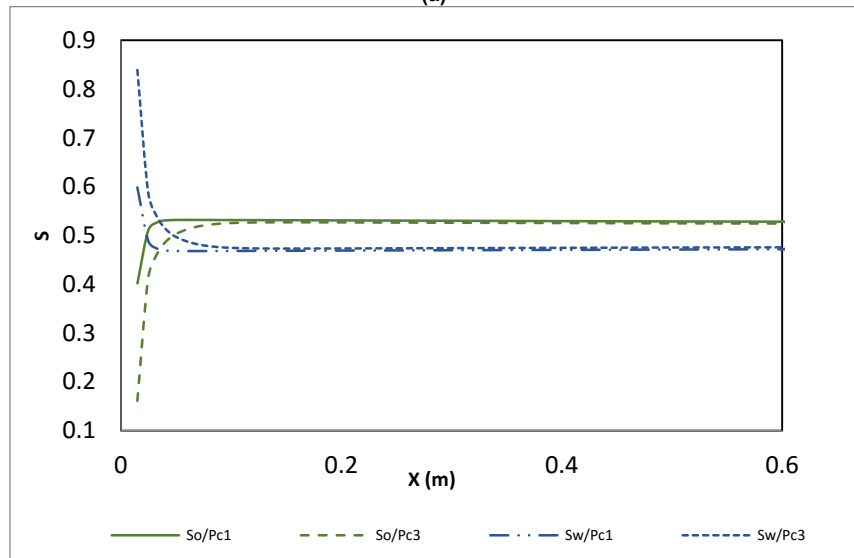
(1)- endpoint of $k_{row}=0.9$; (2)- endpoint of $k_{row}=0.4$

(a)-different P_c in matrix; (b)- water saturation profiles of models with different P_c in matrix;

(c)-oil relative permeability



(a)



(b)

Figure 6.23 Saturation profiles in saturation as a function of distance from the fracture-matrix interface with different capillary pressure in matrix at 30 days:

Endpoint of k_{row} equals to (a)-0.4; (b)- 0.9

Take $k_{row}^o = 0.4$ as an example:

According to Fig 6.23 (a), $\Delta S_w = 0.8750 - 0.6425 = 0.2325$;

According to Fig 6.16, $\Delta k_{row2} = k_{row}(0.6425) - k_{row}(0.8750) = 0.02$

Table 6.2 is list of Δk_{row} . We observe that with increasing the endpoint of oil relative

permeability, Δk_{row} increases. This result demonstrates that Δq_{pc} decreases as oil relative permeability endpoint increases.

Table 6.2 Value of Δk_{row} in conditions of different relative permeability curvature

	Endpoint of $k_{row}=0.4$	Endpoint of $k_{row}=0.9$
Δk_{row}	0.02	0.07

Log-log plots of daily rate versus time with different capillary pressure and relative permeability in matrix are shown in Fig 6.24. Results show that with increasing of k_{row} endpoint, oil rate decreases.

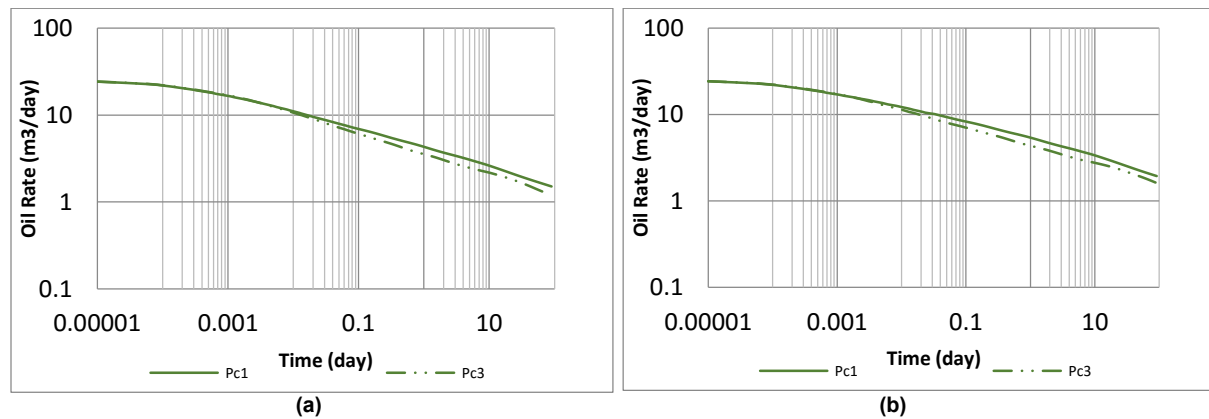


Figure 6.24 Log-log plot of daily rate versus time for the dual-porosity models with different capillary pressure in matrix during 91 days:

endpoint of k_{row} equals to (a)-0.4; (b)- 0.9

Using data shown in Fig 6.23, we calculate Δq_{pc} as a function of time in Fig 6.24. It is obvious that Δq_{pc} increases when endpoint of oil relative permeability increases at the first 50 days. Due to the endpoint increasing, Δk_{row} increases and this leads to Δq_{pc} increasing. This is consistent with what we expected. After 50 days, due to higher oil rate in model with higher k_{row} endpoint,

drainage reaches boundary and Δq_{pc} goes to flat.

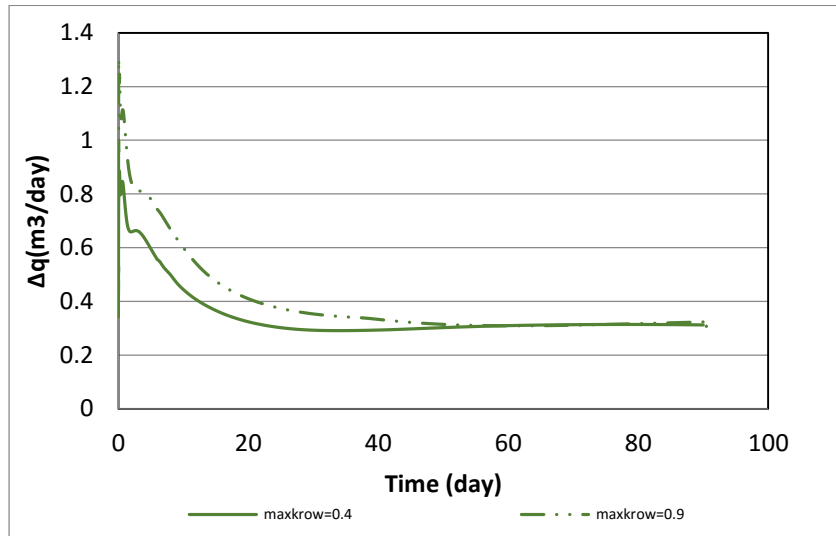


Figure 6.25 Δq as a function of time in models with different endpoint of k_{row}

7 Conclusions and Future Work

7.1 Conclusions

A workflow that integrates numerical simulation results with analytical solutions is implemented to quantify the uncertainty in production performance predictions. Assuming that results obtained from RTA would characterize the mean estimate of the corresponding fracture parameters, additional heterogeneous models of fracture properties are subjected to flow simulations to demonstrate their impact on production performance. Our results highlight the non-uniqueness of fracture characterization in production data analysis. It is illustrated that ignoring the uncertainty in history-matched parameters and assumptions associated with analytical models could potentially over- or under-estimate production by up to 30%.

Certain assumptions in analytical models may not necessarily hold. Numerical models are implemented in this study to assess their limitations and impacts. It is demonstrated that analytical sequential-flow model underestimates drainage with time; therefore, history-matching with analytical models alone would tend to overestimate fracture parameters including natural fracture intensity. The assumption of uniformly-spaced fracture stages, however, could lead to underestimation of hydraulic fracture half-length and the associated stimulated reservoir volume. This could potentially impact future field development decisions such as placement of nearby wells to maximize drainage.

Lengths and spacing between natural fractures play an important role, particularly at mid to late times: higher production and more efficient drainage can be observed when natural fractures are evenly distributed for a given number of natural fractures, especially when matrix permeability is ultra-low. This also implies that the assumption of evenly-distributed natural fractures with

homogeneous properties could lead to underestimation of fracture half-length and the associated stimulated reservoir volume.

A series of simulation models depicting different boundary conditions are also used to evaluate the uncertainties due to pressure interference between natural fractures and inter-well fracture communication. The connectivity of both natural and hydraulic fractures has a pronounced effect on the rate transient behavior. Some of the flow regimes such as fracture linear transient flow disappear as the secondary fractures between hydraulic fractures or hydraulic fractures between lateral wells become disconnected. Oil production decreases more slowly during late time when there is linear flow in natural fractures and bilinear flow in natural fractures and matrix. On the other hand, disconnected short hydraulic fractures may lead to unit slope instead of half slope and quarter slope at early time. The occurrence of early unit-slope and the absence of early half- and quarter-slope indicate that the transient flow in relatively small hydraulic fractures is masked by pseudo steady-state pressure depletion due to limited hydraulic fracture penetration. This may contribute to additional uncertainties in fracture characterization with analytical models.

The approach presented in this study can be used as an avenue to quantify the effects of model uncertainties on production performance prediction, and the method can be readily extended to shale reservoirs. Given the subject of resource/reserve estimation of multi-fractured horizontal wells in unconventional reservoirs remains challenging, this work highlights the importance of adopting a modeling framework that takes into consideration the uncertainties in model parameters when carrying out long-term production forecast.

Ignoring the presence of two phase oil-gas flow or assuming the absence of solution gas in tight oil reservoirs could lead to overestimation of fracture parameters such as effective fracture

volume and fracture length and permeability. In particular, this overestimation would be more severe, if k_{rog} is low and/or gas relative permeability exponent (a_1) is high.

Capillary end-effects do exist at fracture-matrix interface and cause water blockage at this interface. This is similar to the end-effect observed in laboratory coreflooding tests. This capillary discontinuity plays an unignorable role in matrix-fracture flow communication, which in turn, influences water hydrocarbon production. Results show that less water blockage and higher production are observed in cases with lower capillary contrast between fracture and matrix. With higher capillary contrast between fracture and matrix, effects of imbibition become more pronounced and more oil flows into fracture from matrix. However, cumulative oil production does not change much. Also, Capillary end-effect has less influences on oil rate in triple-porosity models compared with impacts on oil rate in dual-porosity models.

It is also observed that initial oil production increases slightly due to the displacement of oil by water (wetting phase) near the fracture-matrix interface. This increase is more pronounced when we increase the capillary pressure or initial water saturation in matrix blocks. However, after this slightly increasing, whole production procedure is hampered as a result of increased water blockage.

Relative permeability effects capillary discontinuity directly. Increasing oil relative permeability endpoint or decreasing oil relative permeability curvature can lead to capillary end-effect more pronounced. Models with different capillary pressure in matrix can have higher oil rate difference as endpoint of oil relative permeability increases.

The results can be applied 1) for a more representative simulation of fractured horizontal wells and 2) for designing efficient treatment technologies for the removal of water blockage which is one of the key mechanisms for the production decline observed in the field.

7.2 *Future Work*

For future multi-phase production from fractured horizontal wells studies, the following future research is recommended:

- Both dual-porosity models and triple-porosity models in tight oil reservoir with three-phase flow can be constructed to figure out three-phase effects on oil production, especially long-term production.
- The presented triple-porosity models in this thesis will be evaluated using more field data from different formations and wells to do production prediction.
- Stochastically distributed discrete fracture networks (DFN) can be employed in future work. Branched natural (secondary) fracture with different length and position will be modeled randomly. This can capture the uncertainties associated with reservoir heterogeneity better.
- An injector can be used in triple-porosity model in this thesis to simulate flow-back and shut-in operation. Effects of capillary discontinuity from fractured horizontal well on hydrocarbon production will be investigated using models with injector.

References

- Abbasi, M. A., Ezulike, D. O., Dehghanpour, H., Hawkes, R. V. 2014. A comparative study of flowback rate and pressure transient behavior in multifracted horizontal wells completed in tight gas and oil reservoirs. *Journal of Natural Gas Science and Engineering*, 17, 82-93. doi:10.1016/j.jngse.2013.12.007
- Abdassah, D., Ershaghi, I. 1986. Triple-porosity systems for representing naturally fractured reservoirs. *SPE Formation Evaluation*, 1(02), 113-127. doi: 10.2118/13409-PA.
- Aguilera, R. 1980. *Naturally fractured reservoirs* (pp. 200-220). Tulsa, Okla.: Petroleum Publishing Company.
- Aguilera, R. 2008. Role of natural fractures and slot porosity on tight gas sands. In *SPE Unconventional Reservoirs Conference*. Society of Petroleum Engineers. doi.org/10.2118/114174-MS
- Al-Ahmadi, H. A., Wattenbarger, R. A. 2011, January. Triple-porosity models: one further step towards capturing fractured reservoirs heterogeneity. In *SPE/DGS Saudi Arabia Section Technical Symposium and Exhibition*. Society of Petroleum Engineers. doi: 10.2118/149054-MS.
- Al-Ghamdi, A., Ershaghi, I. 1996. Pressure transient analysis of dually fractured reservoirs. *SPE Journal*, 1(01), 93-100. doi:10.2118/26959-PA.
- Alahmadi, H. A. H. 2010. *A Triple-porosity model for fractured horizontal wells* (Doctoral dissertation, Texas A&M University). Alberta Geological Survey. Alberta Geological Survey Operational Plan Fiscal Year 2009-2010. www.ags.gov.ab.ca Alberta Research Council, Canadian Society of Petroleum Geologists, and Shetsen, I. 1994. *Geological*

atlas of the Western Canada sedimentary basin. [Calgary]: Published jointly by the Canadian Society of Petroleum Geologists and the Alberta Research Council.

Alcoser, L. A., Ovalle, A., Parsons, M. C. 2012, January. The Bakken: Utilizing a Petroleum System Based Analysis to Optimally Exploit One of the World. In SPE Hydrocarbon Economics and Evaluation Symposium. Society of Petroleum Engineers. doi.org/10.2118/158918-MS

Ali, A. J., Siddiqui, S., Dehghanpour, H. 2013. Analyzing the production data of fractured horizontal wells by a linear triple porosity model: Development of analysis equations. Journal of Petroleum Science and Engineering, 112, 117-128. doi:10.1016/j.petrol.2013.10.016

Alkouh, A. B., Patel, K., Schechter, D., Wattenbarger, R. 2012, January. Practical use of simulators for characterization of shale reservoirs. In SPE Canadian Unconventional Resources Conference. Society of Petroleum Engineers. doi:10.2118/162645-MS.

Allan, J., Sun, S. Q. 2003, January. Controls on recovery factor in fractured reservoirs: lessons learned from 100 fractured fields. In SPE Annual Technical Conference and Exhibition. Society of Petroleum Engineers. doi.org/10.2118/84590-MS

Apotria, T., Kaiser, C. J., Cain, B. A. 1994. Fracturing and stress history of the Devonian Antrim Shale, Michigan basin. In 1st North American Rock Mechanics Symposium. American Rock Mechanics Association. ARMA-1994-0809

Ault, C. H. 1989. Map of Indiana Showing Direction of Bedrock Jointing. Indiana. Geological Survey.

- Baars, D. L. 1972. Devonian system. Geologic Atlas of the Rocky Mountain Region: Denver, Colorado, Rocky Mountain Association of Geologists, 90-99.
- Bahorich, B., Olson, J. E., Holder, J. 2012. Examining the effect of cemented natural fractures on hydraulic fracture propagation in hydrostone block experiments. In SPE Annual Technical Conference and Exhibition. Society of Petroleum Engineers. doi.org/10.2118/160197-MS
- Barthélémy, J. F., Guiton, M. L., Daniel, J. M. 2009. Estimates of fracture density and uncertainties from well data. International Journal of Rock Mechanics and Mining Sciences, 46(3), 590-603. doi:10.1016/j.ijrmms.2008.08.003
- Beliveau, D. 2004, January. Solution Gas Production Profiling. In Canadian International Petroleum Conference. Petroleum Society of Canada. doi.org/10.2118/2004-201
- Bello, R. O. 2009. Rate transient analysis in shale gas reservoirs with transient linear behavior (Doctoral dissertation, Texas A&M University).
- Best, M. E., Katsube, T. J. 1995. Shale permeability and its significance in hydrocarbon exploration. The Leading Edge, 14(3), 165-170. doi: 10.1190/1.1437104
- Blanton, T. L. 1982. An experimental study of interaction between hydraulically induced and pre-existing fractures. In SPE Unconventional Gas Recovery Symposium. Society of Petroleum Engineers. doi.org/10.2118/10847-MS
- Bradley, H. B. 1992. Petroleum Engineering Handbook, 22. Society of Petroleum Engineers, TX, USA.
- Brill, J. P. 1987. Multiphase flow in wells. Journal of petroleum technology, 39(01), 15-21. doi.org/10.2118/16242-PA

- Brooks, R. H., and Corey, A. T. 1964. Hydraulic properties of porous media, Hydrology Papers, No. 3, Colorado State University, Ft. Collins, Colo.
- Brownscombe, E. R., Dyes, A. B. 1952, January. Water-imbibition displacement-a possibility for the Spraberry. In *Drilling and Production Practice*. American Petroleum Institute. API-52-383
- Buchsteiner, H., Warpinski, N. R., and Economides, M. J. 1993, January. Stress-induced permeability reduction in fissured reservoirs. In *SPE Annual Technical Conference and Exhibition*. Society of Petroleum Engineers. doi.org/10.2118/26513-MS
- Castillo, F., Aguilera, R., Lawton, D. 2011, January. Integration of Seismic Data and a Triple Porosity Model for Interpretation of Tight Gas Formations in the Western Canada Sedimentary Basin. In *Canadian Unconventional Resources Conference*. Society of Petroleum Engineers. doi.org/10.2118/149496-MS
- Chen, C. Y., Li, K., Horne, R. N. 2004, January. Experimental Study of Phase Transformation Effects on Relative Permeabilities in Fractures. In *SPE Annual Technical Conference and Exhibition*. Society of Petroleum Engineers. doi.org/10.2118/90233-MS
- Cheng, Y. 2012. Impact of water dynamics in fractures on the performance of hydraulically fractured wells in gas-shale reservoirs. *Journal of Canadian Petroleum Technology*, 51(02), 143-151. doi.org/10.2118/127863-PA
- Cho, Y., Ozkan, E., Apaydin, O. G. 2013. Pressure-dependent natural-fracture permeability in shale and its effect on shale-gas well production. *SPE Reservoir Evaluation & Engineering*, 16(02), 216-228. doi.org/10.2118/159801-PA

- Cinco, L., Samaniego, V., and Dominguez, A. 1978. Transient pressure behavior for a well with a finite-conductivity vertical fracture. *Society of Petroleum Engineers Journal*, 18(04), 253-264. doi.org/10.2118/6014-PA
- Cipolla, C. L., Warpinski, N. R., Mayerhofer, M. J., Lolon, E., and Vincent, M. C. 2008, January. The relationship between fracture complexity, reservoir properties, and fracture treatment design. In *SPE Annual Technical Conference and Exhibition*. Society of Petroleum Engineers. doi.org/10.2118/115769-MS
- Cipolla, C. L., Lolon, E., Mayerhofer, M. J., and Warpinski, N. R. 2009, January. The effect of proppant distribution and un-propped fracture conductivity on well performance in unconventional gas reservoirs. In *SPE Hydraulic Fracturing Technology Conference*. Society of Petroleum Engineers. doi.org/10.2118/119368-MS
- Clark, N. J. 1962. Fundamentals of Reservoir Fluids. *Journal of Petroleum Technology*, 14(01), 11-16. doi: 10.2118/91-PA.
- Clarkson, C. R., Pedersen, P. K. 2011, January. Production analysis of Western Canadian unconventional light oil plays. In *Canadian Unconventional Resources Conference*. Society of Petroleum Engineers. doi.org/10.2118/149005-MS
- Computer Modeling Group. IMEX: Three-phase, black-oil reservoir simulator user's guide (Version 2013). Computer Modeling Group Limited, Calgary, Alberta, Canada, 2013.
- Cox, S. A., Cook, D., Dunek, K., Daniels, G. R., Jump, C. J., and Barree, R. D. 2008, January. Unconventional resource play evaluation: A look at the Bakken Shale Play of North Dakota. In *SPE Unconventional Reservoirs Conference*. Society of Petroleum Engineers. doi.org/10.2118/114171-MS

- Crain's petrophysical handbook. 2012. Shale basics. [Online] <http://www.spec2000.net/11-vshbasics.htm> (accessed 29 Oct 2015).
- Curtis, J. B. 2002. Fractured shale-gas systems. AAPG bulletin, 86(11), 1921-1938.
- Dahi Taleghani, A. 2009. Analysis of hydraulic fracture propagation in fractured reservoirs: an improved model for the interaction between induced and natural fractures.
- Daneshy, A. A. 2004, January. Proppant distribution and flowback in off-balance hydraulic fractures. In SPE Annual Technical Conference and Exhibition. Society of Petroleum Engineers. doi.org/10.2118/89889-MS
- de Swaan O, A. 1976. Analytic solutions for determining naturally fractured reservoir properties by well testing. Society of Petroleum Engineers Journal, 16(03), 117-122. doi: 10.2118/5346-PA.
- Dehghanpour, H., Shirdel, M. 2011, January. A triple porosity model for shale gas reservoirs. In Canadian Unconventional Resources Conference. Society of Petroleum Engineers. doi:10.2118/149501-MS.
- Dershowitz, W. S., Einstein, H. H. 1988. Characterizing rock joint geometry with joint system models. Rock Mechanics and Rock Engineering, 21(1), 21-51. doi: 10.1007/BF01019674
- DOE, U. 2009. Modern Shale Gas Development in the United States: A Primer. Office of Fossil Energy and National Energy Technology Laboratory, United States Department of Energy.
- Duhault, J. L. 2012, November. Cardium Formation Hydraulic "Frac" Microseismic: Observations and Conclusions. In 2012 SEG Annual Meeting. Society of Exploration Geophysicists. SEG-2012-0835
- Dyke, C. G., Wu, B., Milton-Taylor, D. 1995.

- Advances in characterizing natural fracture permeability from mud log data. SPE Formation Evaluation, 10(03), 160-166. doi.org/10.2118/25022-PA
- Eker, I., Kurtoglu, B., Kazemi, H. 2014, September. Multiphase Rate Transient Analysis in Unconventional Reservoirs: Theory and Applications. In SPE/CSUR Unconventional Resources Conference–Canada. Society of Petroleum Engineers. doi.org/10.2118/171657-MS
- El-Banbi, A.H. 1998. Analysis of tight gas wells. PhD Dissertation, Texas A &M U., College Station, Texas.
- Engelder, T., Lash, G. G., Uzcátegui, R. S. 2009. Joint sets that enhance production from Middle and Upper Devonian gas shales of the Appalachian Basin. AAPG bulletin, 93(7), 857-889. doi:10.1306/03230908032
- Ezulike, D. O., Dehghanpour, H. 2013, November. Characterizing tight oil reservoirs using dual- and triple-porosity models. In SPE Unconventional Resources Conference Canada. Society of Petroleum Engineers. doi.org/10.2118/167126-MS
- Ezulike, D. O., Dehghanpour, H. 2014. A model for simultaneous matrix depletion into natural and hydraulic fracture networks. Journal of Natural Gas Science and Engineering, 16, 57-69. doi:10.1016/j.jngse.2013.11.004
- Ezulike, O. D., Ghanbari, E., Siddiqui, S., Dehghanpour, H. 2015. Pseudo-steady state analysis in fractured tight oil reservoirs. Journal of Petroleum Science and Engineering, 129, 40-47. doi:10.1016/j.petrol.2015.01.009
- Fakcharoenphol, P., Torcuk, M. A., Wallace, J., Bertoncello, A., Kazemi, H., Wu, Y. S., Honarpour, M. 2013. Managing Shut-in Time to Enhance Gas Flow Rate in Hydraulic

- Fractured Shale Reservoirs: A Simulation Study. In SPE Annual Technical Conference and Exhibition. Society of Petroleum Engineers. doi.org/10.2118/166098-MS
- Fetkovich, M. 1973. The isochronal testing of oil wells. In Fall Meeting of the Society of Petroleum Engineers of AIME. Society of Petroleum Engineers. doi.org/10.2118/4529-MS
- Fetkovich, M. J. 1980. Decline curve analysis using type curves. *Journal of Petroleum Technology*, 32(06), 1-065. doi.org/10.2118/4629-PA
- Fidler, L. J. 2011. Natural fracture characterization of the New Albany Shale, Illinois Basin, United States. Firoozabadi, A., Markeset, T. 1992. An experimental study of capillary and gravity crossflow fractured porous media. In SPE Annual Technical Conference and Exhibition. Society of Petroleum Engineers. doi.org/10.2118/24918-MS
- Fisher, M. K., Wright, C. A., Davidson, B. M., Goodwin, A. K., Fielder, E. O., Buckler, W. S., Steinsberger, N. P. 2002. Integrating fracture mapping technologies to optimize stimulations in the Barnett Shale. In SPE Annual Technical Conference and Exhibition. Society of Petroleum Engineers. doi.org/10.2118/77441-MS
- Fisher, M. K., Heinze, J. R., Harris, C. D., Davidson, B. M., Wright, C. A., Dunn, K. P. 2004. Optimizing horizontal completion techniques in the Barnett shale using microseismic fracture mapping. In SPE Annual Technical Conference and Exhibition. Society of Petroleum Engineers. doi.org/10.2118/90051-MS
- Fisher, M. K., Warpinski, N. R. 2012. Hydraulic-fracture-height growth: Real data. *SPE Production & Operations*, 27(01), 8-19. doi.org/10.2118/145949-PA

- Firoozabadi, A. 2001. Mechanisms of solution gas drive in heavy oil reservoirs. *Journal of Canadian Petroleum Technology*, 40(03), 15-20. doi.org/10.2118/01-03-DAS
- Fjar, E., Holt, R. M., Raaen, A. M., Risnes, R., and Horsrud, P. 2008. *Petroleum related rock mechanics* (Vol. 53). Elsevier
- Flewelling, S. A., Tymchak, M. P., Warpinski, N. 2013. Hydraulic fracture height limits and fault interactions in tight oil and gas formations. *Geophysical Research Letters*, 40(14), 3602-3606. doi: 10.1002/grl.50707
- Fraim, M. L., Wattenbarger, R. A. 1988, January. Decline Curve Analysis for Multiphase Flow. In *SPE Annual Technical Conference and Exhibition*. Society of Petroleum Engineers. doi.org/10.2118/18274-MS
- Fredd, C. N., McConnell, S. B., Boney, C. L., and England, K. W. 2000, January. Experimental study of hydraulic fracture conductivity demonstrates the benefits of using proppants. In *SPE Rocky Mountain Regional/Low-Permeability Reservoirs Symposium and Exhibition*. Society of Petroleum Engineers. doi.org/10.2118/60326-MS
- Gale, J. F., Reed, R. M., Holder, J. 2007. Natural fractures in the Barnett Shale and their importance for hydraulic fracture treatments. *AAPG bulletin*, 91(4), 603-622. doi:10.1306/11010606061
- Gale, J. F., Holder, J. 2010. Natural fractures in some US shales and their importance for gas production. In *Geological Society, London, Petroleum Geology Conference Series* (Vol. 7, pp. 1131-1140). Geological Society of London. doi:10.1144/0071131

- Gale, J. F., Laubach, S. E., Olson, J. E., Eichhubl, P., Fall, A. 2014. Natural fractures in shale: A review and new observations. *AAPG Bulletin*, 98(11), 2165-2216. doi: 10.1306/08121413151
- Gandossi, L. 2013. An overview of hydraulic fracturing and other formation stimulation technologies for shale gas production. Publications Office.
- Gdanski, R. D., Fulton, D. D., Shen, C. 2006, January. Fracture Face Skin Evolution During Cleanup. In SPE Annual Technical Conference and Exhibition. Society of Petroleum Engineers. doi: 10.2118/101083-PA.
- Ghanbari, E., Dehghanpour, H. 2016. The fate of fracturing water: A field and simulation study. *Fuel*, 163, 282-294. doi:10.1016/j.fuel.2015.09.040
- Gupta, R., Lu, P., Glotzbach, R., Hehmeyer, O. 2015. A Novel, Field-Representative Enhanced-Oil-Recovery Coreflood Method. *SPE Journal*. doi.org/10.2118/169088-PA
- Gupta, R., Maloney, D. R. 2014, November. Intercept Method-A Novel Technique to Correct Steady-State Relative Permeability Data for Capillary End-Effects. In Abu Dhabi International Petroleum Exhibition and Conference. Society of Petroleum Engineers. doi.org/10.2118/171797-MS
- Gutierrez, M., Øino, L. E., Nygård, R. 2000. Stress-dependent permeability of a de-mineralised fracture in shale. *Marine and Petroleum Geology*, 17(8), 895-907. doi:10.1016/S0264-8172(00)00027-1
- Habibi, A., Binazadeh, M., Dehghanpour, H., Bryan, D., and Uswak, G. 2015, September. Advances in Understanding Wettability of Tight Oil Formations. In SPE Annual

- Technical Conference and Exhibition. Society of Petroleum Engineers.
doi.org/10.2118/175157-MS
- Hancock, P. L. 1985. Brittle microtectonics: principles and practice. *Journal of structural geology*, 7(3), 437-457. doi:10.1016/0191-8141(85)90048-3
- Hassen, B. R., Zotskine, Y., and Gulewicz, D. 2012, January. Hydraulic fracture containment in the Bakken with a synthetic polymer water based fracture fluid. In SPE Canadian Unconventional Resources Conference. Society of Petroleum Engineers.
doi.org/10.2118/162670-MS
- Hidek, B. T., Rieb, B. A. 2011. Fracture stimulation treatment best practices in the Bakken oil shale. In SPE Hydraulic Fracturing Technology Conference. Society of Petroleum Engineers. doi: 10.2118/140252-MS.
- Hoch, O., Stromquist, M., Love, G., and Argan, J. 2003, January. Multiple precision hydraulic fractures of low-permeability horizontal openhole sandstone wells. In SPE Annual Technical Conference and Exhibition. Society of Petroleum Engineers.
doi.org/10.2118/84163-MS
- Hodgson, R. A. 1961. Regional study of jointing in Comb Ridge-Navajo mountain area, Arizona and Utah. *AAPG Bulletin*, 45(1), 1-38.
- Holditch, S. A. 1979. Factors affecting water blocking and gas flow from hydraulically fractured gas wells. *Journal of Petroleum Technology*, 31(12), 1-515. doi.org/10.2118/7561-PA
- Horie, T., Firoozabadi, A., Ishimoto, K. 1988. Capillary continuity in fractured reservoirs. SPE, 18282, 2-5.

- Hossain, M. M., and Rahman, M. K. 2008. Numerical simulation of complex fracture growth during tight reservoir stimulation by hydraulic fracturing. *Journal of Petroleum Science and Engineering*, 60(2), 86-104. doi:10.1016/j.petrol.2007.05.007
- Huang, D. D., Honarpour, M. M. 1998. Capillary end effects in coreflood calculations. *Journal of Petroleum Science and Engineering*, 19(1), 103-117. doi:10.1016/S0920-4105(97)00040-5
- Isaacs, E. 2008. Technology innovation and the importance of unconventional gas resources in Canada. In 19th World Petroleum Congress. World Petroleum Congress.
- Iwai, K. 1976. Fundamental studies of fluid flow through a single fracture (Doctoral dissertation, University of California, Berkeley).
- Jones, F. O., Owens, W. W. 1980. A laboratory study of low-permeability gas sands. *Journal of Petroleum Technology*, 32(09), 1-631. doi.org/10.2118/7551-PA
- Kalantari Dahaghi, A., Esmaili, S., Mohaghegh, S. D. 2012. Fast track analysis of shale numerical models. In SPE Canadian Unconventional Resources Conference. Society of Petroleum Engineers. doi:10.2118/162699-MS.
- Kazemi, H. (1969). Pressure transient analysis of naturally fractured reservoirs with uniform fracture distribution. *Society of petroleum engineers Journal*, 9(04), 451-462. doi:10.2118/2156-A.
- Kazemi, H., Merrill Jr, L. S., Porterfield, K. L., Zeman, P. R. 1976. Numerical simulation of water-oil flow in naturally fractured reservoirs. *Society of Petroleum Engineers Journal*, 16(06), 317-326. doi:10.2118/5719-PA.

- Killough, J. E. 1976. Reservoir simulation with history-dependent saturation functions. Society of Petroleum Engineers Journal, 16(01), 37-48. doi:10.2118/5106-PA
- Kim, J. G., Deo, M. D. 2000. Finite element, discrete-fracture model for multiphase flow in porous media. AIChE Journal, 46(6), 1120-1130. doi: 10.1002/aic.690460604
- King, G. E. 2010, January. Thirty years of gas shale fracturing: what have we learned?. In SPE Annual Technical Conference and Exhibition. Society of Petroleum Engineers. doi.org/10.2118/133456-MS
- Kirkpatrick, S. 1973. Percolation and conduction. Reviews of modern physics, 45(4), 574. doi.org/10.1103/RevModPhys.45.574
- Kraus, W. P., McCaffrey, W. J., & Boyd, G. W. (1993, January). Pseudo-bubble point model for foamy oils. In Annual Technical Meeting. Petroleum Society of Canada. doi:10.2118/93-45
- Krause, F. F., Deutsch, K. B., Joiner, S. D., Barclay, J. E., Hall, R. L., and Hills, L. V. 1994. Cretaceous cardium formation of the Western Canada sedimentary basin. Geological Atlas of the Western Canada Sedimentary Basin. GD Mossop and I. Shetson (eds.). Alberta Research Council and Canadian Society of Petroleum Geologists, 485-511.
- Kumar, R., Pooladi-Darvish, M. 2002. Solution-gas drive in heavy oil: Field prediction and sensitivity studies using low gas relative permeability. Journal of Canadian Petroleum Technology, 41(03). doi:10.2118/02-03-01
- Labastie, A. 1990. Capillary continuity between blocks of a fractured reservoir. In SPE Annual Technical Conference and Exhibition. Society of Petroleum Engineers. doi.org/10.2118/20515-MS

- Laubach, S. E. 2003. Practical approaches to identifying sealed and open fractures. AAPG bulletin, 87(4), 561-579.
- Laubach, S. E., Gale, J. F. W. 2006. Obtaining fracture information for low-permeability (tight) gas sandstone from sidewall cores. Journal of Petroleum Geology, 29(2), 147-158. doi: 10.1111/j.1747-5457.2006.00147.x
- Lebel, J. P. 1994. Performance implications of various reservoir access geometries. In 11th Annual Heavy Oil & Oil Sands Tech. Symp., March (Vol. 2).
- Lee, W. J., Sidle, R. 2010. Gas-reserves estimation in resource plays. SPE Economics & Management, 2(02), 86-91. doi:10.2118/130102-MS.
- LeFever, J. A. 2004. Evolution of Oil Production in the Bakken Formation. North Dakota Geological Survey, available from <https://www.dmr.nd.gov/ndgs/bakken/bakken.asp>.
- Liu, J., Bodvarsson, G. S., Wu, Y. S. 2003. Analysis of flow behavior in fractured lithophysal reservoirs. Journal of contaminant hydrology, 62, 189-211. doi:10.1016/S0169-7722(02)00169-9.
- Lopez, B. A., Gonzalez, L., Aguilera, R., Garcia-Hernandez, F. 2012. Effect of Natural Fracture Properties on Production Variability of Individual Wells in Multiphase Oil Reservoirs. In SPE Latin America and Caribbean Petroleum Engineering Conference. Society of Petroleum Engineers. doi:10.2118/153741-MS
- Lu, H., Di Donato, G., Blunt, M. J. 2008. General transfer functions for multiphase flow in fractured reservoirs. SPE Journal, 13(03), 289-297. doi:10.2118/102542-PA
- Marrett, R., Ortega, O. J., Kelsey, C. M. 1999. Extent of power-law scaling for natural fractures in rock. Geology, 27(9), 799-802. doi: 10.1130/0091-7613(1999)027

- Mayerhofer, M. J., Lolon, E. P., Youngblood, J. E., and Heinze, J. R. 2006, January. Integration of microseismic-fracture-mapping results with numerical fracture network production modeling in the Barnett Shale. In SPE Annual Technical Conference and Exhibition. Society of Petroleum Engineers. doi.org/10.2118/102103-MS
- McClure, M. W., Zoback, M. D. 2013, January. Computational investigation of trends in initial shut-in pressure during multi-stage hydraulic stimulation in the Barnett Shale. In 47th US Rock Mechanics/Geomechanics Symposium. American Rock Mechanics Association. ARMA-2013-368
- McClure, M. 2014. The potential effect of network complexity on recovery of injected fluid following hydraulic fracturing. In SPE Unconventional Resources Conference. Society of Petroleum Engineers. doi.org/10.2118/168991-MS
- Medeiros, F., Kurtoglu, B., Ozkan, E., Kazemi, H. 2010. Analysis of production data from hydraulically fractured horizontal wells in shale reservoirs. SPE Reservoir Evaluation & Engineering, 13(03), 559-568. doi:10.2118/110848-PA
- Miller, B. A., Paneitz, J. M., Mullen, M. J., Meijis, R., Tunstall, K. M., and Garcia, M. 2008, January. The successful application of a compartmental completion technique used to isolate multiple hydraulic-fracture treatments in horizontal Bakken shale wells in North Dakota. In SPE Annual Technical Conference and Exhibition. Society of Petroleum Engineers. doi.org/10.2118/116469-MS
- Moore, M. C. 2010, January. Policy and Regulation in the Face of Uncertainty: The Case of Disruptive Markets for Unconventional Natural Gas in North America. In Canadian

- Unconventional Resources and International Petroleum Conference. Society of Petroleum Engineers. doi.org/10.2118/138167-MS
- Muskat, M. 1945. The Production Histories of Oil Producing Gas-Drive Reservoirs. *Journal of Applied Physics*, 16(3). doi:147-159. 10.1063/1.1707566
- Narr, W. 1996. Estimating average fracture spacing in subsurface rock. *AAPG bulletin*, 80(10), 1565-1585.
- Nejadi, S., Leung, J. Y. W., Trivedi, J. J., and Virues, C. J. J. 2014, September. Integrated Characterization of Hydraulically Fractured Shale Gas Reservoirs Production History Matching. In *SPE/CSUR Unconventional Resources Conference—Canada*. Society of Petroleum Engineers. doi.org/10.2118/171664-PA
- Nelson, R. 2001. *Geologic analysis of naturally fractured reservoirs*. Gulf Professional Publishing.
- Nelson, P. H. 2009. Pore-throat sizes in sandstones, tight sandstones, and shales. *AAPG bulletin*, 93(3), 329-340.
- Nickelsen, R. P., VAN NESS, D. H. 1967. Jointing in the Appalachian plateau of Pennsylvania. *Geological Society of America Bulletin*, 78(5), 609-630.
- Ning, X., Fan, J., Holditch, S. A., Lee, W. J. 1993. The measurement of matrix and fracture properties in naturally fractured cores. In *Low Permeability Reservoirs Symposium*. Society of Petroleum Engineers. doi: 10.2118/25898-MS.
- Nolen-Hoeksema, R. 2013. Elements of hydraulic fracturing. *Oilfield Review Summer*, Schlumberger 2013: 25, no. 2.

http://www.slb.com/~media/Files/resources/oilfield_review/ors13/sum13/defining_hydraulic_fracturing.pdf

Norbeck, J. H. 2011. Identification and Characterization of Natural Fractures While Drilling Underbalanced (Doctoral dissertation, Colorado School of Mines).

NoRDQuiST, J. W. 1953. Mississippian stratigraphy of northern Montana.

Obinna, E. D., Hassan, D. 2016. Implications of Characterizing Tight Oil Reservoirs with Dual- and Triple-Porosity Models. *Journal of Energy Resources Technology*.
doi:10.1115/1.4032520

O'Brien, D. G., Larson, R. T., Parham, R., Thingelstad, B. L., Aud, W. W., Burns, R. A., Weijers, L. 2011. Using real-time downhole microseismic to evaluate fracture geometry for horizontal packer-sleeve completions in the Bakken Formation, Elm Coulee Field, Montana. In SPE Hydraulic Fracturing Technology Conference. Society of Petroleum Engineers. doi:10.2118/139774-MS

Ortega, O., Marrett, R. 2000. Prediction of macrofracture properties using microfracture information, Mesaverde Group sandstones, San Juan basin, New Mexico. *Journal of Structural Geology*, 22(5), 571-588. doi:10.1016/S0191-8141(99)00186-8

Ortega, O. J., Marrett, R. A., Laubach, S. E. 2006. A scale-independent approach to fracture intensity and average spacing measurement. *AAPG bulletin*, 90(2), 193-208.
doi:10.1306/08250505059

Ostensen, R. W. 1983. Microcrack permeability in tight gas sandstone. *Society of Petroleum Engineers Journal*, 23(06), 919-927. doi.org/10.2118/10924-PA

- Pagels, M., Hinkel, J. J., Willberg, D. M. 2012. Measuring Capillary Pressure Tells More Than Pretty Pictures. In SPE International Symposium and Exhibition on Formation Damage Control. Society of Petroleum Engineers. doi.org/10.2118/151729-MS
- Papatzacos, P., Skjæveland, S. M. 2002. Relative permeability from capillary pressure. In SPE Annual Technical Conference and Exhibition. Society of Petroleum Engineers. doi:10.2118/77540-MS
- Peters, E. J. 2012. Advanced Petrophysics (Vol. 2). Greenleaf Book Group.
- Petroleum, B. 2011. BP statistical review of world energy.
- Philip, Z. G., Jennings Jr, J. W., Olson, J. E., Holder, J. 2002. Modeling coupled fracture-matrix fluid flow in geomechanically simulated fracture networks. In SPE Annual Technical Conference and Exhibition. Society of Petroleum Engineers. doi.org/10.2118/77340-MS
- Phillips, Z. D., Halverson, R. J., Strauss, S. R., Layman, J., and Green, T. W. 2007, January. A case study in the bakken formation: Changes to hydraulic fracture stimulation treatments result in improved oil production and reduced treatment costs. In Rocky Mountain Oil & Gas Technology Symposium. Society of Petroleum Engineers. doi.org/10.2118/108045-MS
- Pitman, J. K., Price, L. C., and LeFever, J. A. 2001. Diagenesis and fracture development in the Bakken Formation, Williston Basin: Implications for reservoir quality in the middle member. Qadeer, S., Dehghani, K., Ogbe, D. O., Ostermann, R. D. 1991. Correcting oil-water relative permeability data for capillary end effect in displacement experiments (pp. 81-104). Springer US. doi:10.1007/978-1-4899-0617-5_8

- Quirk, D. J., Ziarani, A. S., Mills, S. T., Wagner, K., Chen, S., Chen, C. 2012. Integration of Microseismic Data, Fracture and Reservoir Simulation into the Development of Fractured Horizontal Wells in the Cardium Formation-A Tight Oil Case Study. In SPE Annual Technical Conference and Exhibition. Society of Petroleum Engineers. doi:10.2118/160002-MS
- Raaen, A. M., Skomedal, E., Kjørholt, H., Markestad, P., and Økland, D. 2001. Stress determination from hydraulic fracturing tests: the system stiffness approach. International Journal of Rock Mechanics and Mining Sciences, 38(4), 529-541. doi:10.1016/S1365-1609(01)00020-X
- Rangel-German, E., Akin, S., Castanier, L. 2006. Multiphase-flow properties of fractured porous media. Journal of Petroleum Science and Engineering, 51(3), 197-213. doi:10.1016/j.petrol.2005.12.010
- Rijken, P., Cooke, M. L. 2001. Role of shale thickness on vertical connectivity of fractures: application of crack-bridging theory to the Austin Chalk, Texas. Tectonophysics, 337(1), 117-133. doi:10.1016/S0040-1951(01)00107-X
- Rogers, S., Elmo, D., Dunphy, R., Bearinger, D. 2010. Understanding hydraulic fracture geometry and interactions in the Horn River Basin through DFN and numerical modeling. In Canadian Unconventional Resources and International Petroleum Conference. Society of Petroleum Engineers. doi:10.2118/137488-MS
- Rossen, W. R., Kumar, A. T. 1992. Single-and two-phase flow in natural fractures. In SPE Annual Technical Conference and Exhibition. Society of Petroleum Engineers. doi.org/10.2118/24915-MS

- Rossen, W. R., Kumar, A. T. A. 1994. Effect of fracture relative permeabilities on performance of naturally fractured reservoirs. In International Petroleum Conference and Exhibition of Mexico. Society of Petroleum Engineers. doi:10.2118/28700-MS
- Rubin, B. 2010. Accurate simulation of non Darcy flow in stimulated fractured shale reservoirs. In SPE Western Regional Meeting. Society of Petroleum Engineers. doi.org/10.2118/132093-MS
- Sampath, K. 1982. A new method to measure pore volume compressibility of sandstones. *Journal of Petroleum Technology*, 34(06), 1-360. doi.org/10.2118/10545-PA
- Secor, D. T. 1965. Role of fluid pressure in jointing. *American Journal of Science*, 263(8), 633-646.
- Siddiqui, S. K., Ali, A., and Dehghanpour, H. 2012, January. New advances in production data analysis of hydraulically fractured tight reservoirs. In SPE Canadian Unconventional Resources Conference. Society of Petroleum Engineers. doi.org/10.2118/162830-MS
- Snyder, L. J. 1969. Two-phase reservoir flow calculations. *Society of Petroleum Engineers Journal*, 9(02), 170-182. doi:10.2118/2014-PA.
- Stevens P. 2012. The 'shale gas revolution': Developments and changes. Chatham House Briefing Paper.
- Szymczak, S., Shen, D., Higgins, R., Gupta, D. V. 2012. Minimizing Environmental and Economic Risks with a Proppant-Sized Solid Scale Inhibitor Additive in the Bakken Formation. In SPE Annual Technical Conference and Exhibition. Society of Petroleum Engineers. doi: 10.2118/159701-MS.

- Tabatabaei, M., Mack, D. J., and Daniels, N. R. 2009, January. Evaluating the performance of hydraulically fractured horizontal wells in the Bakken shale play. In SPE Rocky Mountain Petroleum Technology Conference. Society of Petroleum Engineers. doi.org/10.2118/122570-MS
- Talabi, O., Pooladi-Darvish, M. 2004. A simulator for solution-gas drive in heavy oils. *Journal of Canadian Petroleum Technology*, 43(04). doi:10.2118/04-04-02
- Teufel, L. W., and Clark, J. A. 1984. Hydraulic fracture propagation in layered rock: experimental studies of fracture containment. *Society of Petroleum Engineers Journal*, 24(01), 19-32. doi.org/10.2118/9878-PA
- Thomas, L. K., Lumpkin, W. B., Reheis, G. M. 1976. Reservoir simulation of variable bubble-point problems. *Society of Petroleum Engineers Journal*, 16(01), 10-16. doi:10.2118/5107-PA
- Tuckwell, G. W., Lonergan, L., Jolly, R. J. H. 2003. The control of stress history and flaw distribution on the evolution of polygonal fracture networks. *Journal of structural geology*, 25(8), 1241-1250. doi:10.1016/S0191-8141(02)00165-7
- Urbancic, T. I. J., Shumila, V. J., Rutledge, J. T. J., and Zinno, R. J. J. 1999, January. Determining hydraulic fracture behavior using microseismicity. In *Vail Rocks 1999, The 37th US Symposium on Rock Mechanics (USRMS)*. American Rock Mechanics Association. doi: ARMA-99-0991
- US Energy Information Administration. 23 Oct. 2013a. North America leads the world in production of shale gas.. <http://www.eia.gov/todayinenergy/detail.cfm?id=13491> (accessed Oct 18, 2015).

US Energy Information Administration. 23 June. 2013b. Technically Recoverable Shale Oil and Shale Gas Resources: An Assessment of 137 Shale Formations in 41 Countries Outside the United States. <http://www.eia.gov/analysis/studies/worldshalegas/pdf/fullreport.pdf> (accessed Oct 18, 2015)

US Energy Information Administration. 25 November. 2014. Crude oil production.

http://www.eia.gov/dnav/pet/pet_crd_crpdn_adc_mbbldpd_m.htm

US Geological Survey. 2013. Petroleum Resource Assessment of the Bakken and Three Forks Formations.

Veatch Jr, R. W., Moschovidis, Z. A., and Fast, C. R. 1989. An overview of hydraulic fracturing. *Recent Advances in Hydraulic Fracturing*, Edited by JL Gidley, SA Holditch, DE Nierode, and RW Veatch Jr. Society of Petroleum Engineers, Henry L Doherty Series Monograph, 12.

Walsh, J. B., Grosenbaugh, M. A. 1979. A new model for analyzing the effect of fractures on compressibility. *Journal of Geophysical Research: Solid Earth* (1978–2012), 84(B7), 3532-3536. doi: 10.1029/JB084iB07p03532

Walsh, J. B. 1981, October. Effect of pore pressure and confining pressure on fracture permeability. In *International Journal of Rock Mechanics and Mining Sciences & Geomechanics Abstracts* (Vol. 18, No. 5, pp. 429-435). Pergamon. doi:10.1016/0148-9062(81)90006-1

Walton, I., McLennan, J. 2013. The role of natural fractures in shale gas production. In *ISRM International Conference for Effective and Sustainable Hydraulic Fracturing*. International Society for Rock Mechanics. doi: ISRM-ICHF-2013-046

- Warren, J. E., Root, P. J. 1963. The behavior of naturally fractured reservoirs. Society of Petroleum Engineers Journal, 3(03), 245-255. doi: 10.2118/426-PA.
- Warpinski, N. R., Teufel, L. W. 1987. Influence of geologic discontinuities on hydraulic fracture propagation (includes associated papers 17011 and 17074). Journal of Petroleum Technology, 39(02), 209-220. doi.org/10.2118/13224-PA
- Wattenbarger, R. A., Alkough, A. B. 2013. New advances in shale reservoir analysis using flowback data. In SPE Eastern Regional Meeting. Society of Petroleum Engineers. doi.org/10.2118/165721-MS
- Wang, M., Leung, J. 2015. Numerical Investigation of Coupling Multiphase Flow and Geomechanical Effects on Water Loss During Hydraulic Fracturing Flow Back Operation. Unconventional Resources Technology Conference (URTEC).
- Wang, Y., Holditch, S. A., McVay, D. A. 2008. Simulation of Gel Damage on Fracture-Fluid Cleanup and Long-Term Recovery in Tight-Gas Reservoirs. In SPE Eastern Regional/AAPG Eastern Section Joint Meeting. Society of Petroleum Engineers. doi:10.2118/117444-MS
- Warpinski, N. R., and Teufel, L. W. 1987. Influence of geologic discontinuities on hydraulic fracture propagation (includes associated papers 17011 and 17074). Journal of Petroleum Technology, 39(02), 209-220. doi.org/10.2118/13224-PA
- Weber, K. J., Bakker, M. 1981. Fracture and vuggy porosity. In SPE Annual Technical Conference and Exhibition. Society of Petroleum Engineers. doi.org/10.2118/10332-MS

- Wei, Y., Economides, M. J. 2005. Transverse hydraulic fractures from a horizontal well. In SPE Annual Technical Conference and Exhibition. Society of Petroleum Engineers. doi.org/10.2118/94671-MS
- Weijers, L. 1995. The near-wellbore geometry of hydraulic fractures initiated from horizontal and deviated wells (Doctoral dissertation, TU Delft, Delft University of Technology).
- Weng, X., Kresse, O., Cohen, C. E., Wu, R., Gu, H. 2011. Modeling of hydraulic-fracture-network propagation in a naturally fractured formation. SPE Production & Operations, 26(04), 368-380. doi.org/10.2118/140253-PA
- Wiley, C., Barree, B., Eberhard, M., and Lantz, T. 2004, January. Improved Horizontal Well Stimulations in the Bakken Formation, Williston Basin, Montana. In SPE Annual Technical Conference and Exhibition. Society of Petroleum Engineers. doi.org/10.2118/90697-MS
- Wu, Y. S. 2002. Numerical simulation of single-phase and multiphase non-Darcy flow in porous and fractured reservoirs. Transport in Porous Media, 49(2), 209-240. doi:10.1023/A:1016018020180
- Wu, Y. S., Liu, H. H., and Bodvarsson, G. S. 2004. A triple-continuum approach for modeling flow and transport processes in fractured rock. Journal of Contaminant Hydrology, 73(1), 145-179. doi:10.1016/j.jconhyd.2004.01.002.
- Wu, Y. S., Li, J., Ding, D., Wang, C., Di, Y. 2014. A generalized framework model for the simulation of gas production in unconventional gas reservoirs. SPE Journal, 19(05), 845-857. doi:10.2118/163609-PA

- Yan, B., Wang, Y., Killough, J. E. 2013. Beyond dual-porosity modeling for the simulation of complex flow mechanisms in shale reservoirs. In SPE Reservoir Simulation Symposium. Society of Petroleum Engineers. doi.org/10.2118/163651-MS
- Yedlin, D. 2008. Using horizontal drilling techniques in Canada. The Calgary Herald. Retrieved on, 01-23.
- Yue, M., Leung, J., Dehghanpour, H. 2013. Integration of numerical simulations for uncertainty analysis of transient flow responses in heterogeneous tight reservoirs. In SPE Unconventional Resources Conference Canada. Society of Petroleum Engineers. doi:10.2118/167174-MS